博士学位論文

Study on functional soft materials based on ultra-high molecular weight polymers

超高分子量ポリマーからなる機能性ソフトマテリアルに関する研究

Yuji Kamiyama

March 2024

Division of Soft Matter

Graduate School of Life Science

Hokkaido University

CONTENTS

Chapter 1

General Introduction

1.1 Ionic Liquids

Ionic liquids (ILs) are molten salts that have a melting temperature of lower than 100 ºC.[1, 2] In general, ionic substances such as NaCl have much higher melting temperature than room temperature (melting point of NaCl is 801 ºC) because of their strong Coulombic interaction between cations and anions. However, by increasing the ionic radius of the component ions to lower their charge density or by introducing a non-spherical shape of ions to be poorer ion packing, the melting point can be lowered, reaching under 100 ºC. The first IL reported as an "ionic liquid" was a salt with very simple structure called ethylammonium nitrate, $[EtNH_3][NO_3]$, which was reported by Walden in 1914.[3] The melting temperature of $[EtNH_3][NO_3]$ is as low as 12 ºC and regarded as IL. Following this report, chloroaluminate-based ILs, mixtures of aluminum chloride with *N*-alkylpyridinium chloride or alkyl imidazolium chloride, were reported and their applications as solvents for batteries and electrodeposition were explored.[4-7] However, these ILs have the critical disadvantage of being unstable with water and air, which prevented their use in practical applications. In 1992, Wilkes *et al.* reported 1-ethyl-3-methylimidazolium tetrafluoroborate ($[C_2mIm][BF_4]$), which is stable against both air and water.[8] Since then, ILs have been attracted much attention as novel solvents in various research fields such as extraction[9-14], electrochemical devices[1, 15-18], gas separation[19-21], and so on. In general, ILs have unique characteristics such as thermal stability including non-flamability, non-volatility, high ionic conductivity and (electro)chemical stability. Because they are composed solely of ions, they exhibit physical properties that differ from what common molecular liquids such as water and conventional organic solvents possess. For this reason, ILs are often called the "third solvent" following water and organic solvent. The most important characteristic of ILs is that they have infinite number of structural possibilities depending on the chemical structure of the constituent ions and the combination of ions. This enables us the unlimited structural design possibilities, including hydrophilicity. Because of this feature, ILs are also called "designer solvents".

The chemical structures of constituting ions in a typical ILs are shown in **Figure 1-1**. The ions of ILs are mainly bulky structures with cations, resulting in a lower melting point than general salts such as NaCl. These ions in ILs exist in two states, i. e. ion-dissociated and ion-associated. For this reason, a concept of "ionicity" which is degree of dissociation of ion species in ILs is often considered.[22-27] Tokuda *et al.* used the molar conductivity ratio $\Lambda_{imp}/\Lambda_{NMR}$ as a physicochemical parameter to evaluate ionicity, where Λ_{imp} and Λ_{NMR} are the molar ionic conductivities calculated from electrochemical

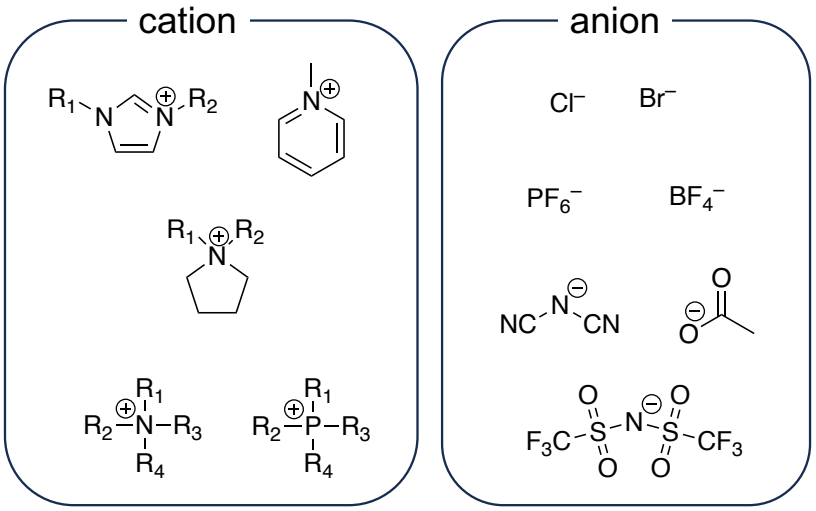

Figure 1-1. Chemical structures of typical cation and anion species of ILs.

impedance measurements and from the self-diffusion coefficients obtained by pulse-field-gradient spin-echo (PGSE) NMR measurements, respectively.[22, 26] They evaluated the ionicity of various ILs and pointed out that the ionicity of IL ions is strongly correlated with the electron accepting nature of cationic species and the electron donating nature of anionic species. They also mentioned that the ionicity of ILs, 1-alkyl-3-methylimidazolium trifluoromethylsulfonylimide ([C$_n$mIm][TFSI]), decreases as the alkyl chain length of the side chain increases, and that ionicity is related not only to Coulombic interactions between ions but also to interactions seen in molecular liquids, such as van der Waals interactions, hydrogen bonding, etc.[24] Another method to evaluate ionicity proposed by MacFarlane is using the Walden plot, which plots the logarithm of ionic conductivity against the logarithm of the reciprocal of viscosity.[28] (**Figure 1-2**) In this case, the straight line with slope 1 obtained from a 1.0 M KCl solution corresponds to the conductivity of an electrolyte solution with 100% dissociation. Based on this plot, Angell *et al.* classified ILs into super ionic liquid, good ionic liquid, and poor ionic liquid according to the deviation from KCl line of Walden plots.[27] The plot shifts upward from this straight line for systems, where conduction in glassy materials or by electron transfer occurs in hopping mechanism. Conversely, the plot shifts downward for systems with low conductivity relative to the viscosity, and for ILs with low ionic dissociation. In practical applications for electrochemical devices, in addition to these criteria, chemical and electrochemical stability, electrode reaction characteristics, and other factors should be comprehensively evaluated.

Furthermore, ILs are also notable for their excellent properties as solvents for other low molecular weight substances, because they can control their affinity against other solutes and solvents such as water. Some ILs, for example, exhibit liquid-liquid phase separation with water or organic solvents so they are thought to have potential applications as extraction solvents for (in)organic substances. In

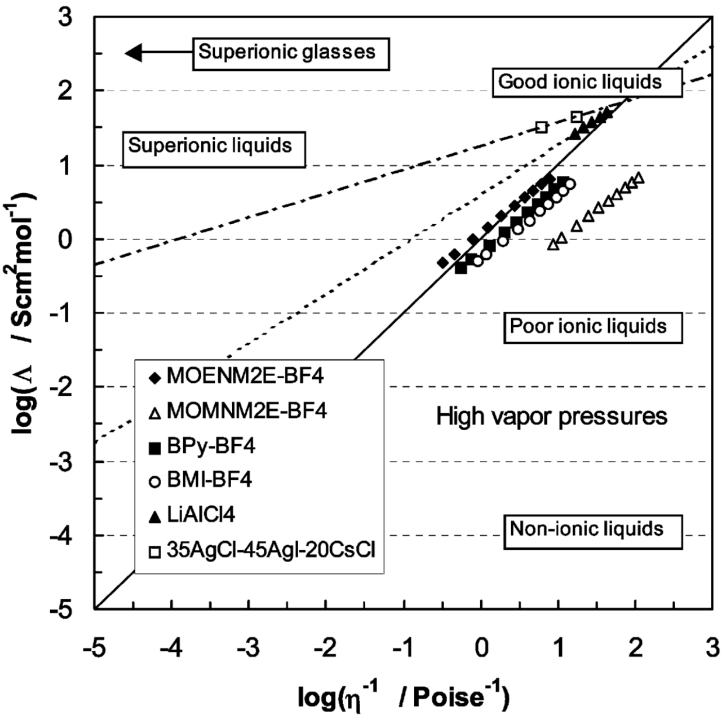

Figure 1-2. Walden plots of tetrafluoroborates salts of various cations. [27]

general, water affinity is strongly dominated by anion structure rather than cation. For example, ILs of combination of certain cation with chloride, acetate, and dicyanamide anions are mostly hydrophilic, while those with PF_6 and TFSI are hydrophobic.[29] Some ILs with certain structures having intermediate hydrophilic and hydrophobic properties, and exhibit temperature responsiveness. Ohno *et al.* developed an extraction system of proteins utilizing lower critical solution temperature (LCST) phase behavior in IL/water solution.[30] Aqueous cytochrome C solution and IL, tetrabutylphosphonium *N*-trifluoromethanesulfonyl leucine, formed a homogeneous phase system below 20°C, but when heated above 25°C, phase separation occurred and all cytochrome C moved to the IL phase. (**Figure 1-3**) Thus, temperature-responsive hydrophilic switching can be used to extract proteins from aqueous solutions by simply changing the temperature.[14] In addition, owing to the non-volatility and chemical stability of ILs, no volatile organic compounds or toxic substances are emitted into the environment during this process. Therefore, ILs are expected to be a new medium for "clean" liquid-liquid extraction. The unique dissolution ability of ILs is not only for water, but ILs also exhibit excellent solubility for aliphatic molecular solvents. Trihexyltetradecylphosphonium trifluoromethylsulfonylimide, $[P_{66614}]$[TFSI] ILs, which is quaternary alkylphosphonium-type IL with long alkyl chains can dissolve hexane up to 80 mol% with persistence of characteristics of the IL structure.[31]

ILs are also expected to be applied as solvents for various “hard-to-soluble” materials such as cellulose, silk and keratin.[32-35] These biogenic naturally occurring polymers are generally insoluble in water and conventional organic solvents because of its strong intra- and intermolecular hydrogen

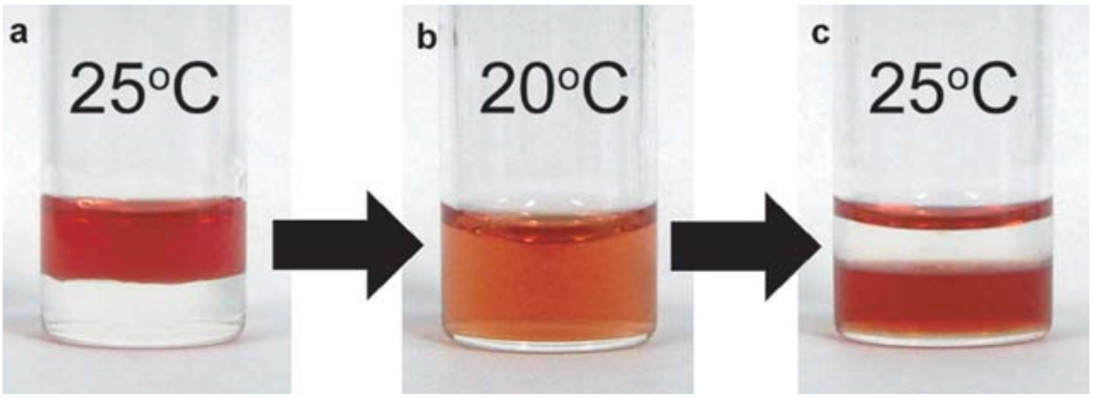

Figure 1-3. Extraction of a protein, cytochrome C from aqueous phase (upper phase) to IL phase (lower phase) by temperature change. (a) an aqueous solution of cytochrome C was added to the IL at 25 ºC; (b) the homogeneous IL/water mixture was obtained at 20 ºC; (c) the solution was heated again to 25 ºC to separate into bi-phases, and cytochrome C was extracted into the IL phase.[14]

bonding networks which hinders attractive interaction with solvent. Since cellulose is a renewable resource, the development of cellulose processing with the aid of ILs solution capability has been expected to establish. Swatloski *et al.* reported for the first time that 1-butyl-3-methylimidazolium chloride, [C_4mIm][Cl] can dissolve cellulose by straightforward heating up to 100 °C. They also reported that the cellulose solubility strongly depends on the anion structure of ILs.[32] Since this discovery, the use of ILs as a solvent of cellulose together with the hydrolysis cellulose processing have been actively explored.[36-39] Carbon nanotubes are cylindrical ring nanostructures consisting of a hexagonal network of carbon rings. They adopt a bundle structure as a result of their low solubility properties due to high cohesive forces resulting from the strong π-π interactions among the tubes.[40-43] Fukushima *et al.* reported that carbon nanotubes and imidazolium-based ILs are mixed and grinded to form a gel-like compound called a Bucky gel.[44] The carbon nanotubes were dispersed by cation-π interactions with imidazolium cations, and the entanglement of the tube bundles contributed to the gelation. This phenomenon was also observed when the alkyl chain length of the cation (C_2mIm, C_4mIm and C_6mIm) and the anion structure (BF_4, PF_6 and TFSI) were varied, and was applied to electrochemical devices such as soft actuators.[45-47] As described above, ILs are considered to have great potential as solvents that can dissolve a variety of solutes by appropriately selecting and designing the ionic structure.

1.2 Polymer Gels

Polymer gels are soft materials consisting of a three-dimensional polymer network swollen by a substantial amount of solvent. Depending on the type of solvent component that swells the polymer network, we can categorize polymer gels into three major types: hydrogels, organogels, and ion gels. If the solvent used to swell the polymer network is water or an organic solvent, it is called a hydrogel or organogel, respectively. If it is swollen with an IL, as in this thesis, it is called an ion gel. In 1978, Tanaka *et al.* has discovered the hydrogels could change their volume in reversible and discontinuous manner in response to external environment such as the changes in composition of solvent (water and acetone).[48] This discovery by Tanaka *et al.* is well known as an epoch-making event in gel science, namely the "discovery of volume phase transition of gels". Since this discovery, fundamental researches in physics have been conducted to elucidate the origin of the volume phase transition of hydrogel and to better understand why proteins having infinite conformational possibilities fold in the one, meaningful conformation. In addition to such basic research, there were a number of material scientific research that attempted to utilize hydrogels for actuators and drug delivery systems (DDS) etc., by transfer reversible swelling-shrinking phase into certain mechanical functions.[48, 49 50-53] Organogels, which are broadly classified by the method of construction of low-molecular weight or polymeric gelators, are have also been studied for applications in gel electrolytes[54, 55], adhesion-resistant materials[56], and DDS.[57]

Recently, the ILs are expected to be a new candidate of solvent for polymer gels. **Figure 1-4** shows a conceptual illustration of a typical chemical ion gel and a physical ion gel. Watanabe *et al.* firstly prepared polymer gels by *in situ* free radical polymerization of methyl methacrylate (MMA) with ethylene glycol dimethacrylate as a bi-functional chemical crosslinker in IL ([C_2mIm][TFSI]), and named them "ion gels".[58] Lodge *et al.* fabricated physically crosslinked ion gels by utilizing self-assembly of block copolymers in ILs: by complexing an ABA-type triblock copolymer consisting of an incompatible A block and a compatible B block in ILs, the A block aggregates to form a micellar

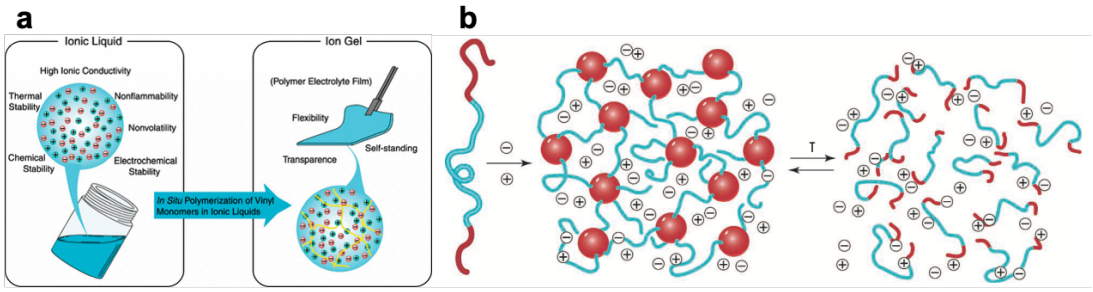

Figure 1-4. Ion gels prepared (a)by *in situ* radical polymerization of vinyl monomers in ILs and (b)by self-assembly of ABA triblock copolymers with different compatibility.[58,59]

structure, and the B block bridges the aggregation points to form a three-dimensional polymer network, resulting in gelation. [59-63] The ion gels with block copolymers as the matrix can be tuned in physical properties by block ratio, molecular weight, and chemical composition of polymers. Since the physical gel is not permanently cross-linked among polymer chain and formed by self-assembled micellar structure formation, and the solvent used to polymer network swell is non-volatile, solution molding of ion gels using co-solvents is possible. [64, 65] Furthermore, the reversible sol-gel transition of ion gels in response to temperature is also realized by introducing thermo-sensitive polymers as A-block. [66, 67] The ion gels possess unique properties, such as high ionic conductivity, non-volatility, non-flammability, and thermal stability derived from ILs, while being soft, wet, and solid consistency of general polymer gels. Given their excellent ionic conductivity and soft texture, they are expected to be applied to flexible electrochemical devices such as strain sensors and smart gels that undergo volume changes in response to external stimuli.[65, 68-76]

Although, I have focused on the solvent component of the polymer gel so far, herein I will briefly summarize the design of polymer network in terms of improvement of mechanical property of hydrogels. Polymer gels are generally mechanically fragile due to the fact that gels contain various types of inhomogeneities.[77] It is desirable to enhance the toughness of polymer gels to ensure that they are robust enough to withstand practical applications. In the past couple of decades, new types of gels capable of large deformations have been developed by sophisticated design of polymer network structures. Four kinds of the representative examples are shown in **Figure 1-5.**[78] The first example was the sliding ring gel realized by Okumura and Ito in 2001.[79] This type of gel was created based on the concept of dynamic cross-linking points and cross-linked by a figure-eight polyrotaxane. Since the cross-linking points are not covalently bonded to the polymer, the cross-links can slide along the axial

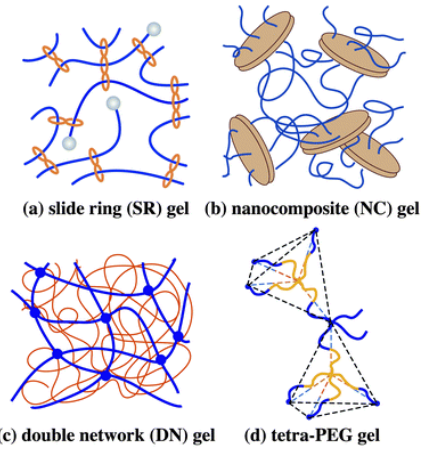

Figure 1-5. Schematic representation of tough polymer gels. (a) slide ring (SR) gel (cyclodextrin (CD) rings threaded by poly(ethylene glycol)(PEG)), (b) nanocomposite (NC) gel (polymer chains crosslinked by clay platelets), (c) double network (DN) gel (polyelectrolyte (thick) and neutral polymer (thin)) and (d) Tetra-PEG gel made by cross-end-coupling tetra-arm PEGs. [78]

direction of polymer chain. Generally, the stress provided for gel deformation is stored at the points of the lowest molecular weight between the cross-linking points, resulting in mechanically rupture. In the slide-ring gel proposed by Okumura and Ito, the mechanical energy originally stored in the gel is converted into moving energy of the cross-linking points because the cross-linking points themselves are freely movable. This unique mechanism allows energy dissipation within the gel, making it possible to prepare mechanically tough gel. The second representative case, called nanocomposite gel (NC gel) proposed by Harada *et al.*, is straightforwardly prepared by radical polymerization of *N*-isopropylacrylamide in the presence of Laponite clay without addition of any typical molecular bifunctional cross-linker such as methylene bisacrylamide.[80] The shape of Laponite is extremely thin disk with a thickness of about a thickness of 10 Å and a diameter of 300 Å, and the physical crosslinking between the homogeneously dispersed clay surface and polymer chains gives NC gels superior elongation properties. Furthermore, NC gels typically shows excellent transparency even at condition of high clay concentration. These properties are suitable not only for mechanical functional materials, but also for application to optical functional materials. In third example, Gong *et al.* have successfully prepared double network (DN) gels utilizing sacrificial bonding, which consist of a rigid and brittle network and a flexible network, exhibiting very large energy dissipation and toughness. Since its compressive fracture stress is extremely high, surpassing that of biological cartilage, its application to artificial articular cartilage was explored.[81] The final representative gel is the tetra-PEG gel, which is fabricated by "cross-end coupling" of two tetra-arm poly(ethylene glycol) (tetra-PEG) macromers with complementary functional groups, that is, an amine group and an active ester group.[82] Tetra-PEG gels have a homogeneous network structure having exactly same molecular weight between cross-linking points. This polymer network design prevents stress concentration during deformation leading to excellent mechanical property. Note that the tetra-PEG gels also provide an opportunity to prepare a predictable model system that can be used to verify and reproduce the classical physical theory of polymer gels.[83, 84] More recently, elongation-induced crystallization of polymer networks has been reported in polymer gels, and high-strength and self-reinforcing gels utilizing this phenomenon are attracting attention.[85-87]

1.3 Self-Healing Polymer Materials

Self-healing materials spontaneously recover from damage or degraded mechanical properties caused in the material. As polymer materials are used, localized damage and microcracks gradually occur. These lead to cracks and fractures, shortening the lifetime of the material. Therefore, early healing of localized damage is important. Overcoming this challenge will extend the lifetime of materials and reduce the environmental burden caused by polymer materials. Here, the classification and principle of self-healing materials are outlined.

Self-healing polymeric materials can be classified into two types in terms of the interaction between healing sites: based on chemical interactions and based on physical interactions. Self-healing by physical interaction has long been studied for its behavior and mechanisms. The very early stage of healing was due to the regeneration of physical cross-links that are inherent to polymers, such as the regeneration of molecular chain entanglement between the damaged surfaces. For example, the recovery of mechanical strength by crack healing in PMMA glass is affected by various factors such as molecular weight, copolymerization ratio, temperature, strain, and the presence of solvent.[88, 89] Wool and O'Connor describe the mechanism of this complicated healing phenomenon in the following five stages by isolating the multi-convoluted time dependencies of the molecular processes: [1] surface rearrangement, [2] surface approach, [3] wetting, [4] diffusion, and [5] randomization.[90] The first stage refers to state of surface, chain-end distribution, and topography and the fact that the damaged surface is rough but must be smoothed in order to recover the surfaces to approach each other in the next second and third stages. In the second and third stages, it was pointed out that in order to heal, damaged surfaces such as cracked surfaces must be close to each other at molecular-scale and must further wet each other, which was described as two-dimensional nucleation and growth process. Steps 4 and 5 mean that strength is recovered only when the damaged surfaces approach each other at the molecular level, after which the molecular chains diffuse into each other, regenerate entanglement, and be equilibrated. In the case of crack healing of PMMA mediated by methanol coated on the surface, methanol acts as a plasticizer for PMMA, lowering the glass transition

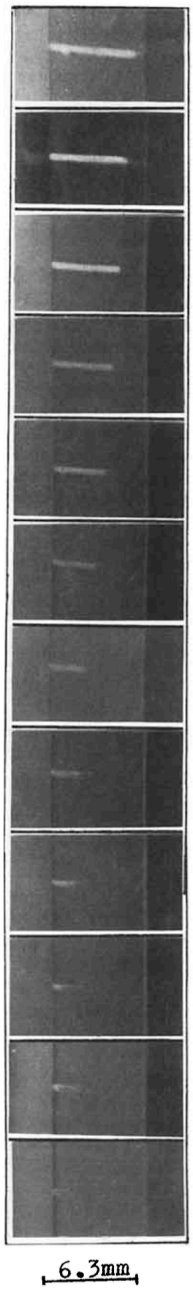

Figure 1-6. Crack healing sequence (interval is 1 minute)[88]

temperature of PMMA and enhancing mobility of molecules, resulting in self-healing only at operating temperature higher than the effective glass transition temperature.[88] (**Figure 1-6**) Such solvent-promoted self-healing is not suitable for good solvents because they immediately dissolve the material, and it is necessary to select a solvent that penetrates only a very thin layer from the top surface of the polymer material.

Most studies to improve healing ability of soft materials have directed to the approach of intentionally introducing chemical interactions. One of the early studies featured microcapsule-based self-healing polymer materials. White *et al.* encapsulated monomers in microcapsules and healed cracks by polymerization of the monomers that leaked from the microcapsules when cracks occurred.[91] (**Figure 1-7(a)**) As a result, the fracture stress is successfully recovered as high as 75%. This report was a breakthrough discovery that strongly pushed the development of self-healing materials worldwide in the following years. Another method for designing self-healing materials is to utilize dynamic bonding such as dynamic covalent bonding or non-covalent bonding such as hydrogen bonding etc. to create a self-healing material that recovers to its original state by re-generating bonding when the cut surfaces come into contact with each other. As an example of dynamic covalent bonding, Wudl *et al.* developed in 2002 a self-healing material based on the Diels-Alder reaction, in which each derivative of diene and ene with a double bond forms a cyclic molecule, which is cleaved by a reverse reaction at high temperature.[92] (**Figure 1-7(b)**) They used multifunctional furan- and maleimide-terminated monomers to obtain a self-healing material. This material showed about 60% self-healing ability by high temperature treatment after fracture. Hydrogen bonds[93, 94], host-guest interactions[95], coordination bonds[96], and ionic bonds[97] are also reversible as well as dynamic covalent bonds[98, 99], and two pairs can form associates through non-covalent interactions resulting in self-healing materials.

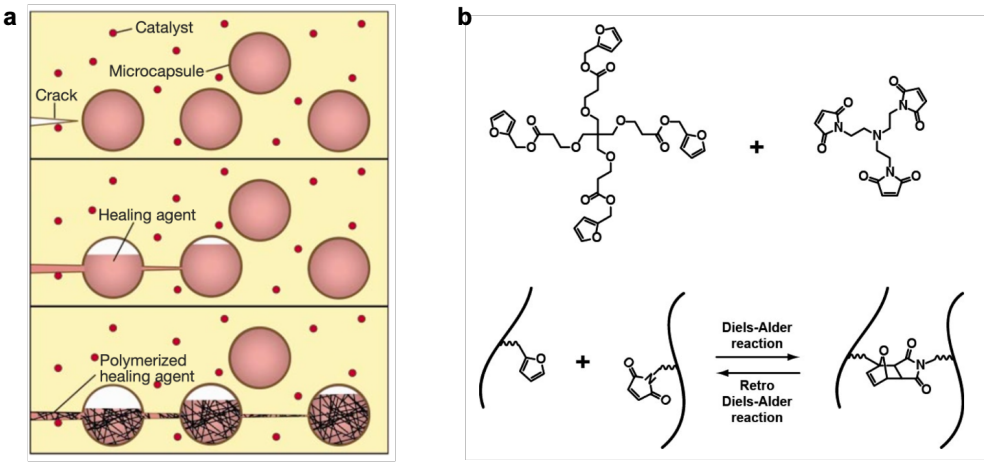

Figure 1-7. Conceptual illustration of self-healing materials using (a)microcapsules and (b)dynamic covalent bonding.[91,92]

In recent years, these methods of developing self-healing materials have been extended to ion gel systems, and the number of reports is increasing every year. For example, self-healing ion gels based on Schiff base reversible bonding[100], hydrogen bonding[72, 74, 101], and ion-dipole interactions[75, 102-104] have been reported. Ion gels created by copolymerization of 2,2,2-trifluoroethyl acrylate and acrylamide in IL [C_2mIm][TFSI] exhibit self-healing properties through hydrogen bonding and ion-dipole interactions.[75] The composition of the fluorine-rich matrix makes it highly resistant to water and several other organic solvents despite the presence of hydrophilic acrylamide, and even allows for self-healing underwater. Self-healing ion gels, stretchable and durable ion-conductive soft materials, are promising for applications in the field of flexible electronics as introduced in following section.

1.4 Application of Composite of Polymers and ILs

Growing health awareness among the increasing older population and the advent of the IoT society have increased the demand for personal health care systems that can detect and analyze an individual's biological signals and health status at any given time and place. The development of such systems will not only facilitate medical assistance for the elderly and infirm, but also provide real-time monitoring to prevent serious illness in chronically ill patients, activity management for athletes, detection and management of physical vital signs of individuals that will play a role in improving the public health and hygiene base, etc. To realize this purpose, the development of wearable flexible electrochemical devices and their materials is required by making the sensors, power supplies, and circuit infrastructure more flexible and durable. As already mentioned, ILs have been considered for application to electrochemical devices such as secondary batteries[105, 106], capacitors[17, 18, 107, 108], sensors[73, 104, 109-112], and actuators[46] because of their high safety, stability, and reliability derived from their nonflammability and nonvolatility, as well as their high ion conductivity. On the other hand, in accordance with the recent social context, there is a growing opportunity to develop it as a flexible and tough ionic conductor by compositing it with polymers, and its application to flexible devices such as touch sensors[113, 114], strain sensors[73, 75, 103, 109], electric double-layer capacitors[107, 108, 115-117], actuators[45, 118-121], displays[65], and organic thin-film transistors[65, 122] has been reported.

Lodge and Frisbie *et al.* used the ion gel with an ABA-type triblock copolymer consisting of polystyrene in the A block and PEG in the B block and IL ([C_2mIm][TFSI]) solvent as a gate insulator for organic thin film transistors.[64] (**Figure 1-8**) The ion gel dielectrics exhibit high capacitance, excellent frequency response, and can be printed with co-solvents, indicating their potential for use in flexible electronics. Recently, 3D printable gel electrolytes and hysteresis-free gels oriented for more practical strain sensor applications have been reported.[123, 124]

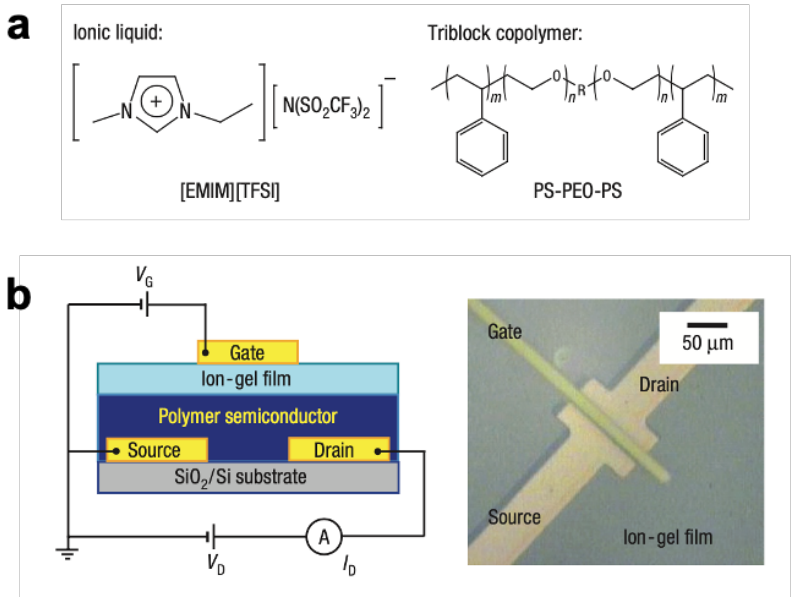

Figure 1-8. Ion gels based on ABA triblock copolymers and their application to organic thin-film transistors.[64]

Ion gel electrolytes that achieve both high robustness and self-healing properties by applying sophisticated synthetic methods to the construction of polymer networks and ensure durability over longer periods of time are being actively investigated.[71, 76, 125] Ion gels with crystalline segments, dynamic urea and hydrogen bonds introduced into the chemical bonding network of the flexible polymers exhibited reproducibility of electrochemical response beyond 10,000 strain cycles and durability of more than 200 days in air, in addition to fully recovered mechanical properties by heating to about 65°C.[74] (**Figure 1-9(a)**) In recent years, several strategies to introduce microphase-separated structures into ion gels by copolymerizing monomers with different compatibility have also been reported. Wang *et al.* found that copolymerization of acrylamide and acrylic acid in the IL 1-ethyl-3-methylimidazolium ethylsulfate ($[C_2mim][EtSO_4]$) induces microphase separation during polymerization, and the resulting ion gels exhibit extremely high mechanical properties (breaking strength: 12.6 MPa, breaking strain 600%), self-healing, and shape memory properties.[126] (**Figure 1-9(b)**) Other reports of various ion gel materials utilizing polymerizable ILs[104, 110, 123, 127], cellulose nanofibrils[128, 129], and covalent organic flameworks[124] have been increasing in recent years. Behind such active material development may be the excellent solubility of various molecules, including polymers, and the designability of their structures, in addition to the excellent material properties of ILs for their applications.

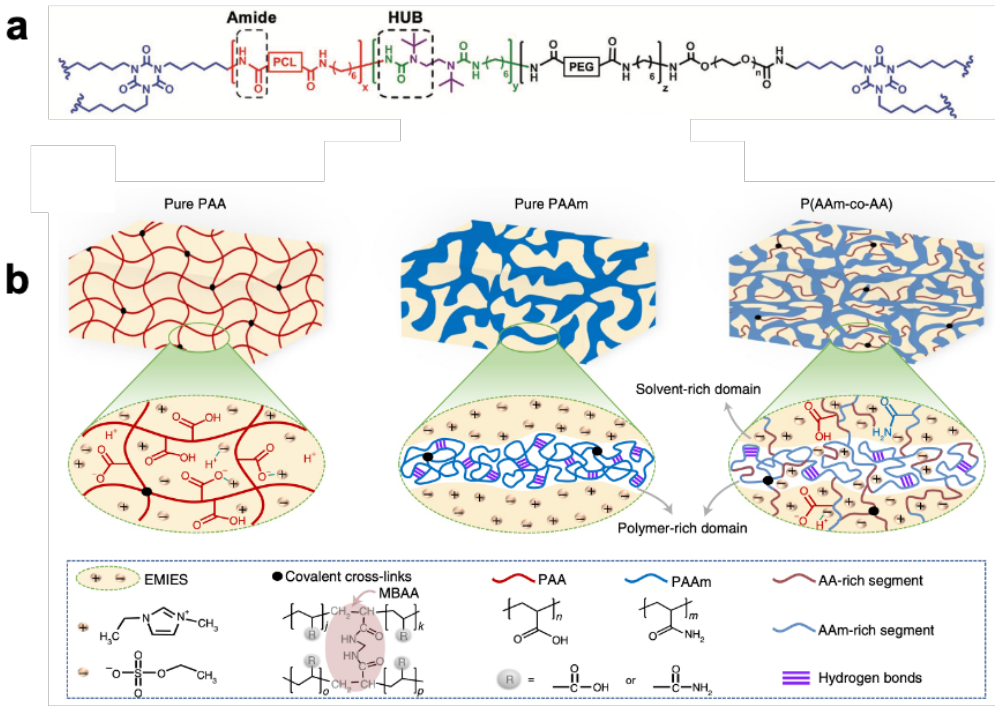

Figure 1-9. High-strength, self-healing ion gels based on (a)poly(urea-urethane) and (b)microphase separation.[74,126]

1.5 Outline of the Dissertation

The history of the development of ILs and ion gels and their applications have been reviewed thus far. The recent development of composite materials of polymers and ILs has been remarkable and their potential as new materials is apparent. The high strength of ion gel materials has been achieved mainly through precise structural design of polymer chains, but the complexity of their synthetic methodologies often prevented their practical application.

In this doctoral dissertation, I have developed an extremely simple method for synthesizing high-toughness and excellent self-healing ion gels. In particular, I will focus on the unique synthetic procedure for the ion gels and mechanical properties of the materials. This study begins with the discovery that radical polymerization of vinyl monomers in ILs is much accelerated compared to polymerization in conventional organic solvents, resulting in polymers with high molecular weights: ultra-high molecular weight polymers with molecular weights exceeding 1 million are generated. As a result, tough ion gels are formed solely by the physical entanglement of ultra-high molecular weight polymers. (Figure 1-10)

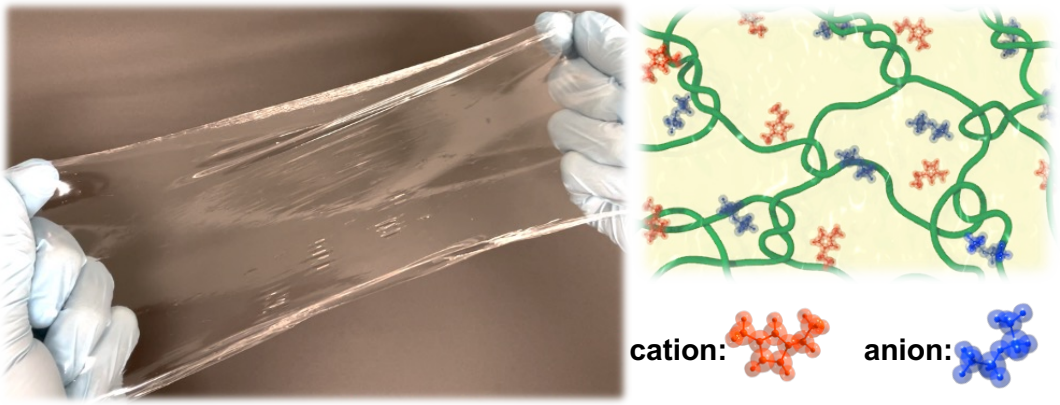

Figure 1-10. Photograph of an ion gel consisting of ultra-high molecular weight polymer entanglement in an IL and illustration of its structure.

First, in Chapter 2, the influence of solvents in radical polymerization was investigated by comparing ILs with conventional solvents, and the conditions under which ultra-high molecular weight polymers are obtained and the mechanism of their formation were discussed. Furthermore, the effects of ultra-high molecular weight on the basic physical properties were highlighted by discussing the results of rheological and dynamic light scattering (DLS) measurements.

In Chapter 3, I focused on the mechanical properties of ion gel materials. The ion gel in this study is essentially different from conventional ion gels where the chemical cross-linking points are replaced by physical entanglement cross-linking points, resulting in new material properties not seen before,

such as high stretchability, recyclability, and self-healing properties. The details of the self-healing behavior, the mechanism of it, and the effect of microscopic dissolved structure on the healing ability were investigated.

In Chapter 4, I finally focused on the structural designability of ILs. While the mechanical properties of gel materials have been generally controlled by the polymer network, here I aimed at controlling the mechanical properties of UHMW ion gels by the chemical structure of the IL, *i.e.*, the solvent engineering of gels. This quite new strategy opens up the new door to tune mechanical property of functional polymer gel materials. *In situ* polymerization and gelation using ILs and monomers with various chemical structures were performed to demonstrate the versatility of UHMW gels. The influence of the chemical structure of the ILs and polymers constituting the gels on the mechanical and self-healing properties of the resulting UHMW gels was investigated, and the correlation between these properties and the chemical structure was screened. Finally, I selected characteristic systems that exhibit different self-healing behaviors, applied micro-solvation structure analysis to them, and summarized the correlation between their micro-solvation state and self-healing behaviors.

Reference

[1] Welton, T. *Chem. Rev.* **1999**, *99*, 2071-2084.

[2] Plechkova, N. V.; Seddon, K. R. *Chem. Soc. Rev.* **2008**, *37*, 123-150.

[3] Walden, P. *Bull. Acad. Imper. Sci.(St. Petersburg)* **1914**, *1800*.

[4] Koch, V. R.; Miller, L. L.; Osteryoung, R. A. *J. Am. Chem. Soc.* **1976**, *98*, 5277-5284.

[5] Robinson, J.; Osteryoung, R. A. *J. Am. Chem. Soc.* **1979**, *101*, 323-327.

[6] Wilkes, J. S.; Levisky, J. A.; Wilson, R. A.; Hussey, C. L. *Inorg. Chem.* **1982**, *21*, 1263-1264.

[7] Gale, R. J.; Gilbert, B.; Osteryoung, R. A. *Inorg. Chem.* **1978**, *17*, 2728-2729.

[8] Wilkes, J.; Zaworotko, M. *J. Chem Soc. Chem. Commun* **1992**, *13*, 965-967.

[9] Huddleston, J. G.; Willauer, H. D.; Swatloski, R. P.; Visser, A. E.; Rogers, R. D. *Chem. Commun.* **1998**, 1765-1766.

[10] Dai, S.; Ju, Y. H.; Barnes, C. E. *J. Chem. Soc., Dalton Trans.* **1999**, 1201-1202.

[11] Visser, A. E.; Swatloski, R. P.; Reichert, W. M.; Griffin, S. T.; Rogers, R. D. *Ind. Eng. Chem. Res.* **2000**, *39*, 3596-3604.

[12] Du, Z.; Yu, Y.-L.; Wang, J.-H. *Chem. Eur. J.* **2007**, *13*, 2130-2137.

[13] Freire, M. G.; Santos, L. M. N. B. F.; Fernandes, A. M.; Coutinho, J. A. P.; Marrucho, I. M. *Fluid Ph. Equilib.* **2007**, *261*, 449-454.

[14] Kohno, Y.; Saita, S.; Murata, K.; Nakamura, N.; Ohno, H. *Polym. Chem.* **2011**, *2*, 862-867.

[15] Holbrey, J. D.; Seddon, K. R. *Clean Products and Processes* **1999**, *1*, 223-236.

[16] Wasserscheid, P.; Keim, W. *Angew. Chem. Int. Ed.* **2000**, *39*, 3772-3789.

[17] Galiński, M.; Lewandowski, A.; Stępniak, I. *Electrochim. Acta.* **2006**, *51*, 5567-5580.

[18] MacFarlane, D. R.; Forsyth, M.; Howlett, P. C.; Pringle, J. M.; Sun, J.; Annat, G.; Neil, W.; Izgorodina, E. I. *Acc. Chem. Res.* **2007**, *40*, 1165-1173.

[19] Aki, S. N. V. K.; Mellein, B. R.; Saurer, E. M.; Brennecke, J. F. *J. Phys. Chem. B* **2004**, *108*, 20355-

20365.

[20] Jacquemin, J.; Husson, P.; Majer, V.; Gomes, M. F. C. *Fluid Ph. Equilib.* **2006**, *240*, 87-95.

[21] Blanchard, L. A.; Hancu, D.; Beckman, E. J.; Brennecke, J. F. *Nature* **1999**, *399*, 28-29.

[22] Ueno, K.; Tokuda, H.; Watanabe, M. *Phys. Chem. Chem. Phys.* **2010**, *12*, 1649-1658.

[23] Tokuda, H.; Hayamizu, K.; Ishii, K.; Abu Bin Hasan Susan, M.; Watanabe, M. *J. Phys. Chem. B* **2004**, *108*, 16593-16600.

[24] Tokuda, H.; Hayamizu, K.; Ishii, K.; Susan, M. A.; Watanabe, M. *J. Phys. Chem. B* **2005**, *109*, 6103-6110.

[25] Tokuda, H.; Ishii, K.; Susan, M. A.; Tsuzuki, S.; Hayamizu, K.; Watanabe, M. *J. Phys. Chem. B* **2006**, *110*, 2833-2839.

[26] Tokuda, H.; Tsuzuki, S.; Susan, M. A. B. H.; Hayamizu, K.; Watanabe, M. *J. Phys. Chem. B* **2006**, *110*, 19593-19600.

[27] Xu, W.; Cooper, E. I.; Angell, C. A. *J. Phys. Chem. B* **2003**, *107*, 6170-6178.

[28] MacFarlane, D. R.; Forsyth, M.; Izgorodina, E. I.; Abbott, A. P.; Annat, G.; Fraser, K. *Phys. Chem. Chem. Phys.* **2009**, *11*, 4962-4967.

[29] Forsyth, S. A.; Pringle, J. M.; MacFarlane, D. R. *Aust. J. Chem.* **2004**, *57*, 113-119.

[30] Fukumoto, K.; Ohno, H. *Angew. Chem. Int. Ed.* **2007**, *46*, 1852-1855.

[31] Liang, M.; Khatun, S.; Castner, E. W., Jr. *J. Chem. Phys.* **2015**, *142*, 121101.

[32] Swatloski, R. P.; Spear, S. K.; Holbrey, J. D.; Rogers, R. D. *J. Am. Chem. Soc.* **2002**, *124*, 4974-4975.

[33] Phillips, D. M.; Drummy, L. F.; Conrady, D. G.; Fox, D. M.; Naik, R. R.; Stone, M. O.; Trulove, P. C.; De Long, H. C.; Mantz, R. A. *J. Am. Chem. Soc.* **2004**, *126*, 14350-14351.

[34] Phillips, D. M.; Drummy, L. F.; Naik, R. R.; Long, H. C. D.; Fox, D. M.; Trulove, P. C.; Mantz, R. A. *J. Mater. Chem.* **2005**, *15*, 4206-4208.

[35] Xie, H.; Li, S.; Zhang, S. *Green Chem.* **2005**, *7*, 606-608.

[36] Kamimura, A.; Okagawa, T.; Oyama, N.; Otsuka, T.; Yoshimoto, M. *Green Chem.* **2012**, *14*.

[37] Rein, D. M.; Khalfin, R.; Szekely, N.; Cohen, Y. *Carbohydr. Polym.* **2014**, *112*, 125-133.

[38] Endo, T.; Hosomi, S.; Fujii, S.; Ninomiya, K.; Takahashi, K. *Molecules* **2017**, *22*.

[39] Hirosawa, K.; Fujii, K.; Hashimoto, K.; Shibayama, M. *Macromolecules* **2017**, *50*, 6509-6517.

[40] Ajayan, P. M.; Schadler, L. S.; Giannaris, C.; Rubio, A. *Adv. Mater.* **2000**, *12*, 750-753.

[41] Chen, R. J.; Zhang, Y.; Wang, D.; Dai, H. *J. Am. Chem. Soc.* **2001**, *123*, 3838-3839.

[42] Bandyopadhyaya, R.; Nativ-Roth, E.; Regev, O.; Yerushalmi-Rozen, R. *Nano Lett.* **2002**, *2*, 25-28.

[43] Hirsch, A. *Angew. Chem. Int. Ed.* **2002**, *41*, 1853-1859.

[44] Fukushima, T.; Kosaka, A.; Ishimura, Y.; Yamamoto, T.; Takigawa, T.; Ishii, N.; Aida, T. *Science* **2003**, *300*, 2072-2074.

[45] Fukushima, T.; Asaka, K.; Kosaka, A.; Aida, T. *Angew. Chem. Int. Ed.* **2005**, *44*, 2410-2413.

[46] Katakabe, T.; Kaneko, T.; Watanabe, M.; Fukushima, T.; Aida, T. *J. Electrochem. Soc.* **2005**, *152*, A1913.

[47] Fukushima, T.; Kosaka, A.; Yamamoto, Y.; Aimiya, T.; Notazawa, S.; Takigawa, T.; Inabe, T.; Aida, T. *Small* **2006**, *2*, 554-560.

[48] Tanaka, T. *Phys. Rev. Lett.* **1978**, *40*, 820-823.

[49] Hirotsu, S.; Hirokawa, Y.; Tanaka, T. *J. Chem. Phys.* **1987**, *87*, 1392-1395.

[50] Tibbitt, M. W.; Anseth, K. S. *Biotechnol. Bioeng.* **2009**, *103*, 655-663.

[51] Burdick, J. A.; Prestwich, G. D. *Adv. Mater.* **2011**, *23*, H41-56.

[52] Hoffman, A. S. *Adv. Drug Deliv. Rev.* **2012**, *64*, 18-23.

[53] Yang, C.; Suo, Z. *Nat. Rev. Mater.* **2018**, *3*, 125-142.

[54] Trung, T. Q.; Lee, N.-E. *Adv. Mater.* **2017**, *29*, 1603167.

[55] Hanabusa, K.; Hiratsuka, K.; Kimura, M.; Shirai, H. *Chem. Mater.* **1999**, *11*, 649-655.

[56] Lv, J.; Yao, X.; Zheng, Y.; Wang, J.; Jiang, L. *Adv. Mater.* **2017**, *29*.

[57] Vintiloiu, A.; Leroux, J. C. *J. Control. Release* **2008**, *125*, 179-192.

[58] Susan, M. A.; Kaneko, T.; Noda, A.; Watanabe, M. *J. Am. Chem. Soc.* **2005**, *127*, 4976-4983.

[59] Lodge, T. P. *Science* **2008**, *321*, 50-51.

[60] Lodge, T. P.; Ueki, T. *Acc. Chem. Res.* **2016**, *19*, 2107-2114.

[61] Tamate, R.; Hashimoto, K.; Ueki, T.; Watanabe, M. *Phys. Chem. Chem. Phys.* **2018**, *20*, 25123-25139.

[62] He, Y.; Boswell, P. G.; Buhlmann, P.; Lodge, T. P. *J. Phys. Chem. B* **2007**, *111*, 4645-4652.

[63] Zhang, S.; Lee, K. H.; Frisbie, C. D.; Lodge, T. P. *Macromolecules* **2011**, *44*, 940-949.

[64] Cho, J. H.; Lee, J.; Xia, Y.; Kim, B.; He, Y.; Renn, M. J.; Lodge, T. P.; Frisbie, C. D. *Nat. Mater.* **2008**, *7*, 900-906.

[65] Moon, H. C.; Lodge, T. P.; Frisbie, C. D. *J. Am. Chem. Soc.* **2014**, *136*, 3705-3712.

[66] He, Y.; Lodge, T. P. *Chem. Commun.* **2007**, 2732-2734.

[67] Kitazawa, Y.; Ueki, T.; Niitsuma, K.; Imaizumi, S.; Lodge, T. P.; Watanabe, M. *Soft Matter* **2012**, *8*, 8067-8074.

[68] Ueki, T.; Watanabe, M. *Langmuir* **2007**, *23*, 988-990.

[69] Ueki, T.; Watanabe, M. *Macromolecules* **2008**, *41*, 3739-3749.

[70] Ishii, S.; Kokubo, H.; Hashimoto, K.; Imaizumi, S.; Watanabe, M. *Macromolecules* **2017**, *50*, 2906-2915.

[71] Kitazawa, Y.; Ueno, K.; Watanabe, M. *Chem. Rec.* **2018**, *18*, 391-409.

[72] Tamate, R.; Hashimoto, K.; Horii, T.; Hirasawa, M.; Li, X.; Shibayama, M.; Watanabe, M. *Adv. Mater.* **2018**, *30*, 1802792.

[73] Kim, Y. M.; Moon, H. C. *Adv. Funct. Mater.* **2019**, *30*.

[74] Li, T.; Wang, Y.; Li, S.; Liu, X.; Sun, J. *Adv. Mater.* **2020**, *32*, e2002706.

[75] Xu, L.; Huang, Z.; Deng, Z.; Du, Z.; Sun, T. L.; Guo, Z.-H.; Yue, K. *Adv. Mater.* **2021**, *33*, 2105306.

[76] Le Bideau, J.; Viau, L.; Vioux, A. *Chem. Soc. Rev.* **2011**, *40*, 907-925.

[77] Shibayama, M.; Norisuye, T. *Bull. Chem. Soc. Jpn.* **2002**, *75*, 641-659.

[78] Shibayama, M. *Soft Matter* **2012**, *8*.

[79] Okumura, Y.; Ito, K. *Adv. Mater.* **2001**, *13*, 485-487.

[80] Haraguchi, K.; Takehisa, T. *Adv. Mater.* **2002**, *14*, 1120-1124.

[81] Gong, J. P.; Katsuyama, Y.; Kurokawa, T.; Osada, Y. *Adv. Mater.* **2003**, *15*, 1155-+.

[82] Sakai, T.; Matsunaga, T.; Yamamoto, Y.; Ito, C.; Yoshida, R.; Suzuki, S.; Sasaki, N.; Shibayama, M.; Chung, U.-i. *Macromolecules* **2008**, *41*, 5379-5384.

[83] Akagi, Y.; Matsunaga, T.; Shibayama, M.; Chung, U.-i.; Sakai, T. *Macromolecules* **2009**, *43*, 488-493.

[84] Akagi, Y.; Katashima, T.; Katsumoto, Y.; Fujii, K.; Matsunaga, T.; Chung, U.; Shibayama, M.; Sakai, T. *Macromolecules* **2011**, *44*, 5817-5821.

[85] Liu, C.; Morimoto, N.; Jiang, L.; Kawahara, S.; Noritomi, T.; Yokoyama, H.; Mayumi, K.; Ito, K. *Science* **2021**, *372*, 1078-1081.

[86] Fujiyabu, T.; Sakumichi, N.; Katashima, T.; Liu, C.; Mayumi, K.; Chung, U.-i.; Sakai, T. *Sci. Adv.* **2022**, *8*, eabk0010.

[87] Hartquist, C. M.; Lin, S.; Zhang, J. H.; Wang, S.; Rubinstein, M.; Zhao, X. *Sci Adv* **2023**, *9*, eadj0411.

[88] Lin, C. B.; Lee, S.; Liu, K. S. *Polym. Eng. Sci.* **2004**, *30*, 1399-1406.

[89] Jud, K.; Kausch, H. H. *Polym. Bull.* **1979**, *1*, 697-707.

[90] Wool, R. P.; O'Connor, K. M. *J. Appl. Phys.* **1981**, *52*, 5953-5963.

[91] White, S. R.; Sottos, N. R.; Geubelle, P. H.; Moore, J. S.; Kessler, M. R.; Sriram, S. R.; Brown, E. N.; Viswanathan, S. *Nature* **2001**, *409*, 794-797.

[92] Chen, X.; Dam, M. A.; Ono, K.; Mal, A.; Shen, H.; Nutt, S. R.; Sheran, K.; Wudl, F. *Science* **2002**, *295*, 1698-1702.

[93] Cordier, P.; Tournilhac, F.; Soulié-Ziakovic, C.; Leibler, L. *Nature* **2008**, *451*, 977-980.

[94] Yanagisawa, Y.; Nan, Y.; Okuro, K.; Aida, T. *Science* **2018**, *359*, 72-76.

[95] Harada, A.; Takashima, Y.; Nakahata, M. *Acc. Chem. Res.* **2014**, *47*, 2128-2140.

[96] Burnworth, M.; Tang, L.; Kumpfer, J. R.; Duncan, A. J.; Beyer, F. L.; Fiore, G. L.; Rowan, S. J.; Weder, C. *Nature* **2011**, *472*, 334-337.

[97] Sun, T. L.; Kurokawa, T.; Kuroda, S.; Ihsan, A. B.; Akasaki, T.; Sato, K.; Haque, M. A.; Nakajima, T.; Gong, J. P. *Nat. Mater.* **2013**, *12*, 932-937.

[98] Amamoto, Y.; Otsuka, H.; Takahara, A.; Matyjaszewski, K. *Adv. Mater.* **2012**, *24*, 3975-3980.

[99] Self, J. L.; Sample, C. S.; Levi, A. E.; Li, K.; Xie, R.; de Alaniz, J. R.; Bates, C. M. *J. Am. Chem. Soc.* **2020**, *142*, 7567-7573.

[100] Zhao, X.; Guo, S.; Li, H.; Liu, J.; Su, C.; Song, H. *RSC Adv.* **2017**, *7*, 38765-38772.

[101] Shi, Y.; Wu, B.; Sun, S.; Wu, P. *Nat. Commun.* **2023**, *14*, 1370.

[102] Cao, Y.; Morrissey, T. G.; Acome, E.; Allec, S. I.; Wong, B. M.; Keplinger, C.; Wang, C. *Adv. Mater.* **2017**, *29*, 1605099.

[103] Shi, P.; Wang, Y.; Tjiu, W. W.; Zhang, C.; Liu, T. *ACS Appl. Mater. Interfaces* **2021**, *13*, 49358-49368.

[104] Yu, Z.; Wu, P. *Adv. Mater.* **2021**, *33*, e2008479.

[105] Kelly, J. C.; Degrood, N. L.; Roberts, M. E. *Chem. Commun. (Camb.)* **2015**, *51*, 5448-5451.

[106] Xue, Z. G.; He, D.; Xie, X. L. *J. Mater. Chem. A* **2015**, *3*, 19218-19253.

[107] Liu, W.; Song, M.-S.; Kong, B.; Cui, Y. *Adv. Mater.* **2017**, *29*, 1603436.

[108] Lu, C.; Chen, X. *Chem. Commun.* **2019**, *55*, 8470-8473.

[109] Zhang, S. H.; Wang, F. X.; Li, J. J.; Peng, H. D.; Yan, J. H.; Pan, G. B. *Sensors (Basel)* **2017**, *17*.

[110] Xiang, S.; Zheng, F.; Chen, S.; Lu, Q. *ACS Appl. Mater. Interfaces* **2021**, *13*, 20653-20661.

[111] Wang, H.; Xu, J.; Li, K.; Dong, Y.; Du, Z.; Wang, S. *J. Mater. Chem. B* **2022**, *10*, 1301-1307.

[112] Wang, M.; Hu, J.; Dickey, M. D. *JACS Au* **2022**, *2*, 2645-2657.

[113] Xia, Y.; Zhu, Y.; Zhi, X.; Guo, W.; Yang, B.; Zhang, S.; Li, M.; Wang, X.; Pan, C. *Adv. Mater.* **2023**, e2308424.

[114] Jin, M. L.; Park, S.; Lee, Y.; Lee, J. H.; Chung, J.; Kim, J. S.; Kim, J. S.; Kim, S. Y.; Jee, E.; Kim, D. W.; et al. *Adv. Mater.* **2017**, *29*.

[115] Lodge, T. P.; Ueki, T. *Acc. Chem. Res.* **2016**, *49*, 2107-2114.

[116] Li, H.; Lv, T.; Sun, H.; Qian, G.; Li, N.; Yao, Y.; Chen, T. *Nat. Commun.* **2019**, *10*, 536.

[117] Lu, C.; Chen, X. *Acc. Chem. Res.* **2020**, *53*, 1468-1477.

[118] Imaizumi, S.; Kokubo, H.; Watanabe, M. *Macromolecules* **2011**, *45*, 401-409.

[119] Lu, W.; Fadeev, A. G.; Qi, B.; Smela, E.; Mattes, B. R.; Ding, J.; Spinks, G. M.; Mazurkiewicz, J.; Zhou, D.; Wallace, G. G.; et al. *Science* **2002**, *297*, 983-987.

[120] Jo, C.; Pugal, D.; Oh, I.-K.; Kim, K. J.; Asaka, K. *Prog. Polym. Sci.* **2013**, *38*, 1037-1066.

[121] Christianson, C.; Goldberg, N. N.; Deheyn, D. D.; Cai, S.; Tolley, M. T. *Sci Robot* **2018**, *3*.

[122] Kim, S. H.; Hong, K.; Xie, W.; Lee, K. H.; Zhang, S.; Lodge, T. P.; Frisbie, C. D. *Adv. Mater.* **2013**, *25*, 1822-1846.

[123] Wang, Z.; Zhang, J.; Liu, J.; Hao, S.; Song, H.; Zhang, J. *ACS Appl. Mater. Interfaces* **2021**, *13*, 5614-5624.

[124] Li, W.; Wang, X.; Liu, Z.; Zou, X.; Shen, Z.; Liu, D.; Li, L.; Guo, Y.; Yan, F. *Nat. Mater.* **2023**.

[125] Tamate, R.; Watanabe, M. *Sci Technol Adv Mater* **2020**, *21*, 388-401.

[126] Wang, M.; Zhang, P.; Shamsi, M.; Thelen, J. L.; Qian, W.; Truong, V. K.; Ma, J.; Hu, J.; Dickey, M. D. *Nat. Mater.* **2022**, *21*, 359-365.

[127] Li, T.; Liu, F.; Yang, X.; Hao, S.; Cheng, Y.; Li, S.; Zhu, H.; Song, H. *ACS Appl. Mater. Interfaces* **2022**, *14*, 29261-29272.

[128] Ye, Y.; Zhang, Y.; Chen, Y.; Han, X.; Jiang, F. *Adv. Funct. Mater.* **2020**, *30*.

[129] Yao, X.; Zhang, S.; Qian, L.; Wei, N.; Nica, V.; Coseri, S.; Han, F. *Adv. Funct. Mater.* **2022**, *32*.

Chapter 2

In Situ Polymerization of Vinyl Monomers in Ionic Liquids and Characterization of UHMW Ion Gels

2-1 Introduction

As mentioned in Chapter 1, numerous robust and self-healing polymer gels have been reported. As in the sliding ring gels[1-3], the topological effect is promising approach for the molecular design of polymer networks to yield mechanically tough polymer gels. Under deformation, the cross-linking points can slide along the axis of polymer main chain, thereby suppressing the stress localization. More recently, the seminal work by Miyata *et al.* demonstrated that tough hydrogels formed by abundant physical entanglement could be prepared by optimizing the monomer concentration and the chemical cross-linker concentration.[4] Suo *et al.* also reported tough hydrogels in which polymer entanglement outnumbered the chemical cross-linking points.[5]

In this chapter, I developed a novel class of stretchable and self-healing polymer gels that are formed solely by the physical entanglement of Ultra-High Molecular Weight (UHMW) polymers, that is, UHMW ion gels. Radical polymerization of vinyl monomers in ILs produces polymers with extremely high molecular weight compared to conventional polymerization in neutral solvents, and the molecular weight exceeds 10^6 g/mol as the initiator concentration decreases. As the polymerization proceeded, transparent polymer gels were formed *in situ* solely by the physical entanglements of the UHMW polymers; this has been already proposed as a class of gel polymerization **(Figure 2-1)**.[6, 7] Details of the formation process of UHMW polymers in ILs and the fundamental physicochemical properties of the resulting ion gels associated with increased molecular weight are discussed.

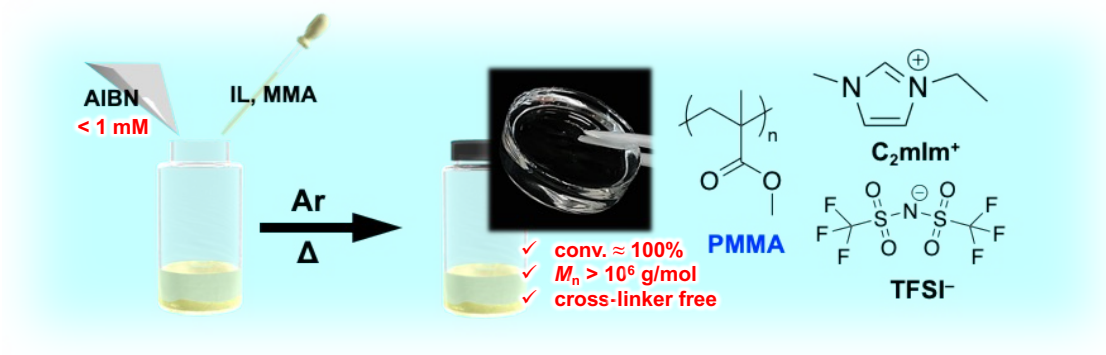

Figure 2-1. Schematic procedure for the synthesis of the UHMW ion gel.

2.2 Experimental

2.2.1 Materials

[C_2mIm][TFSI] was purchased from Kanto Chemical (Japan), and were vacuum dried at 120 °C for 24 h before use. MMA were purchased from Kanto Chemical (Japan) and purified by passing them through basic alumina. 2,2'-Azobis(isobutyronitrile) (AIBN) and toluene were purchased from Wako Pure Chemical Industries (Japan) and used without further purification.

2.2.2 Polymerization and Characterization of Methacrylate Polymers in Ionic Liquids

Herein, a representative synthesis of the UHMW PMMA/[C_2mIm][TFSI] gel is described. MMA (0.300 g, 3.00 mmol), [C_2mIm][TFSI] (0.700 g, 1.79 mmol), and AIBN (0.1 mg, 0.61×10^{-3} mmol) were charged in a glass vial and sealed with a rubber septum, through which argon was bubbled for 15 min at room temperature. Polymerization was conducted at 80 °C for 24 h. Monomer conversion was determined by proton nuclear magnetic resonance (^{1}H-NMR). The molecular weight and polydispersity index (PDI) of the polymer were determined by gel permeation chromatography (GPC) using a 10 mM LiBr/DMF solution as the eluent. The GPC columns (Showa Denko, Japan) were calibrated using PMMA standards. For the characterization by ^{1}H-NMR and GPC, the as prepared UHMW ion gel pieces were dissolved in $CDCl_3$ (ca. 1 wt%) and 10 mL LiBr/DMF (0.1 wt%) under stirring at room temperature overnight.

2.2.3 Transparency Tests

The transparency tests were performed on an UV-Vis spectrophotometer UV-2600 (SHIMADZU, Japan). The sample was prepared in a septum sealed quartz cell of 10 mm thickness. The transmittance spectrum of the ion gel was obtained by subtracting the spectrum of the empty cell. The wavelength for testing were set from 800 to 400 nm.

2.2.4 Rheological Measurements

Rheological measurements were performed using an Anton Paar MCR 102 rheometer (Anton Paar, Austria). A parallel plate geometry with a Ø12-mm plate and a gap spacing of 0.5 mm were used for all the measurements. Temperature sweep measurements were conducted from 10 to 120 °C (heating rate: 1 °C min^{-1}) at a frequency of 1 rad s^{-1} and a strain amplitude of 1%. The time–temperature superposition (tTS) master curves were constructed from the results of the frequency sweep measurements over a frequency range of 0.1–100 rad s^{-1} with a strain amplitude of 1% at different temperatures.

2.2.5 DLS Measurements

A schematic of the developed software-based DLS apparatus is presented in **Figure 2-2**. The output of a single frequency continuous-wave diode-pumped laser (Cobolt Samba, 0532-04-01-0100-700, 100 mW, Sweden) at a wavelength of 532.1 ± 0.3 nm was focused on a quartz cell filled with the sample. The temperature of the sample was maintained at 23 °C during the measurements using a temperature-controlled cuvette holder (qX3, Quantum Northwest, USA). Scattered light was collected at a scattering angle of 90° and guided onto a photon-counting module (C13001-01, Hamamatsu Photonics, Japan) through an optical fiber. The aperture size just before the collection lens was set at 0.8 mm. The electronic signal pulses from the photon-counting module were transferred to a time-to-digital converter (TimeHarp 260 NANO Single, PicoQuant, Germany), which recorded the arrival time of each detected photon. The temporal resolution of the module is 250 ps. All arrival time information was stored in a text file and analyzed after the measurement. The details of the calculation of the time correlation function are described elsewhere.[8]

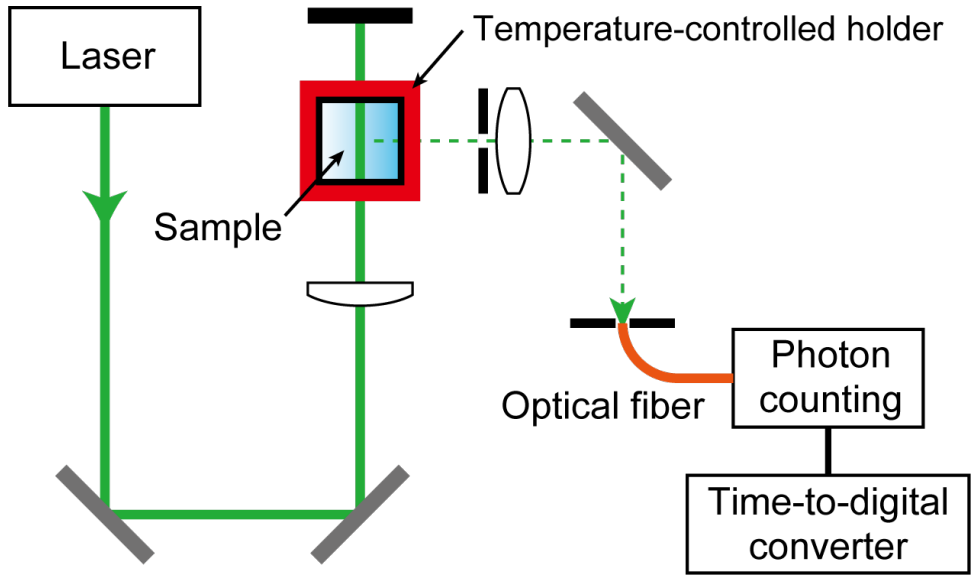

Figure 2-2. Schematic of the software-based dynamic light scattering measurement apparatus.

2.3 Synthesis of UHMW Ion Gels by *In Situ* Radical Polymerization

ILs have been extensively studied as media for various chemical reactions. It is known that free-radical polymerization in ILs leads to a higher molecular weight compared to that in common organic solvents.[9-18] In a report investigating the effect of ILs on the kinetics of polymerization by pulsed laser polymerization[10, 13], the propagation rate coefficient for the polymerization of MMA in 1-butyl-3-methylimidazolium hexafluorophosphate ([C_4mIm][PF_6]) increased approximately twofold. A slight decrease in activation energy was also observed. The termination reaction rate constant was also found to decrease by one order of magnitude, rationalizing the experimental results of accelerated

polymerization in ILs. Although the kinetics of polymerization reactions with various combinations of ILs and monomers have also been discussed, research focus has been limited to living radical polymerization.[19] Herein, I demonstrate that by reducing the amount of the radical initiator in feed extremely, UHMW polymers can be obtained via *in situ* free-radical polymerization of vinyl monomers in ILs without compromising monomer conversion. Although the definition of "UHMW" varies in the literature, in this study, polymers with number-average molecular weights (M_n) exceeding 10^6 g/mol are defined as UHMW polymers according to much of the literature.[7, 20, 21] **Figure 2-3** shows the relationship between the initiator AIBN amount (c_{AIBN}) and M_n for the free-radical polymerization of MMA in a conventional IL [C_2mIm][TFSI] and an organic solvent, toluene. GPC curves, ^{1}H-NMR spectra, and a summary of the polymerization are described in **Figure 2-4, 2-5, and Table 2-1**.

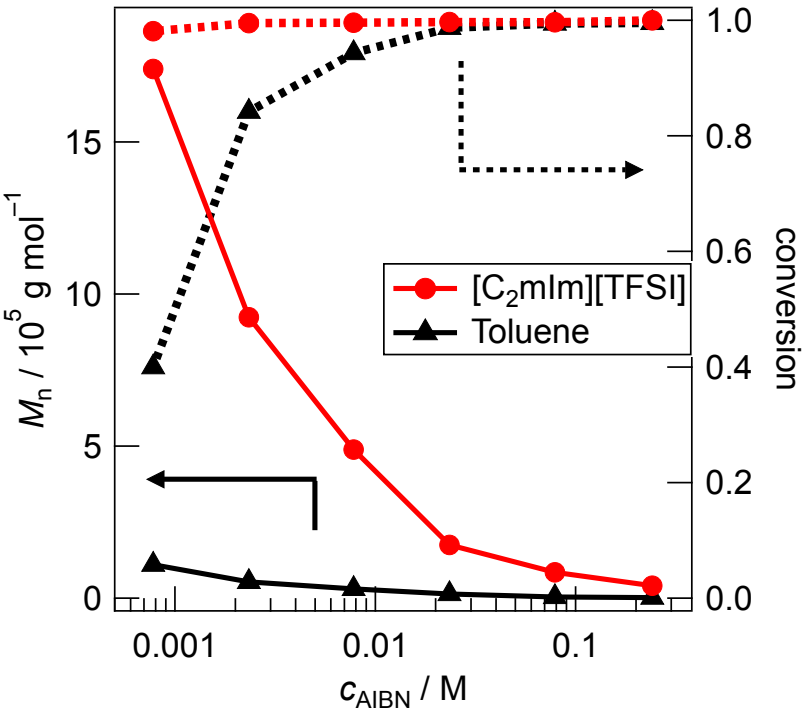

Figure 2-3. Dependence of M_n and monomer conversions on c_{AIBN} for the PMMA/[C_2mIm][TFSI] and PMMA/toluene systems. Polymerization temperature is 80 °C.

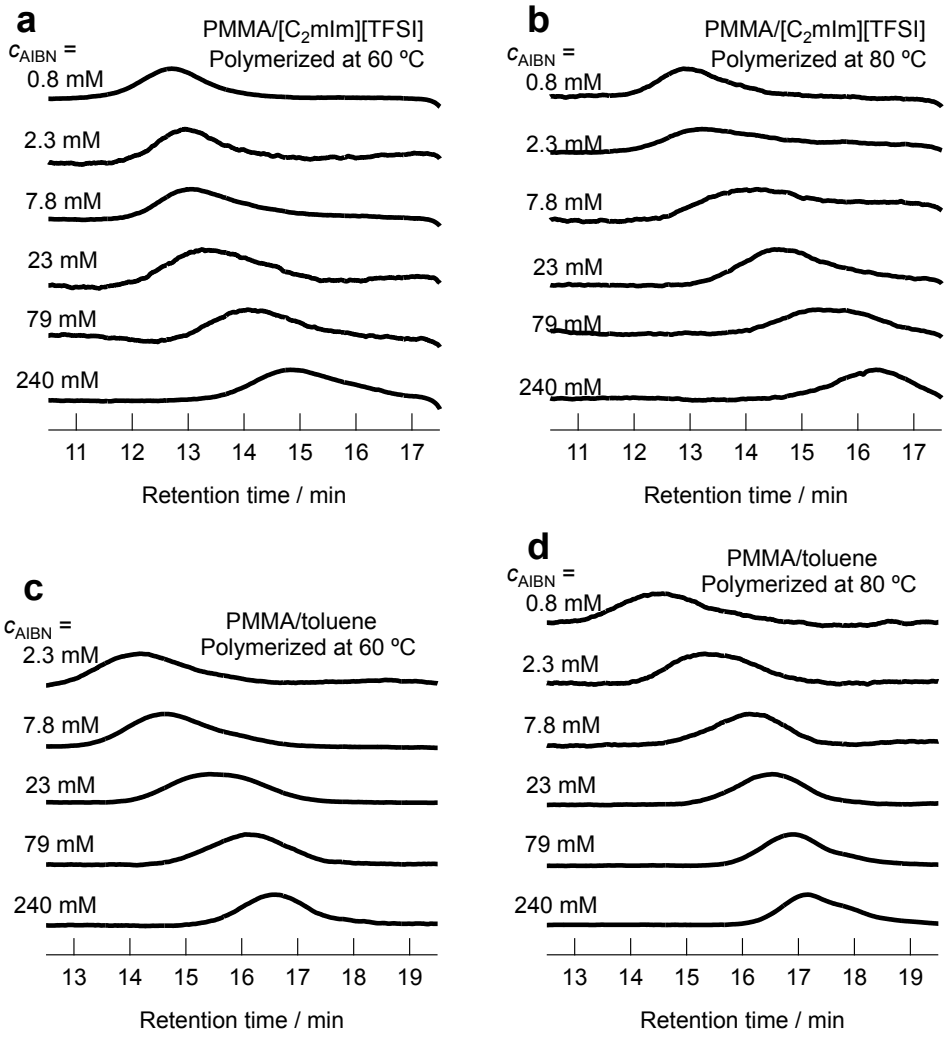

Figure 2-4. GPC curves of PMMA polymerized in [C_2mIm][TFSI] at (a) 60 °C and (b) 80 °C, and in toluene at (c) 60 °C and (d) 80 °C with different initiator concentrations.

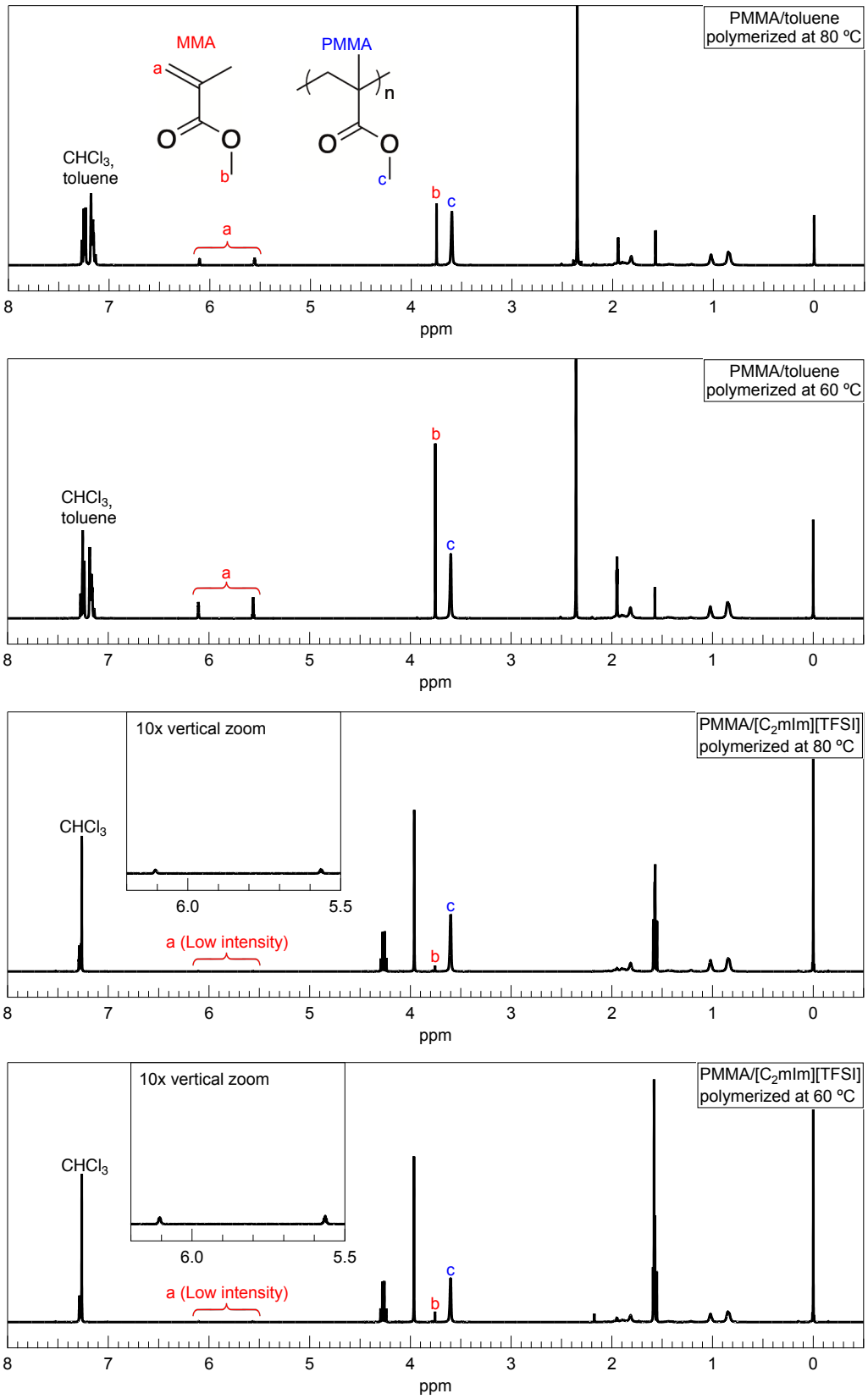

Figure 2-5. ^{1}H-NMR spectra of the polymerization solutions after 24 h at c_{AIBN} = 2.3 mM in $CDCl_3$.

Table 2-1. Polymerization conditions and characterization parameters of the synthesized PMMA in [C_2mIm][TFSI] and toluene.

c_{AIBN} [mM]	solvent	T [°C]	M_n [Da]	M_w [Da]	PDI	conversion
240	[C_2mIm][TFSI]	60	149 000	313 000	2.10	> 0.99
79			271 000	650 000	2.40	> 0.99
23			747 000	1 850 000	2.48	> 0.99
7.8			1 050 000	2 142 000	2.04	0.99
2.3			1 380 000	2 640 000	1.91	0.99
0.78			2 160 000	4 600 000	2.13	0.83
c_{AIBN} [mM]	solvent	T [°C]	M_n [Da]	M_w [Da]	PDI	conversion
240	[C_2mIm][TFSI]	80	41 000	67 000	1.64	> 0.99
79			86 000	137 000	1.60	> 0.99
23			175 000	374 000	2.13	> 0.99
7.8			489 000	816 000	1.67	> 0.99
2.3			924 000	1 820 000	1.97	> 0.99
0.78			1 740 000	2 660 000	1.53	0.99
c_{AIBN} [mM]	solvent	T [°C]	M_n [Da]	M_w [Da]	PDI	conversion
240	Toluene	60	16 000	40 000	2.48	> 0.99
79			38 000	79 000	2.08	> 0.99
23			69 000	154 000	2.22	0.98
7.8			158 000	367 000	2.27	0.93
2.3			291 000	631 000	2.17	0.72
0.78			-	-	-	-
c_{AIBN} [mM]	solvent	T [°C]	M_n [Da]	M_w [Da]	PDI	conversion
240	Toluene	80	2 000	9 000	4.50	> 0.99
79			4 000	17 000	4.11	> 0.99
23			14 000	34 000	2.38	0.99
7.8			31 000	64 000	2.05	0.94
2.3			54 000	123 000	2.30	0.84
0.78			110 000	351 000	3.20	0.40

For the MMA-toluene (representative molecular solvent) system, the monomer conversion significantly decreased with decreasing c_{AIBN}, and M_n did not reach the UHMW range (>10^6 g/mol). On the other hand, in the case of the MMA-[C_2mIm][TFSI] system, a high monomer conversion (>99%) was maintained even at a very low c_{AIBN} (<1 mM), and UHMW PMMA (>10^6 g/mol) was obtained. The polymerization products with the low c_{AIBN} formed transparent gels because of the physical entanglement of the UHMW PMMA chains **(Figure 2-6)**. Generally, high molecular weight

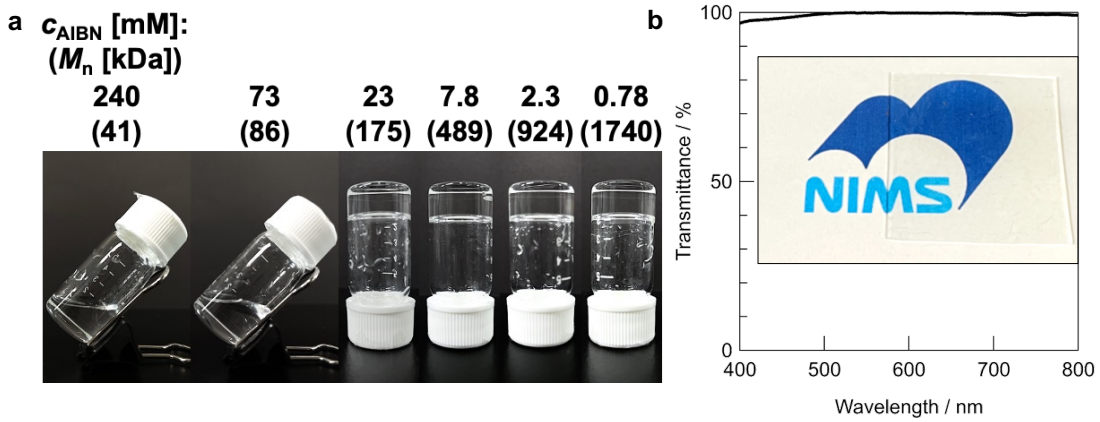

Figure 2-6. (a) Photographs of the PMMA/[C_2mIm][TFSI] solutions polymerized at 80 ºC with various c_{AIBN}, showing the corresponding M_n of PMMA. (b) Transmittance spectrum of the 10-mm-thick UHMW ion gel.

polymers in radical polymerization can be ascribed to the [1] stabilization of the propagation radicals to lower activation energy and [2] slow termination rate derived from high viscosity of the reaction system, so-called the Trommsdorff effect.[22, 23] To validate these assumptions, free-radical polymerization of MMA was carried out in a series of ILs with different viscosities and corresponding toluene systems with controlled viscosities as the reaction media. The viscosities of toluene were controlled by dissolving different concentrations of commercially available PMMA (M_w = 1.5 × 10^4 g/mol). As shown in **Figure 2-7(a)**, the M_n for the IL system slightly increased with an increase in the viscosity of the ILs (i.e., [C_2mIm][NFSI] > [C_2mIm][BETI] > [C_2mIm][TFSI]) (NFSI: nonafluorobutylsulfonylimide, BETI: pentafluoroethylsulfonylimide), however, the difference in molecular weight of resultant polymer is not significant. In addition, there is almost no correlation between the viscosity and M_n for the viscosity-controlled toluene systems. Further, their M_n values are much lower than those of the MMA-IL systems. These results indicate that the high M_n and high monomer conversion for the IL systems are derived not from the high viscosity of the ILs. Consequently, I concluded that the high molecular weight in ILs came from the stabilization of the propagation radicals in the IL systems. The relationship between the monomer concentration and the

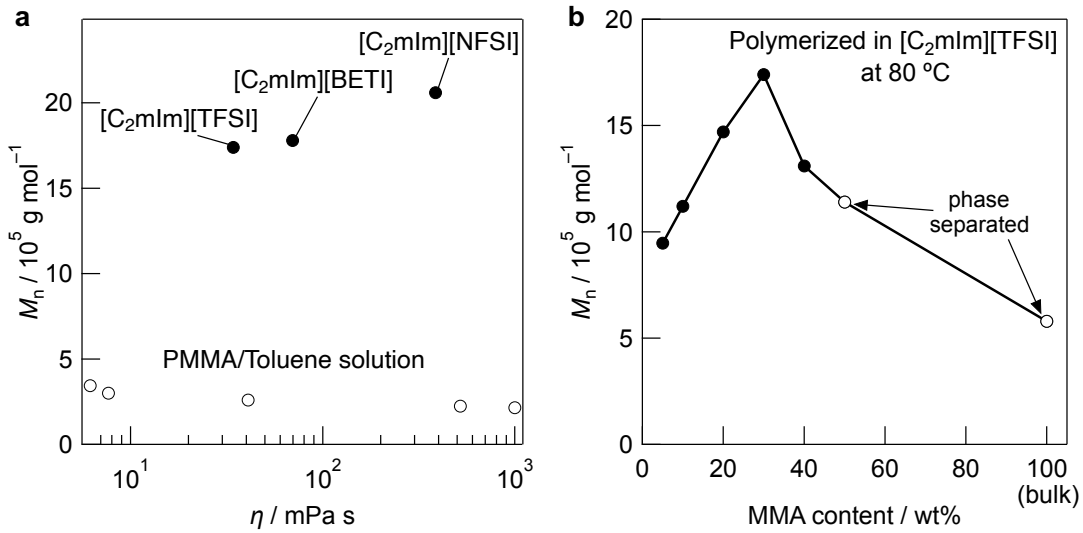

Figure 2-7. (a) The relationship between solvent viscosity and M_n for the PMMA/IL and PMMA/toluene systems. The viscosity of toluene is adjusted by dissolving commercial PMMA (M_w = 1.5 × 10^4 g/mol) at different concentrations. (b) Monomer content versus M_n for the PMMA/[C2mIm][TFSI] system. At a high MMA content, phase separation (denoted by the white circles) into a monomer-rich region and a polymer-rich region was observed.

resultant M_n in [C2mIm][TFSI] is shown in **Figure 2-7(b)**. The maximum M_n value was obtained at a concentration of approximately 30 wt% of monomer content, which exceeded the value obtained by bulk polymerization; this is indicative of the acceleration effect of the ILs that generates the higher-molecular-weight polymers. As another fabrication strategy, by taking advantage of the non-volatility of ILs, it was investigated to prepare the PMMA/[C2mIm][TFSI] UHMW ion gel by using a commercially available UHMW PMMA through the cosolvent evaporation method.[24] However, in the case of UHMW PMMA, it can be dissolved in the cosolvent only at a very low concentration due to its low mutual solubility. In addition, it is difficult to prepare homogeneous UHMW PMMA/[C2mIm][TFSI] ion gels by cosolvent evaporation method because inhomogeneous precipitation of the polymer in ILs occurs during the evaporation of the cosolvent. This is due to the extreme slow down of mass transport because of the high viscosity of the system as the cosolvent evaporates, making a concentration gradient between the interface where the solvent volatiles and the bulk becomes large. Therefore, the one-pot fabrication strategy by mixing low viscous prepolymer (monomer) with IL solvent presented here is the superior way to prepare the homogeneous UHMW ion gels without using volatile organic solvents.

2.4 Physical Properties of UHMW Ion Gels

Notably, owing to the significantly high monomer conversion, the UHMW ion gel formed by the *in situ* polymerization can be used for desired applications without further purification. Temperature sweep measurements of the storage (G') and loss moduli (G'') for the PMMA/[C_2mIm][TFSI] systems with various molecular weights of PMMA at a polymer concentration of 30 wt% are shown in **Figure 2-8(a)**. The UHMW ion gel based on UHMW PMMA (1740 kDa) maintained a gel state (i.e., $G' > G''$) over a wide temperature range despite the absence of a chemical cross-linker. **Figure 2-8(b)** shows temperature dependence of tanδ. Compared to the 41 kDa and 175 kDa PMMA/[C_2mIm][TFSI] systems, the 1740 kDa UHMW PMMA/[C_2mIm][TFSI] ion gel showed tanδ much lower than 1. **Figure 2-8(c)** shows the stress relaxation behavior. The decrease in the relaxation modulus is suppressed by increasing molecular weight, and the UHMW ion gel did not show significant relaxation within the measurement time. Thus, for the 1740 kDa UHMW PMMA/[C_2mIm][TFSI] ion gel, the solid-like integrity is maintained for all temperature range, and energy dissipation is significantly lower than the 41 kDa and 175 kDa PMMA/[C_2mIm][TFSI] systems. The frequency sweep data also shows that the crossover was not observed over the frequency range of 0.1–100 rad s^{-1} at high temperature of 120 °C (**Figure 2-9**). This could be attributed to the large number of transient physical cross-links due to the high entanglement density of the UHMW polymer chains. On the other hand, the crossover of G' and G'' was observed for 175 kDa PMMA/[C_2mIm][TFSI] at approximately 70 °C, indicating the existence of a gel-to-sol transition at high temperatures. The 41 kDa PMMA/[C_2mIm][TFSA] system exhibited liquid-like behavior ($G' < G''$) for all temperature ranges.

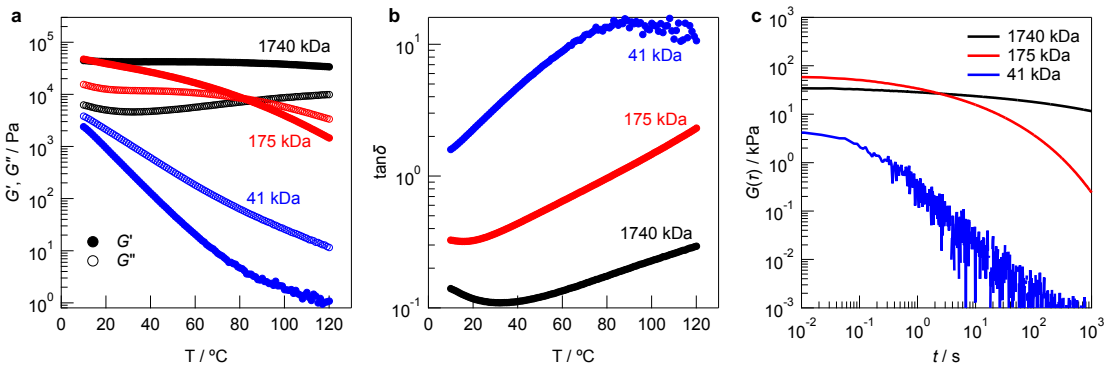

Figure 2-8. Temperature dependence of the (a) storage (G', closed symbols), loss (G'', open symbols) moduli and (b) tanδ, and (c) stress relaxation behavior for 41, 175, and 1740 kDa PMMA/[C_2mIm][TFSI].

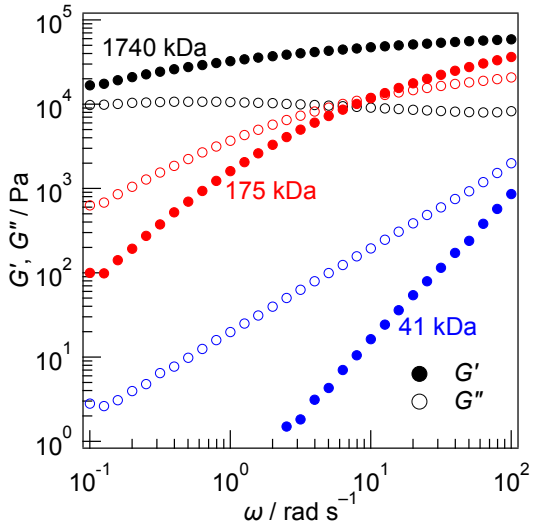

Figure 2-9. Frequency dependence of storage (G', closed) and loss (G'', open) moduli for the 41 kDa, 175 kDa, and 1740 kDa PMMA/[C_2mIm][TFSI] systems at 120 ºC.

Time–temperature superposition (tTS) master curves of G', G'' and tanδ were constructed at a reference temperature of 10 °C (**Figure 2-10**). Consistent with the temperature sweep measurements, the UHMW ion gel showed a significantly wider rubbery plateau compared to the PMMA/[C_2mIm][TFSI] systems with moderate molecular weights[25], while the crossover of G' and G'' was not observed over the entire frequency range. The 175 kDa PMMA/[C_2mIm][TFSI] system exhibits a narrower rubbery plateau and terminal flow behavior ($G' \propto \omega^2$ and G" $\propto \omega$) in the low-frequency region, indicating that it behaves as a liquid over a long time scale. The 41 kDa

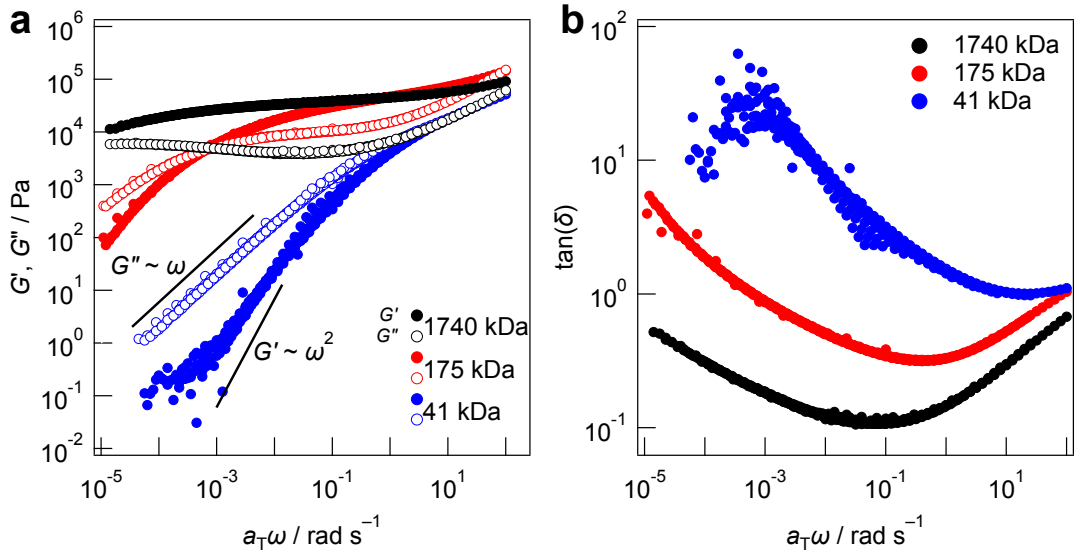

Figure 2-10. Time–temperature superposition (tTS) master curves for 30 wt% PMMA in [C_2mIm][TFSI] with different molecular weights of PMMA. (a) G' (closed symbols) and G'' (open symbols), and (b) tanδ. The reference temperature is 10 ºC.

PMMA/[C_2mIm][TFSI] system shows $G' < G''$; thus, tan$\delta > 1$ over the entire frequency range. Consistent with the rheological properties, the UHMW PMMA/[C_2mIm][TFSI] ion gel exhibited superior long-term shape stability (**Figure 2-11**), the integrity of its shape was maintained even after one week; in contrast, the 175 kDa PMMA/[C_2mIm][TFSI] systems showed significant flow deformation. The UHMW ion gel also exhibited good shape stability at a high temperature of 120 °C.

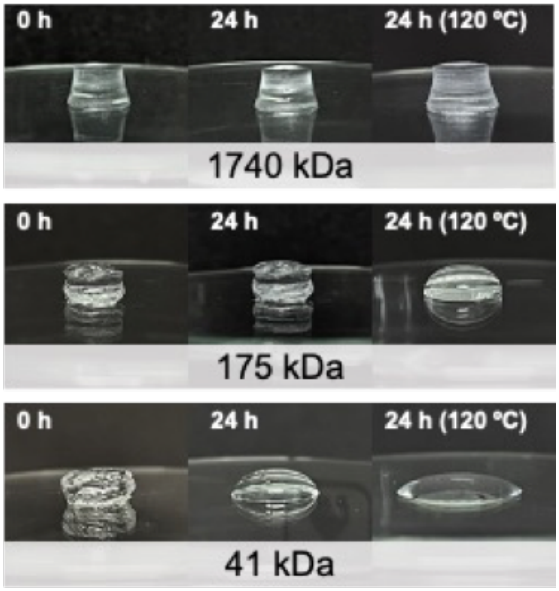

Figure 2-11. Shape stability for the 30 wt% PMMA/[C_2mIm][TFSI] systems with various molecular weights.

The microscopic polymer dynamics in the ion gel were evaluated using software-based dynamic light scattering (DLS) measurements that record both the temporal variation of the scattered light intensity and its time correlation function.[8] **Figure 2-12(a)** shows the temporal variation of the scattered light intensity for the 41 kDa PMMA/[C_2mIm][TFSI] solution and the UHMW PMMA/[C_2mIm][TFSI] ion gel (1740 kDa). It was observed that the absolute scattered light intensity from the UHMW ion gel was approximately one order of magnitude smaller than that of the 41 kDa PMMA/[C_2mIm][TFSI] solution. This suggests the formation of a homogeneous network in the UHMW ion gel by dynamic optimization of the network structure through transient physical cross-links. In addition, a fluctuation of the scattered light intensity over a long time scale was observed for the 41 kDa PMMA/[C_2mIm][TFSI] solution, whereas the UHMW ion gel showed minimal scattering fluctuations. This indicates that the diffusion of the polymer aggregates was restricted by the high entanglement density of the UHMW polymers. The time correlation functions of the scattered light intensity also suggest that there is no long time scale (~1 s) relaxation for the UHMW

PMMA/[C2mIm][TFSI] ion gel, whereas the 41 kDa PMMA/[C2mIm][TFSI] solution showed a long time scale relaxation mode (**Figure 2-12(b)**). In the case of the 41 kDa PMMA/[C2mIm][TFSI] solution, the number of crosslinks made from entanglements is not enough to construct a robust 3D polymer network. As a result, a part of PMMA aggregates can move freely in the network, which is detected as long time scale relaxation in the time correlation function of the scattered light intensity. In contrast, the UHMW PMMA/[C2mIm][TFSI] ion gel is robust enough to trap all of the PMMA polymer chains in the network. In this situation, the detected fluctuation of the scattered light intensity originates from only the restricted fluctuations of polymers between crosslinking points, which is detected as short time scale relaxation similar to the conventional polymer gels.[23] Therefore, the lack of long time scale relaxation for the DLS result implies the formation of a robust 3D network that is consistent with the temporal variation of the scattered light intensity.

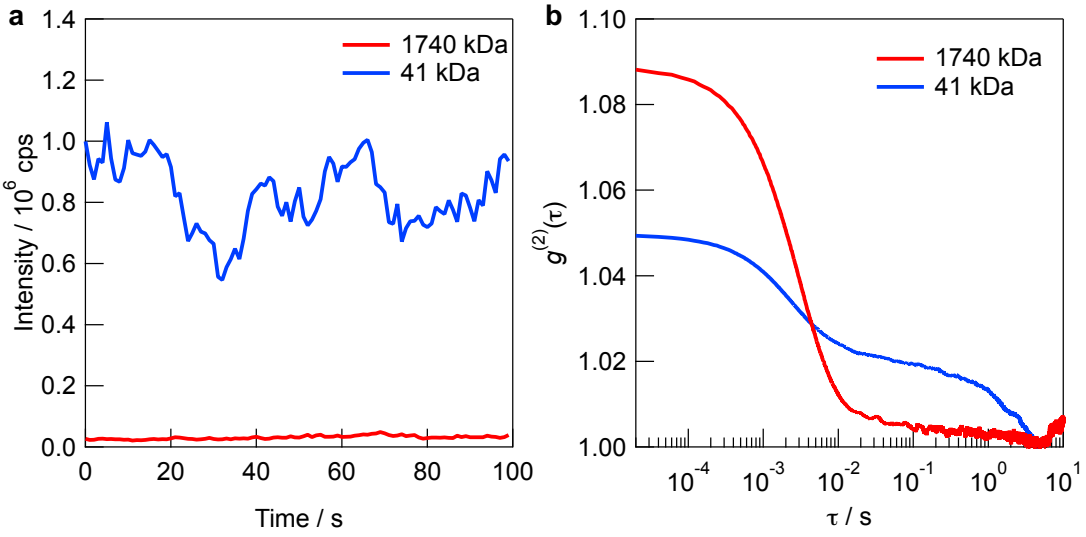

Figure 2-12. Temporal variation of the scattered light intensity for the 41 kDa PMMA/[C2mIm][TFSI] and 1740 kDa PMMA/[C2mIm][TFSI] systems. cps, count per second. The 1740 kDa PMMA/[C2mIm][TFSI] system is referred to as the UHMW ion gel in this study. (b) Time correlation functions of the scattered light intensity, $g^{(2)}(\tau)$, for the 30 wt% PMMA/[C2mIm][TFSI] systems with different molecular weights (1740 kDa and 41 kDa).

2.5 Conclusions

In situ radical polymerization of MMA in an IL [C_2mIm][TFSI] resulted in a significant increase in molecular weight compared to that in toluene, a common organic solvent. Even at very low initiator concentrations, UHMW PMMA was formed while maintaining almost 100% conversion, and a transparent freestanding gel was formed solely by physical entanglement of polymer chains. The relationship between the viscosity of the polymerization system and the molecular weight of resultant polymers was investigated by comparing the viscosity different ILs system with a viscosity-tuned molecular liquid (PMMA dissolved toluene) system. The viscosity of the polymerization solvent had little effect on the increment of the molecular weight of polymer, suggesting a decrease in the activation energy due to the interaction between the IL and the propagation radicals. In addition, the molecular weight of PMMA obtained by polymerization in IL was larger than that obtained by bulk polymerization. This also means that the propagation rate increases in the presence of ILs, which strongly suggests that ILs possess a specific ability to accelerate polymerization. Rheological measurements revealed that the terminal relaxation behavior at high temperatures and low frequencies is suppressed with increasing molecular weight, resulting in excellent shape stability of UHMW ion gels. Dynamic light scattering measurements also confirmed the disappearance of the flow-diffusion mode of the polymer with increasing molecular weight, suggesting the formation of a robust 3D network with entangled cross-linking points.

Reference

[1] Okumura, Y.; Ito, K. *Adv. Mater.* **2001**, *13*, 485-487.

[2] Ito, K. *Polym. J.* **2012**, *44*, 38-41.

[3] Liu, C.; Morimoto, N.; Jiang, L.; Kawahara, S.; Noritomi, T.; Yokoyama, H.; Mayumi, K.; Ito, K. *Science* **2021**, *372*, 1078-1081.

[4] Norioka, C.; Inamoto, Y.; Hajime, C.; Kawamura, A.; Miyata, T. *NPG Asia Mater.* **2021**, *13*, 34.

[5] Kim, J.; Zhang, G.; Shi, M.; Suo, Z. *Science* **2021**, *374*, 212-216.

[6] Read, E.; Guinaudeau, A.; James Wilson, D.; Cadix, A.; Violleau, F.; Destarac, M. *Polym. Chem.* **2014**, *5*, 2202-2207.

[7] An, Z. *ACS Macro Lett.* **2020**, *9*, 350-357.

[8] Hiroi, T.; Samitsu, S.; Ishioka, K. *Sci. Technol. Adv. Mater. Methods* **2021**, *1*, 134-142.

[9] Hong, K.; Zhang, H.; Mays, J. W.; Visser, A. E.; Brazel, C. S.; Holbrey, J. D.; Reichert, W. M.; Rogers, R. D. *Chem. Commun.* **2002**, 1368-1369.

[10] Harrisson, S.; Mackenzie, S. R.; Haddleton, D. M. *Chem. Commun.* **2002**, 2850-2851.

[11] Strehmel, V.; Laschewsky, A.; Wetzel, H.; Görnitz, E. *Macromolecules* **2006**, *39*, 923-930.

[12] Kubisa, P. *Prog. Polym. Sci.* **2004**, *29*, 3-12.

[13] Harrisson, S.; Mackenzie, S. R.; Haddleton, D. M. *Macromolecules* **2003**, *36*, 5072-5075.

[14] Vygodskii, Y. S.; Mel'nik, O. A.; Lozinskaya, E. I.; Shaplov, A. S.; Malyshkina, I. A.; Gavrilova, N. D.; Lyssenko, K. A.; Antipin, M. Y.; Golovanov, D. G.; Korlyukov, A. A.; et al. *Polym. Adv. Technol.* **2007**, *18*, 50-63.

[15] Schmidt-Naake, G.; Schmalfuss, A.; Woecht, I. *Chem. Eng. Res. Des.* **2008**, *86*, 765-774.

[16] Thurecht, K. J.; Gooden, P. N.; Goel, S.; Tuck, C.; Licence, P.; Irvine, D. J. *Macromolecules* **2008**, *41*, 2814-2820.

[17] Woecht, I.; Schmidt‐Naake, G.; Beuermann, S.; Buback, M.; García, N. *J. Polym. Sci., Part A: Polym. Chem.* **2008**, *46*, 1460-1469.

[18] Jeličić, A.; García, N.; Löhmannsröben, H.-G.; Beuermann, S. *Macromolecules* **2009**, *42*, 8801-8808.

[19] Kubisa, P. *Eur. Polym. J.* **2020**, *133*, 109778.

[20] Carmean, R. N.; Becker, T. E.; Sims, M. B.; Sumerlin, B. S. *Chem* **2017**, *2*, 93-101.

[21] Liu, Z.; Lv, Y.; An, Z. *Angew. Chem. Int. Ed.* **2017**, *56*, 13852-13856.

[22] Tulig, T. J.; Tirrell, M. *Macromolecules* **1982**, *15*, 459-463.

[23] Shibayama, M. *Macromol. Chem. Phys.* **1998**, *199*, 1-30.

[24] Tamate, R.; Hashimoto, K.; Horii, T.; Hirasawa, M.; Li, X.; Shibayama, M.; Watanabe, M. *Adv. Mater.* **2018**, *30*, 1802792.

[25] Mok, M. M.; Liu, X.; Bai, Z.; Lei, Y.; Lodge, T. P. *Macromolecules* **2011**, *44*, 1016-1025.

Chapter 3

Mechanical and Self-Healing Properties of UHMW Ion Gels

3.1 Introduction

In Chapter 2, I focused on the formation process of UHMW polymers by *in situ* radical polymerization in ILs. From fundamental rheological measurements and DLS, I also demonstrated that the entanglement of polymer become less likely to pull-out and become stronger as the molecular weight of polymer increases, which is the driving force behind the excellent shape stability of the UHMW ion gels despite the absence of chemically constrained cross-linking points. On the other hand, mechanical properties, including stress-strain behavior, which is an important mechanical characteristic for flexible electronics applications such as strain sensor, remains still unclear.

In this Chapter 3, I investigated the mechanical properties of UHMW ion gels and evaluate their potential application as strain sensors. In particular, I focused on their high stretchability and recyclability in detail, which have never been found in conventional chemically crosslinked ion gels. The UHMW ion gels also showed excellent self-healing properties at room temperature due to the reformation of the entanglements of polymers across the damaged interface. Although self-healing hydrogels based on dangling chain entanglement have been reported, their mechanical properties were sacrificed due to the need to control gelation near the sol-gel transition point in order to achieve self-healing ability.[1, 2] The micro-solvation and dissolved structure of polymers in ILs are investigated by molecular dynamics (MD) simulations. The effect on self-healing ability will be discussed with the results of the microscopic depiction of polymers in ILs.

3.2 Experimental

3.2.1 Materials

Most of the ILs, monomers, and radical polymerization initiators were purchased and treated as in chapter 2. ILs composed of anions except for TFSI were synthesized according to a method described in a previous report with slight modifications.[3] Ethyl methacrylate (EMA) was purchased from Kanto Chemical (Japan) and purified by passing them through a basic alumina column.

3.2.2 Tensile and Compressive Tests

The tensile and compressive tests of the gels were performed using a Shimadzu AGS-X tester

(Shimadzu, Kyoto, Japan). For the tensile test, gels cut into a dumbbell-shape (size of the rectangular portion: 2.0 × 12.0 × 1.0 mm) were stretched at a speed of 10 cm min^{-1} using a 100 N load cell. To investigate the self-healing behavior, the gel was cut at the center into two equal pieces. Then, the two cut surfaces were gently attached and allowed to stand for various healing times at room temperature, after which tensile tests were performed. For the compressive test, gels molded into a cylindrical shape (Ø10 mm × 10 mm height) were compressed at a speed of 100 % min^{-1} using a 10 kN load cell.

3.2.3 Thermal Analysis

Differential scanning calorimetry (DSC) was performed using an X-DSC7000 instrument (Hitachi High-Tech, Japan). The samples were semi-sealed in aluminum pans. The samples were heated to 200 °C, followed by cooling to −150 °C, and then reheated to 200 °C at a cooling and heating rate of 10 °C min^{-1}. The glass transition temperature T_g (the midpoint temperature of the heat capacity change) and melting point (the onset temperature of the endothermic peak, T_m) were determined from the DSC thermograms during the programmed reheating steps. Thermogravimetric (TG) measurements of the samples were conducted in open Al pans using a thermogravimetry/differential thermal analyzer (TG-DTA 6200, Seiko Instruments, Japan) from room temperature to 550 °C at a heating rate of 10 °C min^{-1}.

3.2.4 Electrochemical Measurements

The ionic conductivity of the gel was evaluated by impedance measurements using a VMP3 potentiostat/galvanostat (Bio-Logic Science Instruments, France) over a frequency range of 0.1 Hz–1 MHz with an AC of 10 mV amplitude. The gel was held between two stainless steel disk electrodes using a polytetrafluoroethylene spacer (1.0 mm (T) × 8.5 mm (ID)). The measurements were conducted over a temperature range of 20–120 °C at intervals of 10 °C. The sample was allowed to equilibrate for at least 1 h at each temperature prior to each measurement.

The impedance tests for the stretched and unstretched gels were conducted using a rectangular gel sheet (60 mm (L) × 10 mm (W) × 2.5 mm (T)). Copper electrodes (10 × 10 mm) were attached to both ends of the sample. The impedance measurements were then performed with (300%) and without stretching strain. For the self-healing test, the gel sheet was cut at the center, and the two cut surfaces were brought into contact. After 6 h at room temperature, impedance measurements were performed on the healed gel sheet.

3.2.5 Molecular Dynamics Simulations

An all-atom MD simulation was conducted using the GROMACS 2020.1 program under the isobaric-isothermal (NTP) ensemble (298 K and 1 atm) in a cubic cell controlled by a Nosé-Hoover thermostat[4, 5] and a Parrinello-Rahman barostat[6]. The long-range interactions were treated using the

Particle mesh Ewald method with real-space cutoff distance of 1.2 nm. The compositions (i.e., number of ILs and polymers) in the simulation box are listed in **Table 3-1**. A 20-mer equivalent of approximately 2 kDa was used as the polymer moiety owing to computing performance issues. The molecules were randomly placed in the simulation box in the order of cations, anions, and PMMA which was structurally relaxed in vacuum. After that, stirring under pressurized and high temperature conditions, and then allowed to settle to room temperature and pressure conditions over 5 ns. The total simulation time was set to 25.0 ns. An equilibration of 10 ns was performed to ensure that the density was constant during the simulation. The data collected at 0.1 ps intervals from the last 500 ps were analyzed to determine the radial distribution function $G(r)$. The resulting density values from the current MD simulations are in good agreement with the corresponding density values estimated from the respective densities of the IL and polymer, which are listed in **Table 3-1**. CLaP and OPLS-AA force fields, including intermolecular Lennard–Jones (LJ), coulombic interactions, and intramolecular interactions (i.e., bond stretching, angle bending, and torsion of dihedral angles) were used for C_2mIm, TFSI, and the polymers.[7-9] The radius of gyration (R_g) of the polymer was calculated using intramolecular $G_{intra}(r)$ according to the following equation:

$$R_g^2 = \frac{\int_0^{r_{max}} r^2 4\pi r^2 G(r) \mathrm{d}r}{\int_0^{r_{max}} 4\pi r^2 G(r) \mathrm{d}r}$$

Table 3-1. Density d, compositions (number of ion-pairs and polymer molecules), and box length of the systems for MD simulations.

System	d [g mL^{-1}]		[C$_2$mIm][TFSI]	PMMA (20mer)	PEMA (20mer)	Box length [Å]
	Calc	MD				
PMMA/[C$_2$mIm][TFSI]	1.399	1.395	256	21	-	55.98
PEMA/[C$_2$mIm][TFSI]	1.372	1.368	256	-	19	55.49

3.3 Mechanical Properties of UHMW Ion Gels

Despite the absence of chemical cross-linking, the UHMW ion gel exhibited excellent stretchability and toughness because the high density of the entangled chains behaved as transient physical cross-links. **Fig. 3-1(a)** shows the tensile stress–strain curves of the UHMW ion gels and a conventional gel of comparable Young's modulus that involved a chemical cross-links.[10] The UHMW ion gel exhibited a high fracture stress and strain of 0.12 MPa and 570%, respectively. Comparison of stress-strain curves for PMMA/[C_2mIm][TFSI] systems with different molecular weight of PMMA are shown in **Figure 3-1(b)**. Moreover, **Figure 3-2** shows cyclic tensile stress-strain curves for the PMMA/[C_2mIm][TFSI] gel and PMMA/[C_2mIm][TFSI] systems with lower molecular weight PMMA. Hysteresis observed in the UHMW PMMA/[C_2mIm][TFSI] gel could be attributed to the energy dissipation resulting from relaxation of physical entanglement between UHMW polymers. The residual strain gradually increases with cyclic testing, indicating the disentanglement of the polymer chains. However, the hysteresis and residual strain of the UHMW gel are significantly low compared to the lower molecular weight PMMA/[C_2mIm][TFSI] systems, suggesting that the disentanglement of polymer chains during the cyclic tensile testing is greatly suppressed for the UHMW PMMA/[C_2mIm][TFSI] ion gel. The UHMW ion gel also showed excellent compressive strength with a fracture stress of over 100 MPa (**Figure 3-3**). Owing to the negligible volatility of the ILs (**Figure 3-4**) and the absence of covalent bonding in the gel network, recycling of the UHMW gel was also

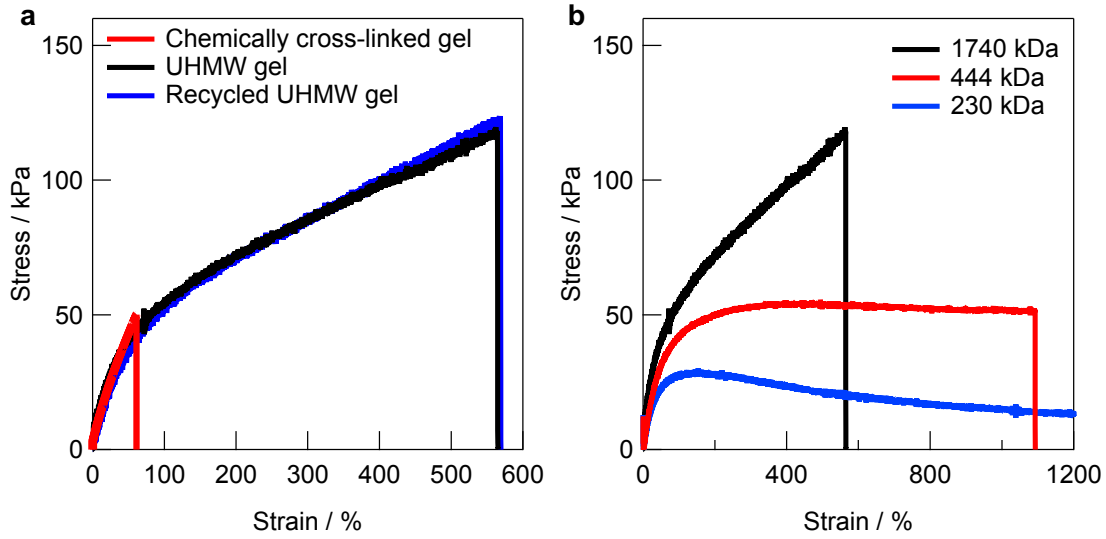

Figure 3-1. Tensile stress–strain curves of the chemically cross-linked PMMA/[C_2mIm][TFSI] gel [red, reproduced with permission from ref[10], American Chemical Society 2017], UHMW PMMA/[C_2mIm][TFSI] gel (black), and recycled UHMW PMMA/[C_2mIm][TFSI] gel (blue). (b) Tensile stress-strain curves of PMMA/[C_2mIm][TFSI] systems with different molecular weight of PMMA. The PMMA/[C_2mIm][TFSI] system with the molecular weight of 230 kDa was elongated to the limit of the apparatus without breakage.

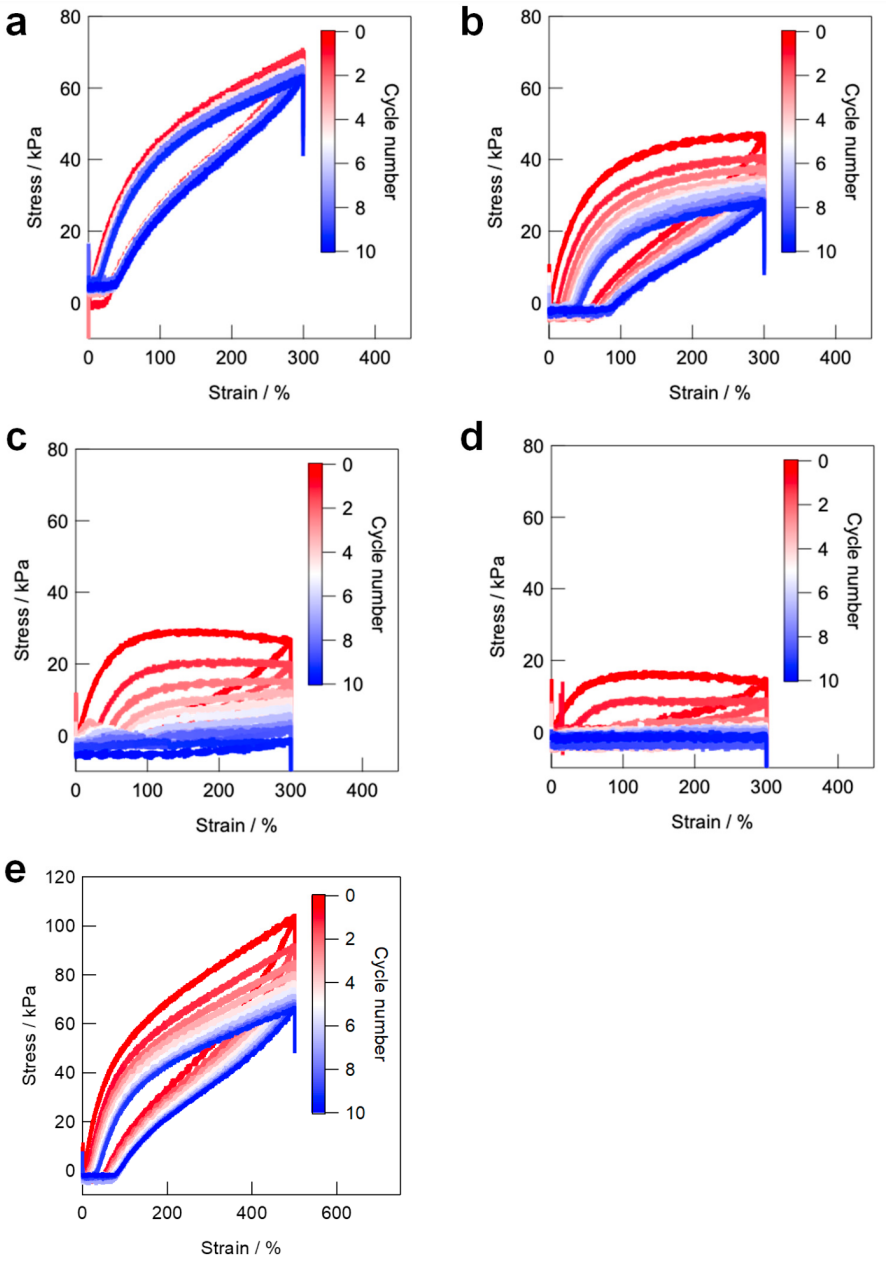

Figure 3-2. The cyclic stress-strain curves at the strain of 300% for PMMA/[C_2mIm][TFSI] systems with different molecular weight of PMMA, with 600 s waiting times between each cycle. (a) 1740 kDa (i.e., the ultrahigh molecular weight (UHMW) gel). (b) 444 kDa. (c) 240 kDa. (d) 123 kDa. The hysteresis and residual strain of the UHMW PMMA/[C_2mIm][TFSI] gel were significantly lower than those of the lower molecular weight PMMA/[C_2mIm][TFSI] systems. (e) The cyclic stress-strain curve at the strain of 500% for the UHMW PMMA/[C_2mIm][TFSI] gel. The hysteresis and residual strain at the strain of 500% were larger than those of 300%, indicating that the disentanglement or chain scission of UHMW polymers more likely occurred at the strain of 500%.

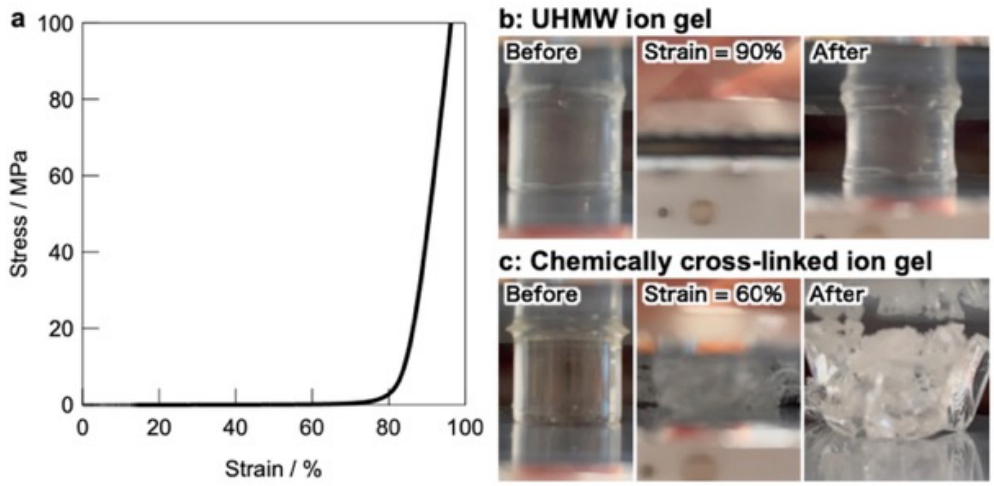

Figure 3-3. (a) Compressive stress–strain curves of the ultrahigh molecular weight (UHMW) PMMA/[C_2mIm][TFSI] ion gel. (b, c) Photographs before and after compression of UHMW PMMA/[C_2mIm][TFSI] gel (b) and chemically cross-linked PMMA/[C_2mIm][TFSI] gel (c).

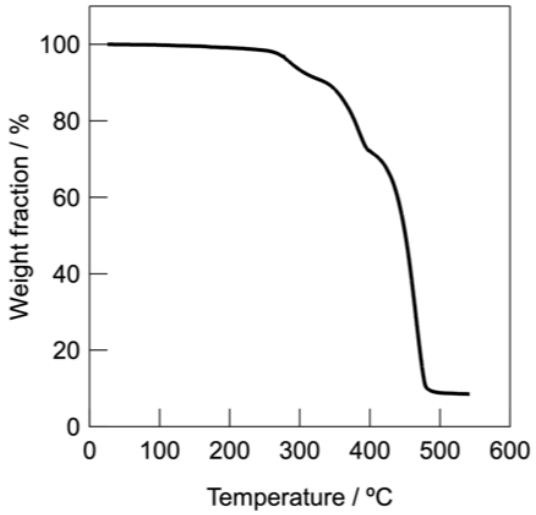

Figure 3-4. Thermogravimetric analysis of the ultrahigh molecular weight PMMA/[C_2mIm][TFSI] gel. The measurement was performed under nitrogen atmosphere at a heating rate of 10 °C min^{-1}.

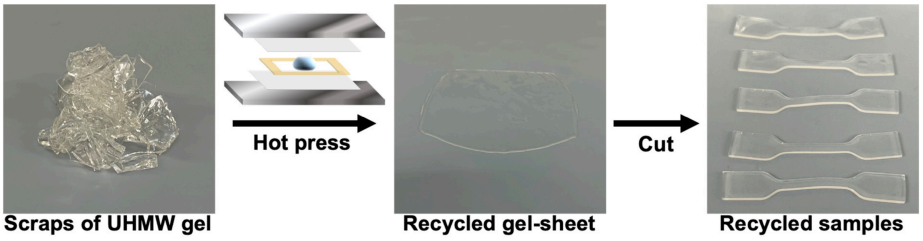

Figure 3-5. Recyclability of the UHMW ion gel. Photographs of the fragmented gels (left), a hot-pressed gel (center), and reproduced dumbbell-shaped gels (right).

possible by the facile hot pressing process **(Figure 3-5).** The stress–strain curve of the UHMW ion gel remained unchanged before and after reprocessing, indicating that neither the degradation of the polymer nor the evaporation of the solvent occurred during the recycling process **(Figure 3-1(a))**. **Figure 3-6** shows the effect of the repeated recycling process on the tensile properties of the UHMW gel; nearly identical stress-strain curves and toughness were maintained up to 10 recycling cycles. Furthermore, as the UHMW polymers can be polymerized *in situ* in different ILs, the physical properties of the UHMW ion gels can be largely modulated by selecting a suitable combination of monomer and IL chemical structures **(Figure 3-7)**. In general, to control the mechanical properties of polymer gels, the molecular design of polymer networks has been extensively investigated.[11-14] In sharp contrast to the conventional system, the mechanical properties of present system can be easily and effectively modulated by the molecular design of the solvent.

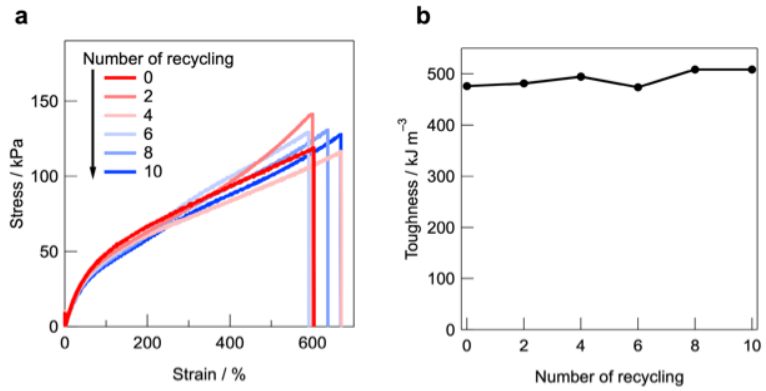

Figure 3-6. Repeated recycling test for the UHMW ion gels. (a) Tensile stress-strain curves for the UHMW PMMA/[C_2mIm][TFSI] ion gels with different number of recycling processes. (b) Relationship between the number of recycling and the toughness of the recycled UHMW ion gels. Each recycling process was conducted by hot pressing the UHMW ion gel at 130 °C for 15 min.

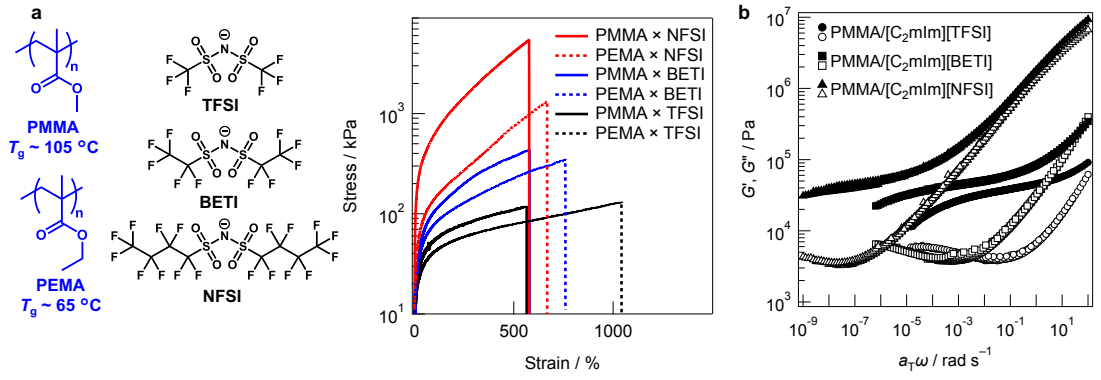

Figure 3-7. (a) Tensile stress–strain curves of the UHMW ion gels with various polymer/IL combinations. A logarithmic scale on the vertical axis is used. (b) Time–temperature superposition (tTS) master curves of G' (closed symbols) and G'' (open symbols) for the ultrahigh molecular weight gels with different ionic liquid structures. The reference temperature is 10 °C.

3.4 Self-Healing Properties of UHMW Ion Gels

Remarkably, the UHMW PMMA/[C_2mIm][TFSI] gel exhibited outstanding self-healing capabilities. Upon cutting the gel sheet into two pieces and then immediately bringing them into contact, spontaneous self-healing behavior was observed under ambient conditions without applying any external stimuli **(Figure 3-8(a))**. The self-healing efficiency was evaluated by tensile testing the UHMW gel with different healing times. With increasing healing time, the tensile strength gradually recovered, and the stress–strain curve and fracture energy of the healed gel after 6 h were almost the same as those of the pristine sample **(Figure 3-8(b, c))**. This indicates that the entanglements of the PMMA chains reformed across the cut surface during the healing process. The speed of healing is faster for lower molecular weight PMMA/[C_2mIm][TFSI] systems, however, the mechanical properties were deteriorated **(Figure 3-9)**. Furthermore, by exploiting the mechanical robustness of the UHMW gel at high temperature, the self-healing rate can be accelerated by conducting the healing process at elevated temperatures **(Figure 3-10)**. In addition to its superior mechanical properties, the UHMW gel exhibited good electrochemical properties, such as ionic conductivity of 0.23 mS cm^{-1} at 25 °C, which can be attributed to the high IL content **(Figure 3-11(a)).** The Nyquist plots showing the impedance spectra of the stretched and unstretched UHMW gels before and after self-healing suggest that the electrochemical properties were also recovered after the self-healing process, rendering the UHMW gel as a promising stretchable electrolyte for flexible/wearable devices **(Figure 3-12(b))**.

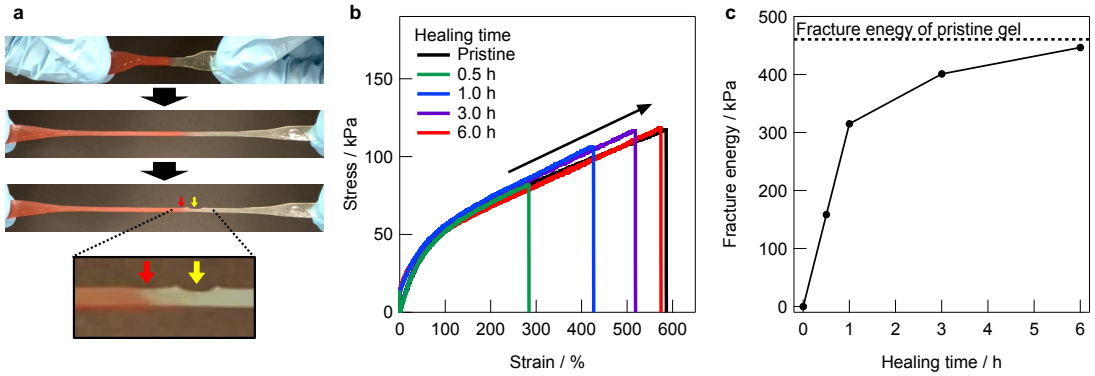

Figure 3-8. (a) Photographs of the UHMW PMMA/[C_2mIm][TFSI] ion gel after healing at room temperature for 6 hours. The red and yellow arrows indicate the contact point of two cut gel pieces and a breaking point of the healed gel, respectively. The fact that the breaking point of the gel does not start from the contact point implies that the healing process at the interface completed. (b) Tensile stress–strain curves of the pristine and healed UHMW ion gels with different healing times. (c) Relationship between healing time and toughness of the UHMW PMMA/[C_2mIm][TFSI] ion gel. Toughness is defined as the area under the stress-strain curve to fracture in the tensile tests. The dotted solid line indicates the toughness of the pristine gel.

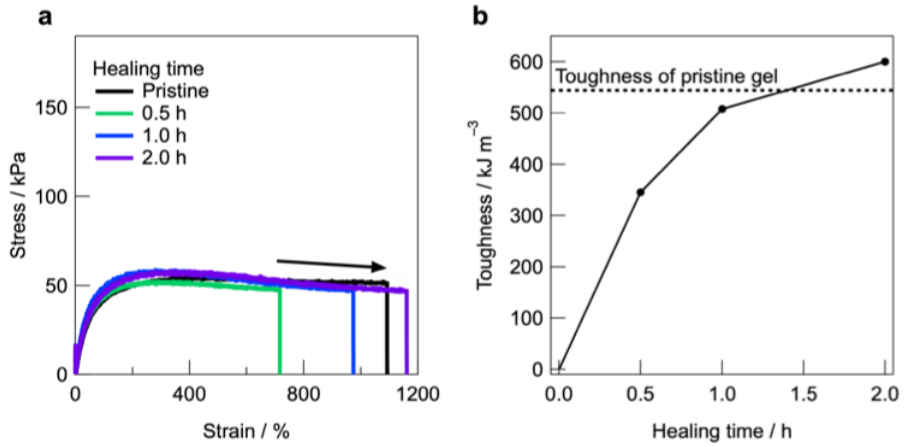

Figure 3-9. Self-healing properties for the 444 kDa PMMA/[C_2mIm][TFSI] system. (a) Tensile stress-strain curves and (b) mechanical toughness of the pristine and healed 444 kDa PMMA/[C_2mIm][TFSI] systems with different healing times.

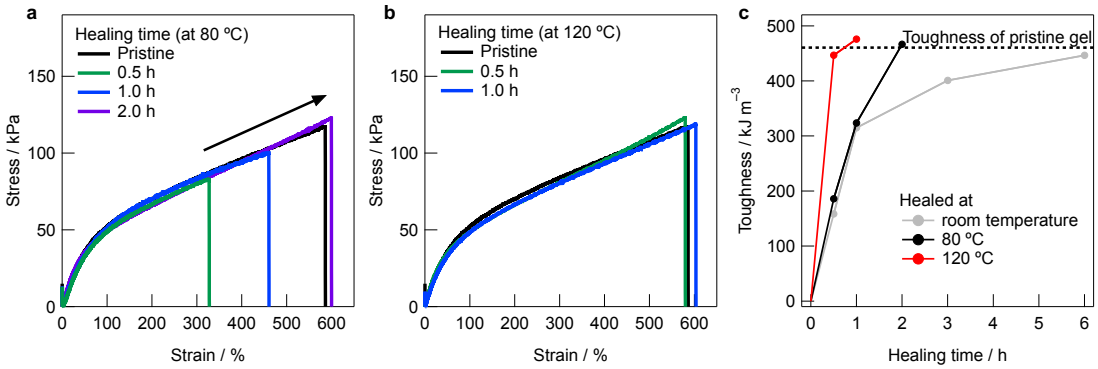

Figure 3-10. Self-healing at high temperatures. (a, b) Tensile stress–strain curves of the pristine and healed UHMW PMMA/[C_2mIm][TFSI] ion gels with different healing time. The healing process was conducted at 80 °C (a) and 120 °C (b). (c) Relationship between healing time and toughness of the UHMW ion gel with different healing temperatures.

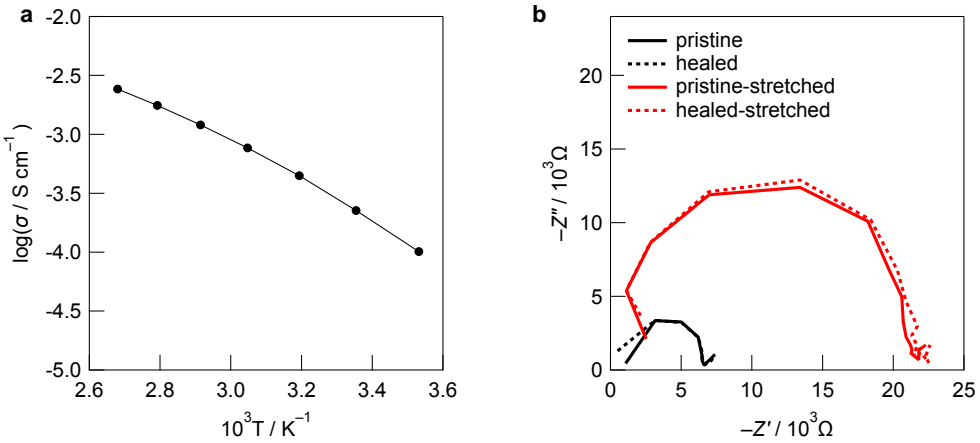

Figure 3-11. (a) Temperature dependence of ionic conductivity for the ultrahigh molecular weight PMMA/[C_2mIm][TFSI] ion gel. (b) Nyquist plots of impedance spectra for the 300% stretched and unstretched UHMW gels before and after the self-healing process.

As demonstrated above, the UHMW PMMA/[C$_2$mIm][TFSI] gel exhibited self-healing ability at room temperature within 6 h even though the gel was formed by the physical entanglement of the UHMW polymers with a long relaxation time; the point of a crossover of G' and G'' was much larger than 105 s (~28 h) **(Figure 2-10)**. Notably, when the cut samples were brought into contact after some waiting time, the healing efficiency decreased with longer waiting times **(Figure 3-12(a))**, although complete healing was also achieved for the sample with the waiting time of 72 h by extending the healing time to 24 h **(Figure 3-12(b, c))**. These results indicate that the waiting time has a significant impact to decelerate the speed of self-healing process. This phenomenon was also observed for self-healing supramolecular polymers[15, 16] and the crack healing of glassy polymers[17, 18]. In the case of the self-healing supramolecular polymers, the ratio of non-associated free stickers at the cut surfaces decreased with longer delays, leading to a deteriorated self-healing efficiency. This suggests that immediately after cutting, a large number of the UHMW PMMA chains at the cut surfaces are in a nonequilibrium disentangled state, which more rapidly reform entanglements than two equilibrated surfaces **(Figure 3-13)**.

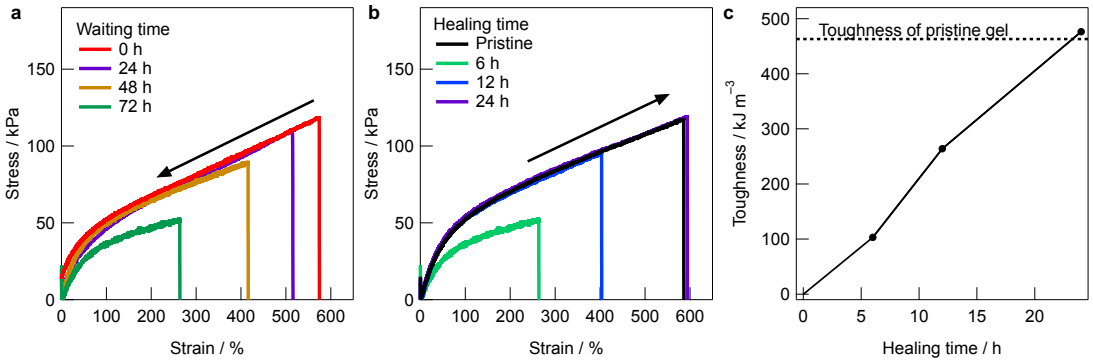

Figure 3-12. (a) Tensile stress–strain curves for UHMW PMMA/[C$_2$mIm][TFSI] ion gels after the self-healing process for 6 hours with different waiting times. (b) Tensile stress-strain curves for the UHMW PMMA/[C$_2$mIm][TFSI] ion gel with different healing times after the waiting time of 72 h. (c) Relationship between healing time and toughness with the waiting time of 72 h.

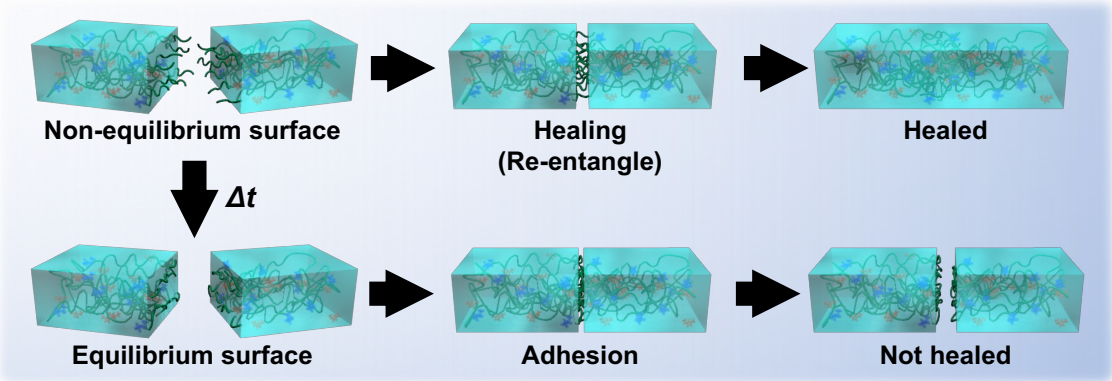

Figure 3-13. Schematic illustration for the healing process of UHMW ion gels with/without the waiting time.

Furthermore, it was revealed that the chemical structure of the polymer chain greatly affects the self-healing efficiency of the UHMW gel. The tensile properties before and after the self-healing process were compared for PMMA/[C_2mIm][TFSI] and poly(ethyl methacrylate) (PEMA)/[C_2mIm][TFSI] UHMW gels **(Figure 3-14)**. PEMA is also compatible with [C_2mIm][TFSI], and the T_g of the PEMA/[C_2mIm][TFSI] UHMW gel (T_g = −74 °C) was lower than that of the PMMA/[C_2mIm][TFSI] UHMW gel (T_g = −71 °C) **(Figure 3-15)**, suggesting that the PEMA polymer chains were more mobile in the IL at the same temperature because of the large free volume. Nevertheless, the UHMW gel with PEMA showed a poor self-healing efficiency of approximately 50% than that with PMMA **(Figure 3-14)**. This implies that the self-healing behavior of the UHMW gels is affected not only by the T_g, but also by the microscopic interactions between the solvent molecules and polymer chains.

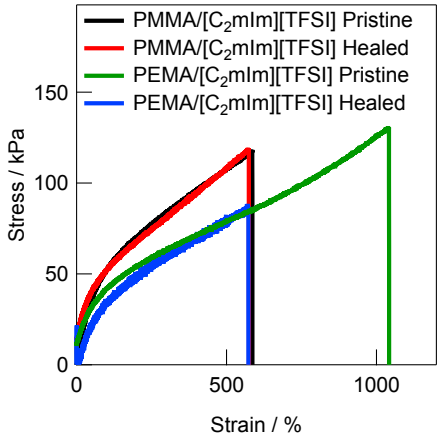

Figure 3-14. Tensile stress–strain curves for the pristine and healed PMMA/[C_2mIm][TFSI] and PEMA/[C_2mIm][TFSI] ion gels.

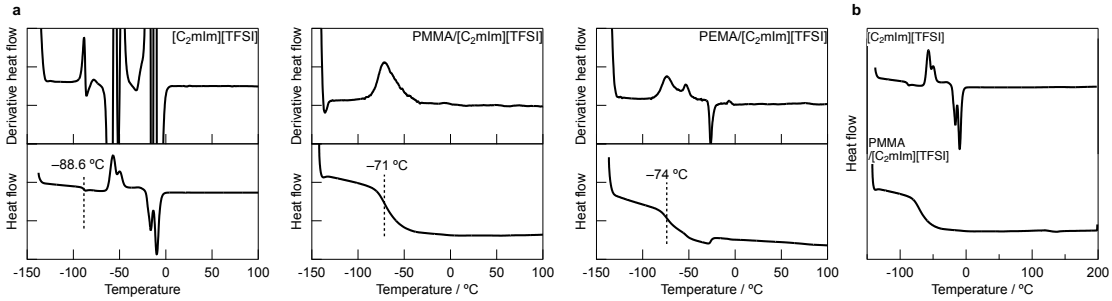

Figure 3-15. Differential scanning calorimetry (DSC) measurements. (a) Heat flow and derivative heat flow curves of the neat [C_2mIm][TFSI], UHMW PMMA/[C_2mIm][TFSI] ion gel, and UHMW PEMA/[C_2mIm][TFSI] ion gel. The samples were heated to 200 °C, followed by cooling to −150 °C, and then reheated to 200 °C at a cooling and heating rate of 10 °C min−1. The 2nd heating step from −150 °C to 100 °C was shown in this figure. (b) DSC thermograms for the bulk [C_2mIm][TFSI] and the UHMW PMMA/[C_2mIm][TFSI] ion gel from −150 °C to 200 °C. It shows that there is no peak between 100 to 200 °C.

3.5 Microscopic Structure of Polymers in Ionic Liquids

Thus, the solvation structures of PMMA and PEMA (20-mer) in [C_2mIm][TFSI] were analyzed by MD simulations, and the difference in the self-healing behavior is discussed from the perspective of the solvation structures and polymer conformation. The MD simulations were carried out in the isobaric-isothermal (NTP) ensemble, and the radial distribution function ($G_{total}(r)$) was calculated from the trajectory obtained from the MD calculations **(Figure 3-16)**. $G_{total}(r)$ is separated into intra- ($G_{intra}(r)$) and intermolecular ($G_{inter}(r)$) contributions, and $G_{inter}(r)$ can be further divided into partial functions of (i) polymer–cation ($G_{poly-cation}(r)$), (ii) polymer–anion ($G_{poly-anion}(r)$), and (iii) cation–anion ($G_{cation-anion}(r)$) interactions. The extracted $G_{poly-cation}(r)$ and $G_{poly-anion}(r)$ of the PMMA/[C_2mIm][TFSI] and PEMA/[C_2mIm][TFSI] systems are shown in **Figure 17(a).** Atom-atom contribution for $G_{poly-cation}(r)$ and $G_{poly-anion}(r)$ indicates that the C_2mIm cations were in the first solvation zone and the TFSI anions in the second solvation zone of PMMA and PEMA **(Figure 3-**

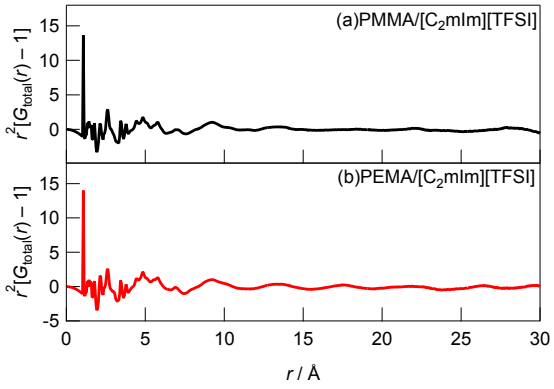

Figure 3-16. $G_{total}(r)$ functions obtained from molecular dynamics simulations for the 30 wt% (a) PMMA/[C_2mIm][TFSI] and (b) PEMA/[C_2mIm][TFSI] systems.

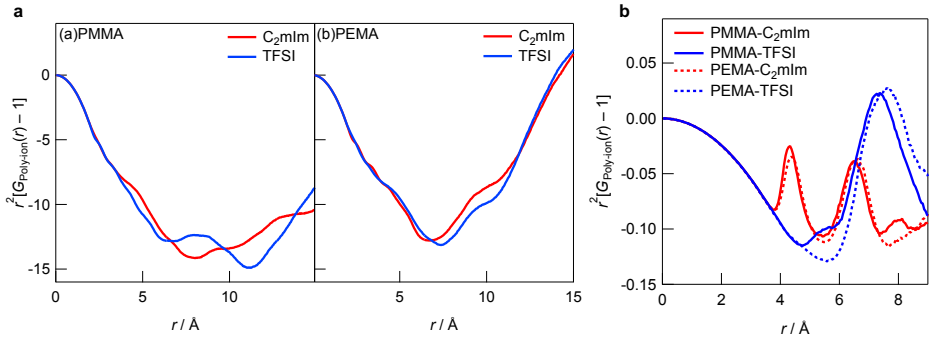

Figure 3-17. (a) Partial $G(r)$ for the intermolecular component of the polymer–cation ($G_{poly-cation}(r)$) (red) and polymer–anion ($G_{poly-anion}(r)$) (blue) for PMMA/[C_2mIm][TFSI] and PEMA/[C_2mIm][TFSI] systems. (b) Atom-atom contributions for $G_{poly-cation}(r)$ and $G_{poly-anion}(r)$. Atom-atom contributions for $G_{poly-ion}(r)$ between carbonyl carbon of polymers and 2nd carbon of [C_2mIm] cation (red solid line: PMMA-C_2mIm, red dotted line: PEMA-C_2mIm), and those between carbonyl carbon of polymers and central nitrogen of TFSI anion (blue solid line: PMMA-TFSI, blue dotted line: PEMA-TFSI). Peaks for the polymer–cation interactions near 5 Å and polymer– anion interactions near 8 Å were observed, suggesting that the C_2mIm cations were in the first solvation zone and the TFSI anions in the second solvation zone of PMMA and PEMA.

17(b)). The atom–atom pair correlation function between the oxygen atom of the methacrylate polymers and the proton atoms of the imidazolium cations shows that the height of the nearest peak ~2.5 Å for C_2mIm-PMMA is larger than that for C_2mIm-PEMA **(Figure 3-18(a))**. This implies that PMMA is better solvated by the C_2mIm cations than PEMA. Consistent with this result, the intramolecular radial distribution function $G_{intra}(r)$ for PEMA has a narrower peak than that for PMMA, suggesting that PMMA adopts a more extended conformation in [C_2mIm][TFSI] **(Figure 3-18(b), 3-19(a))**. Consequently, the calculated radius of gyration (R_g) for PMMA is larger than that for PEMA. Furthermore, intermolecular contribution of the radial distribution function ($G_{Poly\text{-}Poly}(r)$) revealed that different polymer chains is located in more proximity for the PMMA/[C_2mIm][TFSI] system than the PEMA/[C_2mIm][TFSI] system **(Figure 3-19(b))**. These results indicate that the interfacial entanglement is more likely to occur for the PMMA/[C_2mIm][TFSI] UHMW ion gel than the PEMA/[C_2mIm][TFSI] UHMW ion gel. Therefore, microscopic polymer–solvent interactions seem to play a crucial role in the self-healing capability of the UHMW ion gels.

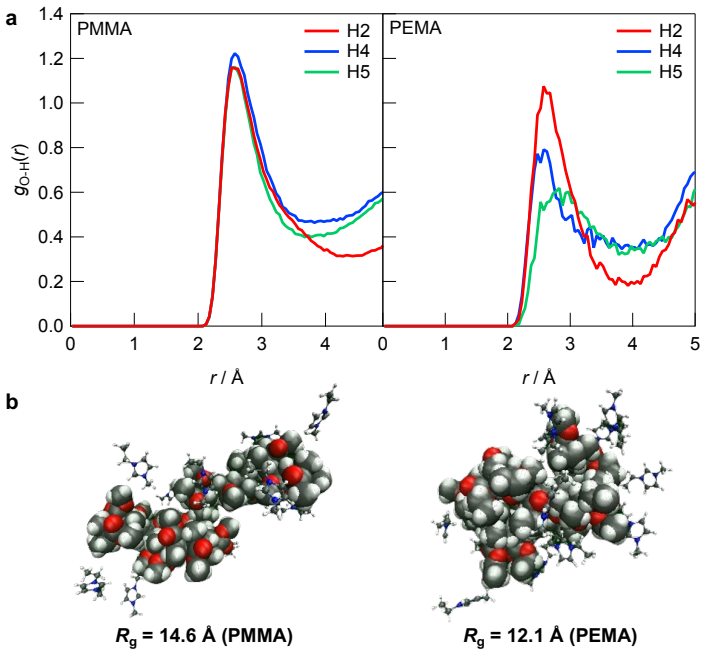

Figure 3-18. Pair correlation functions between the oxygen atom of the methacrylate polymers and proton atoms of the C_2mIm cations for (a) PMMA/[C_2mIm][TFSI] and PEMA/[C_2mIm][TFSI]. (b) Typical snap shot of PMMA (left) and PEMA (right) in [C_2mIm][TFSI] extracted from simulation box and their calculated R_g.

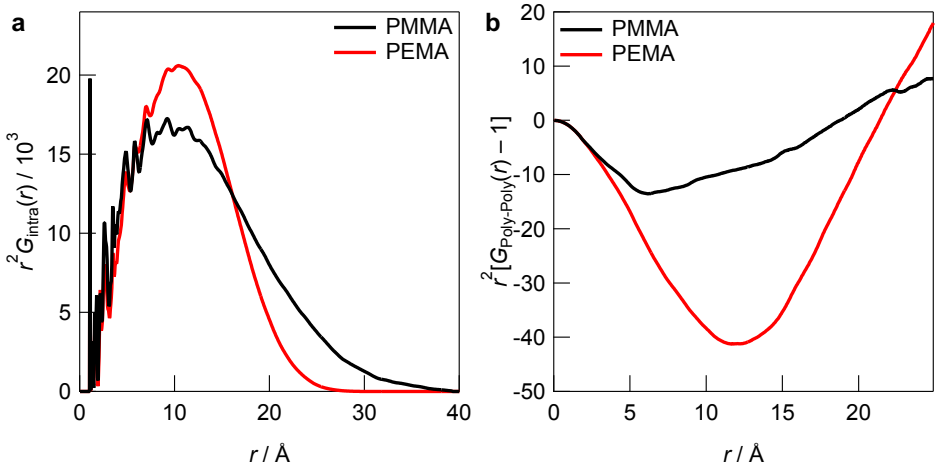

Figure 3-19. (a) Intramolecular contribution of the radial distribution function (r-weighted $G_{intra}(r)$) for the 30 wt% PMMA/[C_2mIm][TFSI] and PEMA/[C_2mIm][TFSI] systems. (b) Intermolecular contribution of the radial distribution function ($G_{Poly-Poly}(r)$) for the 30 wt% PMMA/[C_2mIm][TFSI] and PEMA/[C_2mIm][TFSI] systems.

3.6 Conclusions

The mechanical properties of ion gels consisting of the entanglement of ultra-high molecular weight PMMA in ionic liquids were investigated by tensile tests, and the results showed that UHMW ion gels exhibit excellent mechanical properties, such as [1] excellent stretchability, [2] recyclability by hot-pressing, [3] rapid self-healing at room temperature, which are not observed in conventional chemically cross-linked ion gel. The self-healing properties of the ion gels are attributed to the diffusion of polymer chains across the cut interface followed by the formation of physical entanglement. This is in contrast to self-healing materials based on reversible bonds such as hydrogen bonding, host-guest interactions, and dynamic covalent bonds, which have been extensively studied in recent years. It is also suggested that the nonequilibrium state of the cut interface plays an important role in the self-healing process. With the appropriate combination of polymer and solvent structures, UHMW gels exhibit rapid self-healing behavior at room temperature. MD simulation results suggest that the self-healing properties of ion gels depend on slight differences in chemical structure and may be influenced by the micro-solvation of the polymer in IL.

Reference

[1] Yamaguchi, M.; Ono, S.; Okamoto, K. *Mater. Sci. Eng. B* **2009**, *162*, 189-194.

[2] Yamaguchi, M.; Maeda, R.; Kobayashi, R.; Wada, T.; Ono, S.; Nobukawa, S. *Polym. Int.* **2012**, *61*, 9-16.

[3] Noda, A.; Hayamizu, K.; Watanabe, M. *J. Phys. Chem. B* **2001**, *105*, 4603-4610.

[4] Nosé, S. *Mol. Phys.* **1984**, *52*, 255-268.

[5] Hoover, W. G. *Phys. Rev. A* **1985**, *31*, 1695-1697.

[6] Parrinello, M.; Rahman, A. *Phys. Rev. Lett.* **1980**, *45*, 1196-1199.

[7] Jorgensen, W. L.; Maxwell, D. S.; Tirado-Rives, J. *J. Am. Chem. Soc.* **1996**, *118*, 11225-11236.

[8] Cornell, W. D.; Cieplak, P.; Bayly, C. I.; Gould, I. R.; Merz, K. M.; Ferguson, D. M.; Spellmeyer, D. C.; Fox, T.; Caldwell, J. W.; Kollman, P. A. *J. Am. Chem. Soc.* **1995**, *117*, 5179-5197.

[9] Canongia Lopes, J. N.; Pádua, A. A. H. *J. Phys. Chem. B* **2006**, *110*, 19586-19592.

[10] Ishii, S.; Kokubo, H.; Hashimoto, K.; Imaizumi, S.; Watanabe, M. *Macromolecules* **2017**, *50*, 2906-2915.

[11] Creton, C. *Macromolecules* **2017**, *50*, 8297-8316.

[12] Sakai, T.; Matsunaga, T.; Yamamoto, Y.; Ito, C.; Yoshida, R.; Suzuki, S.; Sasaki, N.; Shibayama, M.; Chung, U.-i. *Macromolecules* **2008**, *41*, 5379-5384.

[13] Gong, J. P. *Soft Matter* **2010**, *6*, 2583-2590.

[14] Zhao, X.; Chen, X.; Yuk, H.; Lin, S.; Liu, X.; Parada, G. *Chem. Rev.* **2021**, *121*, 4309-4372.

[15] Cordier, P.; Tournilhac, F.; Soulié-Ziakovic, C.; Leibler, L. *Nature* **2008**, *451*, 977-980.

[16] Stukalin, E. B.; Cai, L.-H.; Kumar, N. A.; Leibler, L.; Rubinstein, M. *Macromolecules* **2013**, *46*, 7525-7541.

[17] Wool, R. P.; O'Connor, K. M. *J. Appl. Phys.* **1981**, *52*, 5953-5963.

[18] Prager, S.; Tirrell, M. *J. Chem. Phys.* **1981**, *75*, 5194-5198.

Chapter 4

Effects of Chemical Structure of Monomers and Ionic Liquids on Mechanical Properties of UHMW Ion Gels

4.1 Introduction

In Chapters 2 and 3, I discussed the synthesis process, viscoelasticity, stress-strain behavior, and self-healing behavior of ion gels consisting of entangled UHMW PMMA in the IL [C_2mIm][TFSI]. In Chapter 3, I pointed out the possibility that the chemical structure of the constituents of the ion gel can affect its mechanical and self-healing properties, but the detailed mechanism of their correlation has not been understood, yet. In addition, due to the unique feature of structural designability of ILs, it is very important to elucidate the correlation between chemical structure and material properties.

In this Chapter, UHMW ion gels were synthesized from various combinations of IL and monomer structures to investigate the effect of their chemical structures on the *in situ* formed UHMW polymers. The rheological, mechanical properties, and self-healing ability of UHMW ion gels composed of various IL and polymer structures were investigated in detail to elucidate the structure-property relationship of UHMW ion gels. Furthermore, molecular dynamics (MD) simulations were performed to decipher the influence of IL and polymer structures on self-healing ability of UHMW ion gels at microscopic level.

4.2 Experimental

4.2.1 Materials

1-Alkyl-3-methylimidazolium trifluoromethylsulfonylimide ([C_nmIm][TFSI], n = 1, 2, 8, 12) and 1-ethyl-2,3-dimethylimidazolium trifluoromethylsulfonylimide ([C_2dmIm][TFSI]) were purchased from Kanto Chemical (Japan). [C_3mIm][TFSI] was purchased from TCI (Japan). [C_2mIm][BETI] (BETI: pentafluoroethylsulfonylimide and [C_2mIm][IM_{14}] (IM_{14}: (trifluoromethylsulfonyl)(nonafluorobutylsulfonyl)imide) were synthesized according to a literature with slight modifications.[1] Lithium salts, Li[BETI] and Li[IM_{14}], which were used for synthesis of these ILs, were purchased from Mitsubishi Materials Electronic Chemical Co., Ltd. (Japan). All the ILs were dried under vacuum at 120 °C for 24 h prior to use. Methyl methacrylate (MMA) and ethyl methacrylate (EMA) were purchased from Kanto Chemical (Japan), and propyl methacrylate (PMA) was purchased from TCI (Japan). All monomers were purified by passing them through the basic alumina column to remove polymerization inhibitor. 2,2'-Azobis(isobutyronitrile) (AIBN) were

purchased from FUJIFILM Wako Pure Chemical Corporation (Japan) and used as received.

4.2.2 Polymerization and Characterization of Methacrylate Polymers in Ionic Liquids

A representative synthetic procedure for the PMMA/[C_2mIm][TFSI] UHMW ion gel is described as follows. MMA (1.6 mL, 15.0 mmol), [C_2mIm][TFSI] (2.4 mL, 9.32 mmol), and AIBN (0.49 mg, 3.0×10^{-3} mmol) were charged in a glass cup and sealed with a rubber septum, through which argon was bubbled for 15 min at room temperature. Subsequently, polymerization reaction was carried out at 80 °C for 24 h, resulting in the formation of the transparent ion gel. Monomer conversion was determined using ^{1}H-NMR measurements for the as prepared UHMW gels dissolved in deuterated chloroform ($CDCl_3$). For the determination of molecular weight of *in situ* formed UHMW polymers, UHMW gels were purified by reprecipitation with acetone as good solvent and methanol as poor solvent twice and then vacuum dried at 60 °C, resulting in white powder of UHMW polymers. The molecular weight and polydispersity index (PDI) of the polymers were determined using gel permeation chromatography (GPC), in which 10 mM lithium bromide (LiBr) in *N*, *N*-dimethylformamide (DMF) solution was used as the eluent. The GPC columns (Showa Denko, Japan) were calibrated using PMMA standards. Prior to use for rheological measurements and mechanical measurements, UHMW gels were dried in vacuo at 80 °C overnight to remove residual monomers.

4.2.3 Rheological Measurements

Oscillatory shear measurements were performed with an Anton Paar MCR 102 rheometer (Anton Paar, Austria) using the parallel plate geometry with a 12 mm diameter plate. The detailed procedure is described in Chapter 2. Gap spacing was kept at 0.5 mm for all the measurements. Frequency sweep measurements were performed over a frequency range of 0.1–100 rad/s with a strain amplitude of 1% at constant temperatures from 10 to 120 °C at intervals of 10 °C. The time-temperature superposition (tTS) master curves for UHMW gels were constructed from the frequency sweep data at different temperatures.

4.2.4 Tensile Tests

Tensile tests of UHMW gels were carried out using a Shimadzu AGS-X tester (Shimadzu, Japan). The gels cut into a dumbbell-shape (JIS K 6251-7 size, width: 2 mm, gauge length: 12 mm) were stretched at a speed of 10 cm/min with a 100 N load cell. For the self-healing test, the dumbbell-shaped gels were cut at the center, subsequently the two cut surfaces were contacted and allowed to heal at room temperature for 24 h, after which tensile tests were performed for the healed samples.

4.2.5 Thermal Analyses

Differential scanning calorimetry (DSC) measurements were performed using a DSC250 instrument

(TA Instruments, USA) under a nitrogen atmosphere. The samples were placed on an open aluminum pan and heated from 40 °C to 200 °C, followed by cooling to −120 °C, and then reheated to 200 °C at a cooling and heating rate of 10 °C/min. The glass transition temperature (T_g) (the temperature at the peak top of derivative heat flow) were determined from the DSC thermograms during the 2nd heating step.

4.2.6 MD Simulations

All-atom molecular dynamics (MD) simulations were carried out using the GROMACS 2020.1 program under the isobaric-isothermal (NTP) ensemble (298 K and 1 atm) in a cubic cell. The detailed procedure is described in Chapter 3. Number of ILs and polymers in the simulation boxes are listed in **Table 4-1**. A 20-mer (approximately 2 kDa) was used as the polymer due to computing performance issues. The total simulation time was set to be 25 ns. From the last 500 ps, the data was collected with 0.1 ps intervals, and analyzed to determine the radial distribution function $G(r)$. The density values calculated from the present MD simulations are consistent with the density values estimated from the respective densities of the IL and the polymer, which are also listed in **Table 4-1**. CLaP and OPLS-AA force fields, including intermolecular Lennard–Jones (LJ), coulombic interactions, and intramolecular interactions (bond stretching, angle bending, and torsion of dihedral angles) were used for the C_2mIm and C_{12}mIm cations, TFSI anion, and PMMA and PEMA polymers.[2-4] The radius of gyration (R_g) for the polymer was calculated from the intramolecular component $G_{intra}(r)$, according to the following equation, where r_{max} represents the upper limit of the integration, and here I assumed a sufficiently large r (35 Å) that there is no intramolecular correlation of the polymers:

$$R_g^2 = \frac{\int_0^{r_{max}} r^2 4\pi r^2 G(r) \mathrm{d}r}{\int_0^{r_{max}} 4\pi r^2 G(r) \mathrm{d}r}$$

Table 4-1. Density d, compositions (number of ion-pairs and polymer molecules), and box length of the systems for MD simulations.

System	d [g mL^{-1}]		IL	PMMA	PEMA	Box length [Å]
	Calc	MD	(ion pair)	(20mer)	(20mer)	
PMMA/[C2mIm][TFSI]	1.402	1.403	256	20	-	55.45
PMMA/[C12mIm][TFSI]	1.223	1.214	256	34	-	65.50
PEMA/[C2mIm][TFSI]	1.379	1.373	256	-	18	55.64

4.3 Synthesis of UHMW Ion Gels from Various IL and Monomer Structures

To prepare UHMW ion gels with different IL structures, methyl methacrylate (MMA) monomer was polymerized in a wide variety of ILs consisting of combinations of different imidazolium-based cations; 1-alkyl-3-methylimidazolium ([C_nmIm]: n = 2-12), 1-ethyl-2,3-dimethylimidazolium ([C_2dmIm]) and sulfonylimide anions with different lengths of perfluoroalkyl groups (TFSI, BETI, and IM_{14}). In addition to MMA, ethyl methacrylate (EMA) and propyl methacrylate (PMA) were polymerized in [C_2mIm][TFSI] and [C_2mIm][BETI], respectively to investigate how monomer structures affect mechanical property of UHMW ion gel. Note that when PMA was polymerized in [C_2mIm][TFSI], it was too soft to be molded for mechanical tests probably due to its very low glass transition temperature (T_g). Therefore, polymerization of PMA monomer was performed in [C_2mIm][BETI] (T_g = −82.3) to increase T_g of resultant ion gel compared to much lower T_g solvent of [C_2mIm][TFSI] (T_g = −93.4). The chemical structures of ILs and monomers used in this study are summarized in **Figure 4-1**. For the synthesis of UHMW ion gels, the monomer concentration was fixed to be 40 vol% and the initiator (2,2'-Azobis(isobutyronitrile), AIBN) content was set at as low as 0.02 mol% vs. monomer concentration. After argon bubbling of precursor solutions containing ILs, monomers and initiator, polymerization was allowed to proceed at 80 °C for 24 h. For all combinations of monomers and ILs, transparent ion gels without any macroscopic phase separation of polymer and an IL were formed *in situ* as polymerization proceeded, indicating that the robust physical entanglement of UHMW polymers were formed in ILs. The results of polymerization (molecular weight, polydispersity index (PDI), and monomer conversion) are summarized in **Table 4-2**. GPC traces of synthesized polymers extracted from UHMW ion gels and ^{1}H-NMR spectra of as prepared UHMW ion gels after polymerization are shown in **Figure 4-2 and 4-3**. For all monomer-IL combinations used in this study, UHMW polymers with molecular weights near or above 10^6 g mol^{-1} were obtained with high monomer conversion of over 95%. These results indicate that the fabrication strategy of UHMW ion gels can be applicable for wide variety of methacrylate polymer and IL structures, which would render tunability of physicochemical properties of UHMW ion gels. Previous

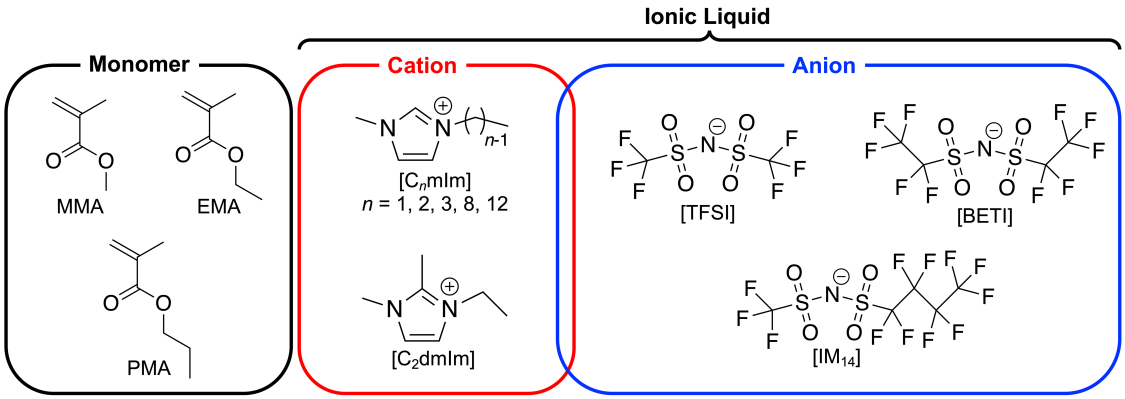

Figure 4-1. The chemical structures of monomer, IL cation, and anions used in this study.

experimental and computational investigations for the radical polymerization in ILs suggested that the rate constant of propagation (k_p) was enhanced with decrease in activation energy due to the charge-dipole or dipole-dipole interaction between solvent(IL)-radical.[5, 6] Consistent with the previous results, the molecular weight of the obtained PMMA in ILs tended to increase with increasing ionic concentration in the precursor solutions **(Figure 4-4)**, suggesting that the more the ionic moieties around the propagation radicals, the higher the k_p due to the IL-radical interaction. Interestingly, the PDIs of obtained UHMW polymers were slightly below 2.0, which were significantly lower than those of high molecular weight polymers produced as a result of decreased termination rate due to high viscosity, which was well-known as the Trommsdorff effect.[7] In the bulk polymerization of MMA, the Trommsdorff effect, which occurs late in the polymerization, leads to the formation of high molecular weight products and the consequent bimodalization of the GPC trace, resulting in a PDI above 4.0. The relatively low PDI in this study could be attributed to the enhanced k_p and significantly low concentration of radicals in this polymerization condition that might lower the influence of the termination reaction.

Table 4-2. Characterization results of UHMW polymers synthesized in ILs. [a]calculated by GPC using PMMA standards (eluent: 10 mM LiBr/DMF). For the characterization by GPC, polymers were extracted from ILs as follows: UHMW ion gels were dissolved in acetone, subsequently UHMW polymers were reprecipitated into excess amount of methanol. [b]calculated from ^{1}H-NMR. As prepared UHMW ion gels were dissolved in $CDCl_3$, and the monomer conversion was calculated by comparing the residual vinyl peaks of monomers with polymer peaks.

Monomer	Solvent	M_n / kDa[a]	M_w / kDa[a]	PDI[a]	Conversion[b]
MMA	[C_1mIm][TFSI]	1,587	2,896	1.83	98.0
	[C_2mIm][TFSI]	1,280	2,377	1.85	98.1
	[C_3mIm][TFSI]	1,216	2,400	1.97	97.3
	[C_8mIm][TFSI]	1,274	2,235	1.75	95.9
	[C_{12}mIm][TFSI]	1,169	2,263	1.94	97.0
	[C_2dmIm][TFSI]	1,492	2,773	1.86	96.8
	[C_2mIm][BETI]	1,473	2,693	1.83	97.9
	[C_2mIm][IM_{14}]	1,162	2,652	2.28	97.8
EMA	[C_2mIm][TFSI]	988	1,700	1.72	95.8
PMA	[C_2mIm][BETI]	1,019	1,820	1.79	95.9

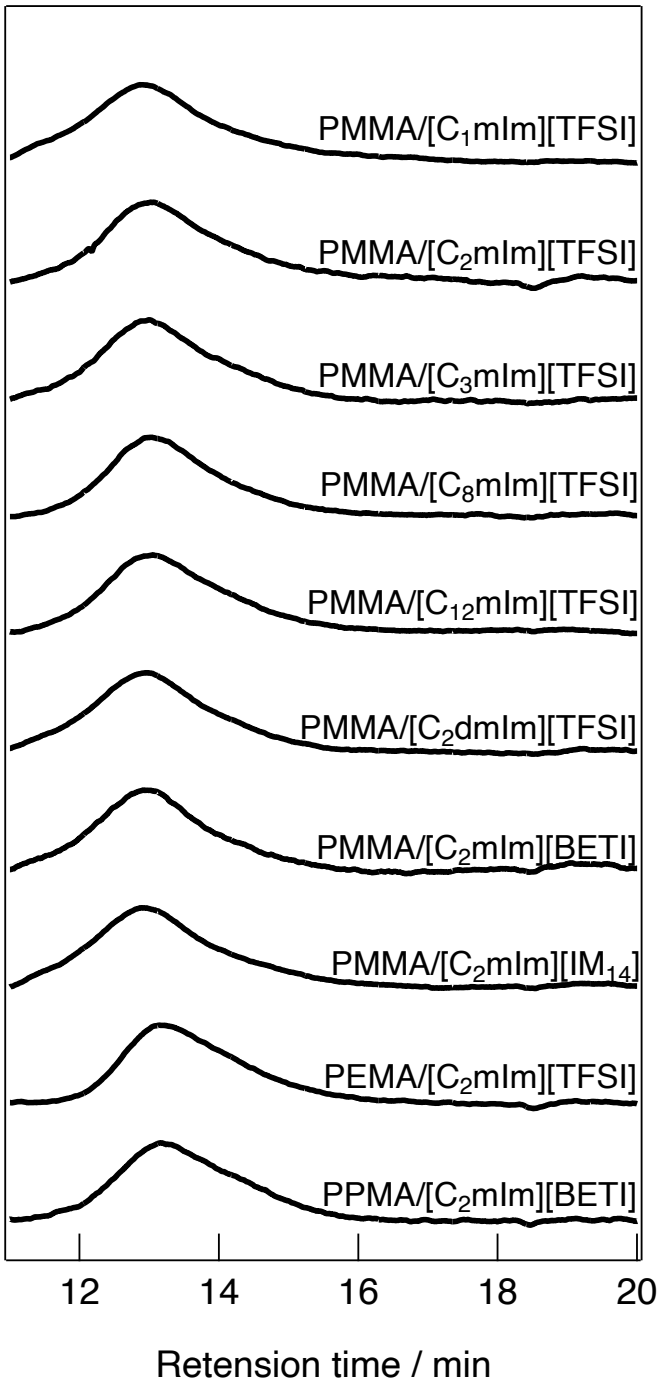

Figure 4-2. GPC traces for UHMW polymers, which were extracted from the as prepared UHMW ion gels.

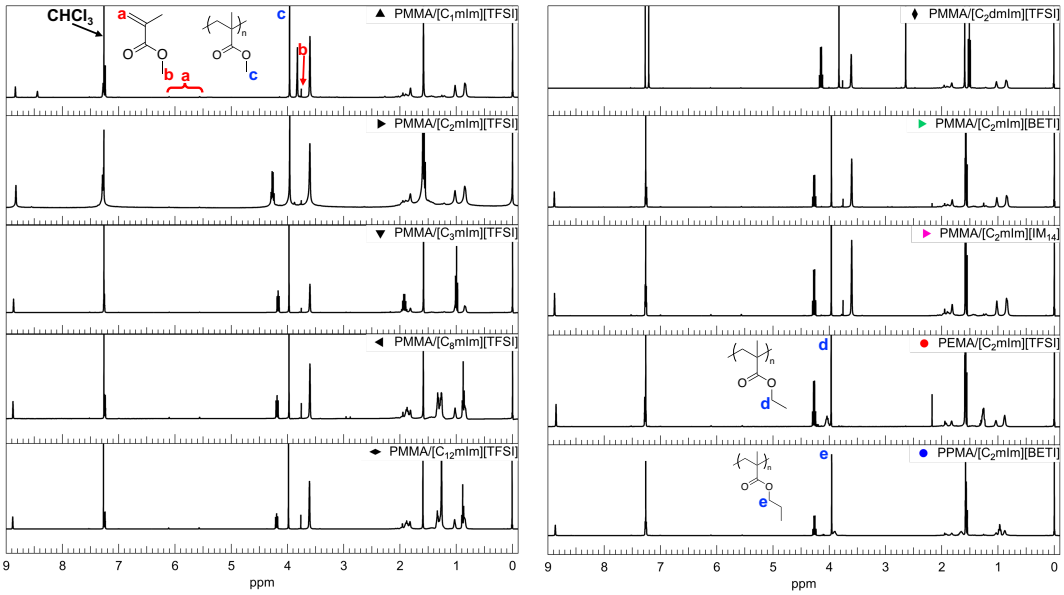

Figure 4-3. ^{1}H-NMR spectra for as prepared UHMW ion gels in $CDCl_3$. Monomer conversions were calculated by comparing the residual vinyl peak with the polymer peaks. The methyl peak for PMMA, the methylene peaks for PEMA and PPMA were used for calculation.

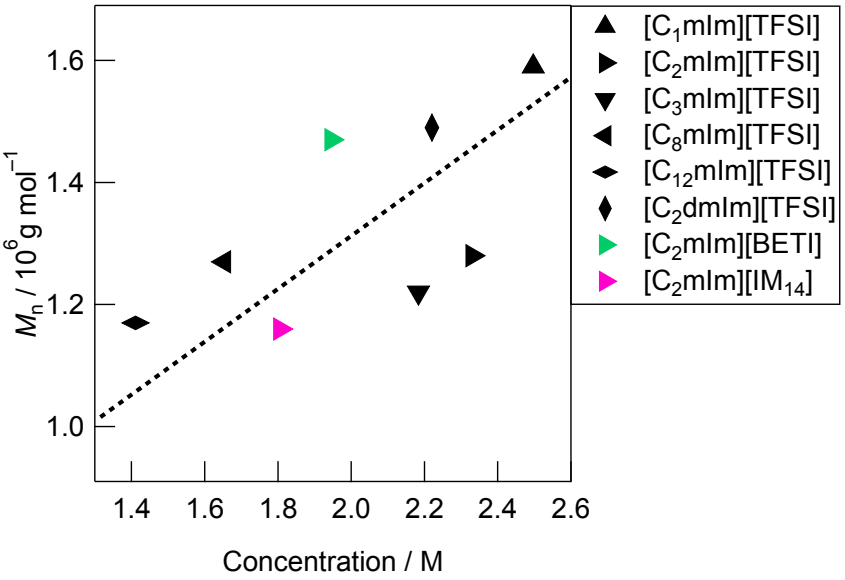

Figure 4-4. Dependence of molecular weight of PMMA synthesized by *in situ* radical polymerization in various ILs on ionic strength of the precursor solutions. The dotted line is a guide to the eye.

4.4 Rheological Properties of UHMW Ion Gels

Rheological properties of UHMW ion gels with different polymers and IL structures were evaluated by frequency sweep measurements at different temperatures ranging from 10 to 120 °C. Next, time–temperature superposition (tTS) master curves for storage modulus (G'), loss modulus (G''), and tanδ for each UHMW ion gel was obtained at a reference temperature of 10 °C **(Figure 4-5(a, b))**. Note that, although the tTS principle was well applicable, there was a deviation for G'' and tanδ at high frequency region for all UHMW ion gels. This phenomenon has been already reported for other conventional ion gel systems that the relaxation was related to solvent viscosity.[8-10]

In all systems, a rubbery plateau region was observed over a wide frequency range; crossover of G' and G'' and subsequent terminal relaxation ($G' \propto \omega^2$ and $G'' \propto \omega$) did not appear at least within this measurement condition, which indicates that UHMW gels behave as viscoelastic solids over very long timescales. This is due to the significantly slow relaxation of physical crosslinking owing to the extremely high molecular weight of the polymers, as the reptation theory suggests that the relaxation time of polymer entanglement correlates with the 3rd power of molecular weight. Even at frequency sweep measurement at 120 °C, G' was higher than G'' for all frequency region, indicating excellent mechanical robustness against temperature for UHMW ion gels **(Figure 4-6)**. Furthermore, the plateau G' at which the tanδ takes a minimum value, varied depending on the structure of the ILs. The plateau G' reflects the entanglement network structure, such as the number density of topological constraints.[11, 12] This indicates that the entanglement network structure and entanglement crosslink density of UHMW ion gels may depend on the structure of the IL solvents and thus differ from polymer melt systems.[13-15]

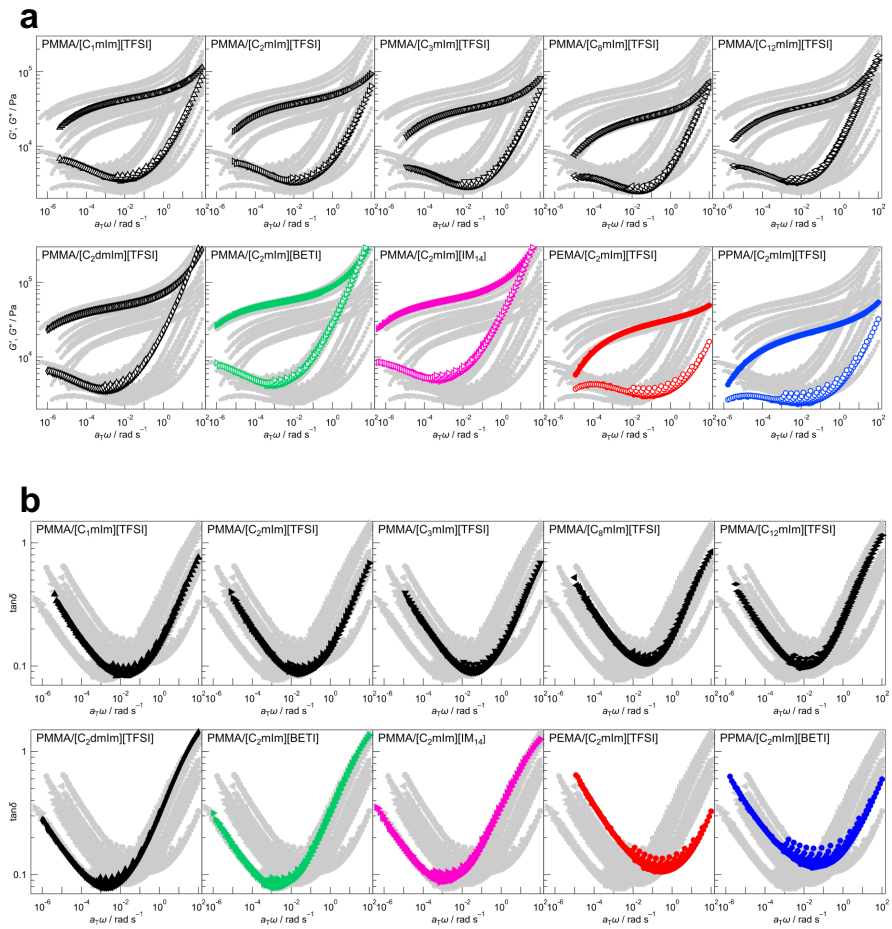

Figure 4-5. Time–temperature superposition (tTS) master curves of (a) G' (closed symbols), G'' (open symbols) and (b) tanδ (= G''/G') for UHMW ion gels with different combinations of polymers and ILs constructed from the frequency sweep measurements at the temperature range from 10 to 120 °C. The reference temperature = 10 °C. In each graph, only the master curve of interest is highlighted, while the other curves are shown in grey to clarify their relative positions.

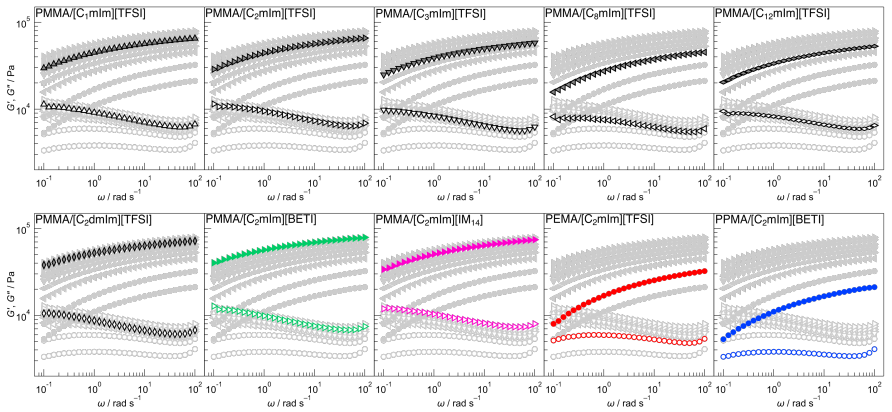

Figure 4-6. Frequency sweep measurements of G'(closed) and G''(open) moduli for UHMW ion gels at a temperature of 120 °C with a strain amplitude of 1%. In each graph, only the master curve of interest is highlighted, while the other curves are shown in grey to clarify their relative positions.

4.5 Mechanical Properties of UHMW Ion Gels

Figure 4-7 shows the uniaxial tensile stress-strain curves for UHMW ion gels obtained with various polymer/IL combinations. The mechanical strength of all the UHMW ion gels was much better than that of a conventional PMMA ion gel using a chemical crosslinker.[16] Tensile properties and T_gs of UHMW ion gels are summarized in **Table 4-3**. When the cation structures of UHMW ion gels were changed **(Figure 4-7(a))**, Young's modulus (E) varied from 94 to 167 kPa, and the fracture stress and strain varied from 182 to 353 kPa and 578 to 853%, respectively. On the other hand, when the anion and polymer structures were changed **(Figure 4-7(b))**, the stress-strain curves changed much significantly compared to changes in the UHMW ion gels with different cation structures. In particular, UHMW gels from PMMA/[C_2mIm][BETI] and PMMA/[C_2mIm][IM14] exhibited significantly high fracture stress. One of the possible reasons for high mechanical strength in the PMMA/[C_2mIm][BETI] UHMW ion gel could be attributed to its relatively high T_g of −57.2 °C (**Table 4-3**), which possibly contributed to stresses associated with micro-Brownian motion of polymer segment. In contrast, the PMMA/[C_2mIm][IM_{14}] UHMW gel showed the highest fracture stress among UHMW gels in this study despite possessing relatively low T_g of −69.7 °C. A recent study suggested that nanoscale phase separation occurred in [C_2mIm][IM_{14}] due to the aggregation of the long perfluoroalkyl chains of [IM_{14}] anions.[17] The different compatibility of UHMW PMMA with each domain might contribute to the polymer concentration gradient, resulting in higher fracture stress as the polymer-rich domain and the polymer-poor domain, respectively, play the role of stress storage and dissipation. Although the detailed mechanism is still unclear, this result implies that the mechanical strength of UHMW ion gels can be further improved by properly controlling the nanophase

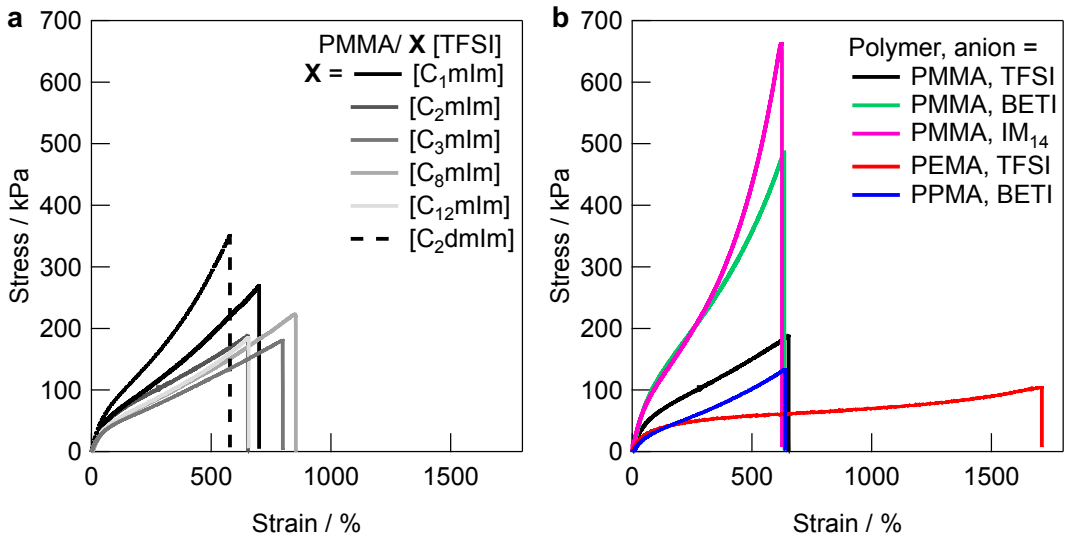

Figure 4-7. Tensile stress–strain curves for UHMW ion gels with (a) different cation structures with the fixed polymer and anion structures (PMMA and [TFSI] anion), and (b) different polymer and anion structures with the fixed cation structure ([C_2mIm] cation).

separation structure in the (ion) gel. On the other hand, although the PMMA/[C_{12}mIm][TFSI] UHMW ion gel had relatively high T_g of −56.1 °C, comparable to that of PMMA/[C_2mIm][BETI], the UHMW ion gel showed much lower Young's modulus and fracture stress than those of PMMA/[C_2mIm][BETI]. The long alkyl chain of [C_{12}mIm] cation is known to cause polar-apolar nanophase separation,[18] suggesting that nanophase of cation polar-apolar domain nanophase separation might have a negative effect on mechanical properties. Although the PMMA/[C_{12}mIm][TFSI] UHMW ion gel is transparent and thus PMMA and [C_{12}mIm][TFSI] are macroscopically compatible, low affinity between the IL and the polymer on the microscopic scale may degrade the mechanical properties. This consideration will be discussed later in molecular dynamics (MD) simulations section. It was also revealed that the PEMA/[C_2mIm][TFSI] UHMW ion gel showed the highest fracture strain and the lowest fracture stress among all UHMW ion gels. This can be attributed to the lowest T_g of –78.7 °C and slightly lower molecular weight of PEMA/[C_2mIm][TFSI] gel compared to other systems (**Table 4-2 and Table 4-3**), which may lead to low mechanical strength and large elongation at break due to the disentanglement of polymer chains under the timescale of the tensile test.

Table 4-3. Summary of the tensile properties and glass transition temperature (T_g) for UHMW ion gels. [a]measured by tensile tests. [b]determined by DSC measurements.

Polymer	Solvent	Young's modulus (E) / kPa[a]	Fracture stress / kPa[a]	Fracture strain / %[a]	T_g / °C[b]
PMMA	[C_1mIm][TFSI]	147	271	700	-62.1
	[C_2mIm][TFSI]	124	190	653	-70.0
	[C_3mIm][TFSI]	94	182	799	-68.0
	[C_8mIm][TFSI]	120	225	853	-60.3
	[C_{12}mIm][TFSI]	101	187	656	-56.1
	[C_2dmIm][TFSI]	167	353	578	-62.4
	[C_2mIm][BETI]	196	467	454	-57.2
	[C_2mIm][IM_{14}]	180	665	625	-69.7
PEMA	[C_2mIm][TFSI]	71	106	1711	-78.7
PPMA	[C_2mIm][BETI]	69	135	639	-74.5

4.6 Self-Healing Properties of UHMW Ion Gels

Next, I evaluated the self-healing behavior of UHMW ion gels prepared in different combinations of polymer network and ILs. In Chapter 3, I demonstrated that the PMMA/[C_2mIm][TFSI] UHMW ion gel showed remarkable self-healing ability in a unique molecular mechanism at room temperature.

The driving force of self-healing of UHMW ion gel is due to the entanglement of the constituent "un-crosslinked" linear polymers. However, the self-healing efficiency is highly dependent on the chemical structure of ILs and polymers. For example, PMMA/[C_2mIm][TFSI] exhibits a good self-healing efficiency, while PEMA/[C_2mim][TFSI] shows a poor self-healing rate. Herein, how chemical structure of polymer and ILs affect self-healing ability of the UHMW ion gels in detail will be investigated. **Figure 4-8** shows the tensile stress-strain curves for the pristine and healed ion gels for each UHMW ion gel with different polymer and IL structures. For the preparation of healed ion gel samples, dumbbell-shaped ion gels were cut at the center, after that the two cut surfaces were brought into contact immediately and allowed to heal at room temperature for 24 h. In contrast to conventional chemically cross-linked ion gels having no self-healing ability, all UHMW ion gels exhibited self-healing properties, although healing efficiencies were different. For UHMW ion gels with different cation structures, the healing efficiency reached to 100% for PMMA/[C_2mIm][TFSI] and PMMA/[C_3mim][TFSI], whereas complete healing was not observed for other gels. When the anion structure was varied from TFSI to BETI and IM_{14}, the healing efficiency was decreased to less than as low as 40%. One of the possible reasons of low healing efficiency for the PMMA/[C_2mIm][BETI] and PMMA/[C_2mIm][IM_{14}] could be attributed to the trade-off relationship between self-healing ability and stiffness. The higher Young's modulus is related to lower dynamic properties of physical cross-linking by entanglement, which might lead to low self-healing properties. The trade-off relationship

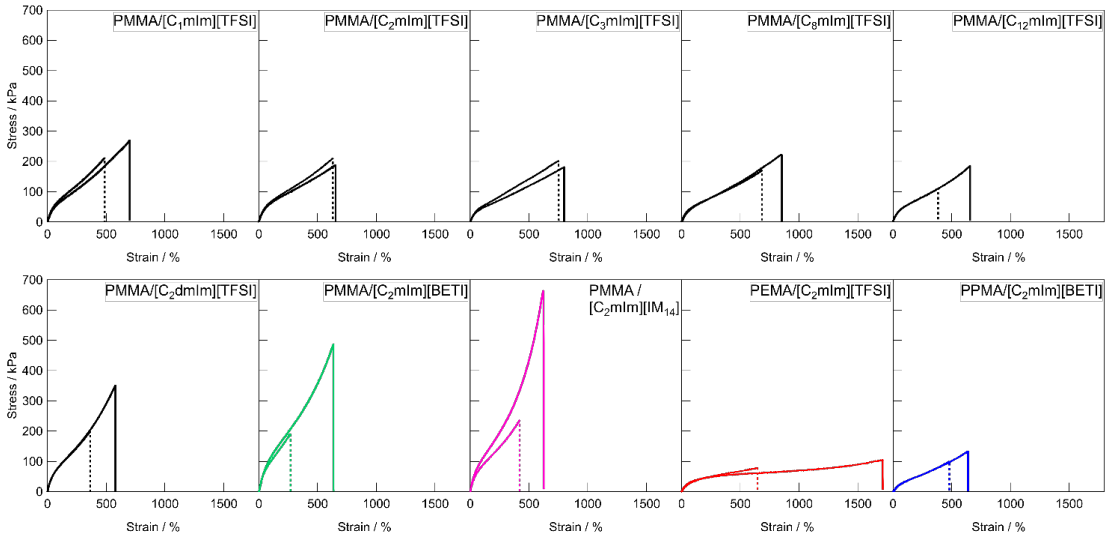

Figure 4-8. Tensile stress-strain curves for pristine and healed UHMW ion gels with different polymer and IL structures. Solid and dashed lines indicate pristine and healed samples, respectively.

was also reported in other self-healable polymeric materials.[19, 20]

Figure 4-9 shows the relationship between Young's modulus and healing efficiency for UHMW gels. While several UHMW ion gels obeyed the trade-off relationship between Young's modulus and healing efficiency shown by the dotted straight line, some UHMW ion gels deviated upward and downward from the line. The PMMA/[C_2mIm][TFSI] UHMW gel exhibited upward deviation from

the line, indicating that there exists a driving force which accelerates the reformation of entanglement across the cut surfaces. On the other hand, PMMA/[C_{12}mIm][TFSI], PEMA/[C_2mIm][TFSI], and PPMA/[C_2mIm][TFSI] UHMW ion gels deviated significantly downward from the trade-off line. Notably, although the tensile stress-strain curves for pristine PMMA/[C_{12}mIm][TFSI] and PMMA/[C_2mIm][TFSI] UHMW gels were nearly identical, the healing efficiencies were quite different **(Figure 4-10)**.

These results suggest that the self-healing behavior of UHMW gels is not governed only by the trade-off relationship between the stiffness and the healing efficiency, other factors also contribute to the self-healing phenomena. In our previous study, MD simulations for PMMA/[C_2mIm][TFSI] and PEMA/[C_2mIm][TFSI] systems suggested that PMMA and PEMA showed different solvation structure in [C_2mIm][TFSI]. Therefore, the deviation from the trade-off relationship might be originated from the difference in the microscopic interaction among polymers and IL cations and anions, which would lead to the acceleration or deceleration of reformation of entanglement across cut surfaces.

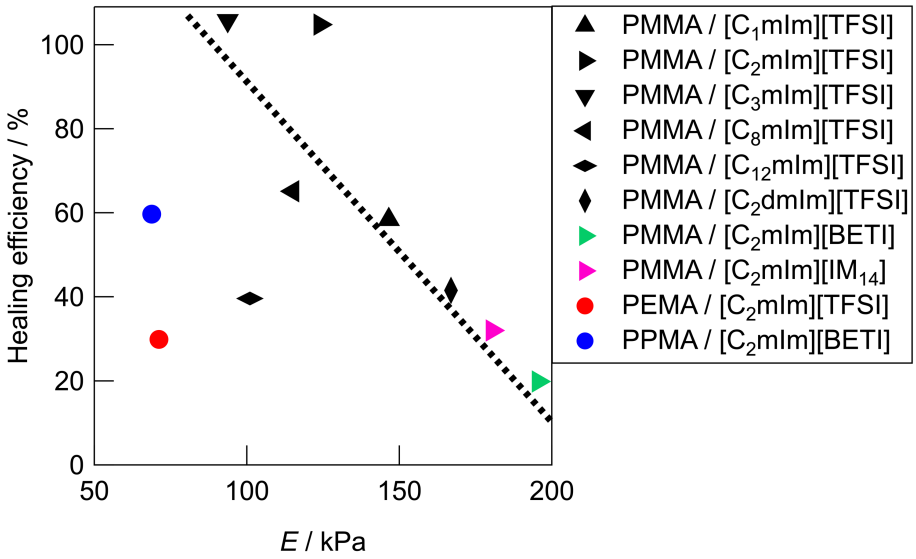

Figure 4-9. Relationship between the Young's modulus (E) and the healing efficiency of UHMW ion gels. The dotted line is a guide to the eye. The healing efficiency was defined as the ratios of mechanical toughness (the area under the stress-strain curve) between pristine and healed gels.

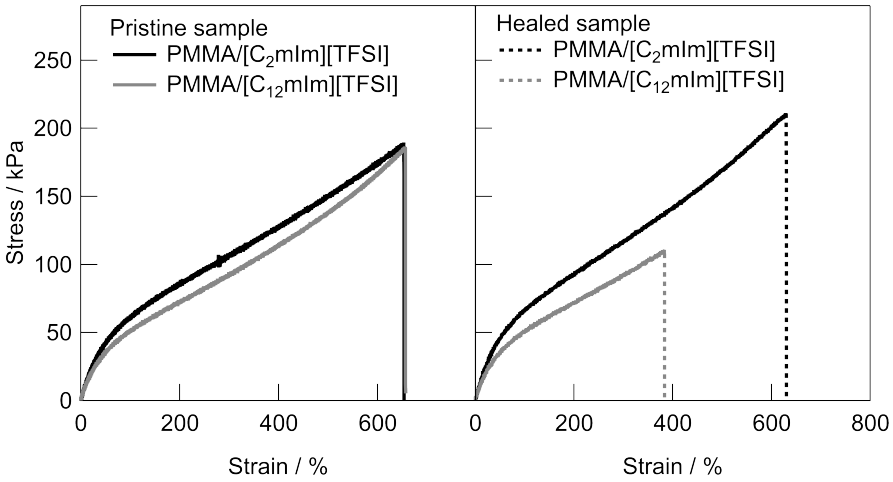

Figure 4-10. Comparison of the stress-strain curves for pristine (left) and healed (right) PMMA/[C_2mIm][TFSI] and PMMA/[C_{12}mIm][TFSI] UHMW ion gels.

4.7 MD Simulations for Different Polymer/IL Systems

To gain further insight into the polymer-IL and polymer-polymer interactions at the microscopic scale, all-atom MD simulations and detailed statistical analysis were performed on the PMMA/[C_2mIm][TFSI] (upward deviation from trade-off line), PMMA/[C_{12}mIm][TFSI] (downward deviation), and PEMA/[C_2mIm][TFSI] (downward deviation) systems, in which healing efficiency was quite different. The simulations were carried out in an NTP ensemble. The radial distribution functions for all atoms ($G_{total}(r)$ as an r-weighted difference form, $r^2[G(r) - 1]$, is shown in **Figure 4-11**) were calculated from the trajectory data obtained from the 500 ps calculations. The radial

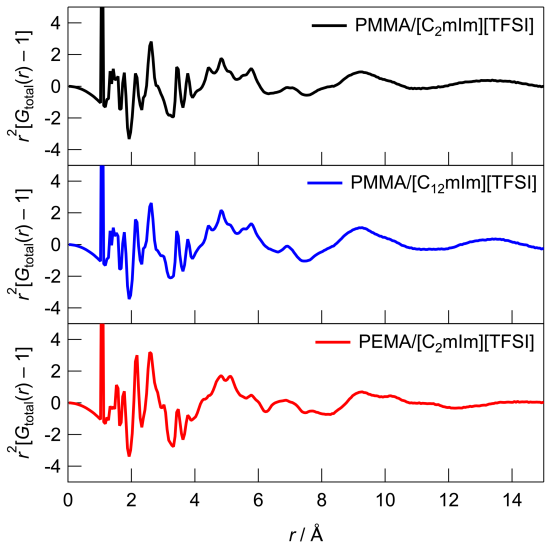

Figure 4-11. $G_{total}(r)$ functions for the PMMA/[C_2mIm][TFSI], PMMA/[C_{12}mIm][TFSI], and PEMA/[C_2mIm][TFSI] systems.

distribution function consists of intramolecular and intermolecular correlations for each component. The intramolecular radial distribution function for the polymer ($G_{intra}(r)$) is shown in **Figure 4-12(a).** The jagged peaks appearing below 5 Å corresponded to correlations between directly bonded atoms or their neighbors in the polymer molecule. On the other hand, the broad peak with a peak top near 10 Å can be attributed to the summation of atomic correlations within non-bonded atoms. Therefore, the broadness of these peaks is an indicator for the degree of expansion of individual polymers solvated by ILs. It was observed that the PMMA/[C_2mIm][TFSI] system had a broader peak than those of PMMA/[C_{12}mIm][TFSI] and PEMA/[C_2mIm][TFSI] systems, suggesting that the polymer conformation was most extended in the PMMA/[C_2mIm][TFSI] system compared to PMMA/[C_{12}mIm][TFSI] and PEMA/[C_2mIm][TFSI] systems. In fact, the R_g calculated from the intramolecular radial distribution function was 14.2, 13.1, and 12.3 Å for PMMA/[C_2mIm][TFSI], PMMA/[C_{12}mIm][TFSI], and PEMA/[C_2mIm][TFSI], respectively. **Figure 4-12(b)** shows representative polymer conformations for three systems.

Furthermore, to obtain insight into the polymer-polymer interactions in ILs, I evaluated the intermolecular radial distribution function ($G_{poly\text{-}poly}(r)$) that represents the correlation between the different polymer chains (**Figure 4-13(a)**). In the PMMA/[C_2mIm][TFSI] system, the upturn of the intensity was observed around 6 Å, which indicates that the correlation between polymers starts to exist from this distance. On the other hand, in the PMMA/[C_{12}mIm][TFSI] and the PEMA/[C_2mIm][TFSI] systems, the upturns were observed from around 9 and 12 Å, respectively, which were farther than that of the PMMA/[C_2mIm][TFSI] system. In addition, the depth of the convex curve for the PMMA/[C_{12}mIm][TFSI] and the PEMA/[C_2mIm][TFSI] systems in **Figure 4-13(a)** was much deeper than that of the PMMA/[C_2mIm][TFSI] system, suggesting the probability of having different polymer chains in the proximity is low. These results suggest that in the PMMA/[C_2mIm][TFSI] system, individual polymer chain has a more extended conformation in the IL, and different polymer chains are more likely to exist in the vicinity (**Figure 4-13(b)**). Therefore, even at the cut surfaces of the PMMA/[C_2mIm][TFSI] UHMW gel, the polymer chains may take an expanded form and different polymer chains are more likely to be present in the vicinity, which facilitates the reformation of entanglement, resulting in the excellent self-healing ability. However, it should be noted that, MD calculations were performed for polymers with a low polymerization degree of 20-mers, which is quite different from the degree of polymerization for UHMW polymers (> 10,000-mers). Further studies to clarify the polymer conformations and interpolymer interactions in UHMW ion gels more accurately by combining the large-scale MD calculations at polymerization degree that exceeds the entanglement molecular weight is under progress along with high-energy X-ray total scattering experiments.

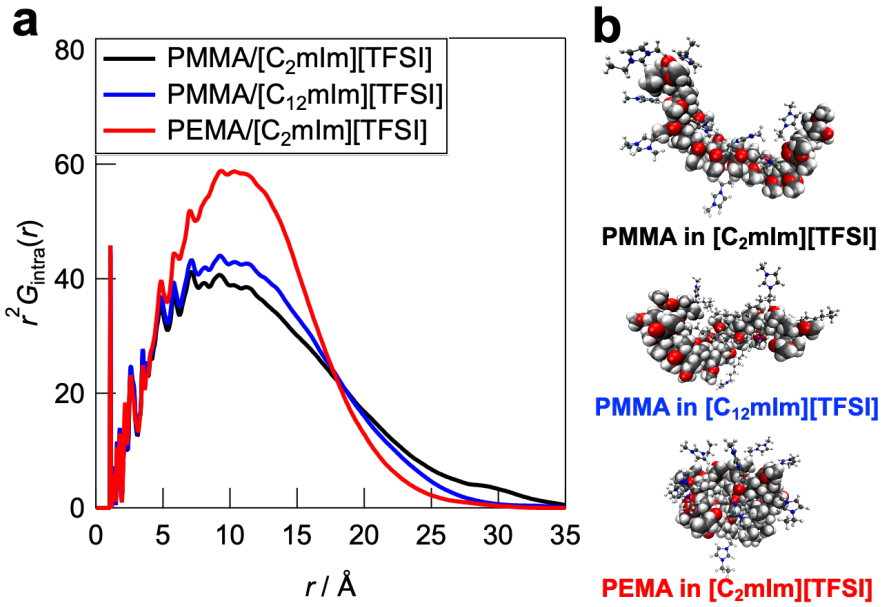

Figure 4-12. (a) Intramolecular contribution of the radial distribution function ($G_{intra}(r)$) for the PMMA/[C2mIm][TFSI], PMMA/[C12mIm][TFSI], and PEMA/[C2mIm][TFSI] systems. (b) Representative snapshot of individual polymer conformations in ILs extracted from the MD simulation boxes.

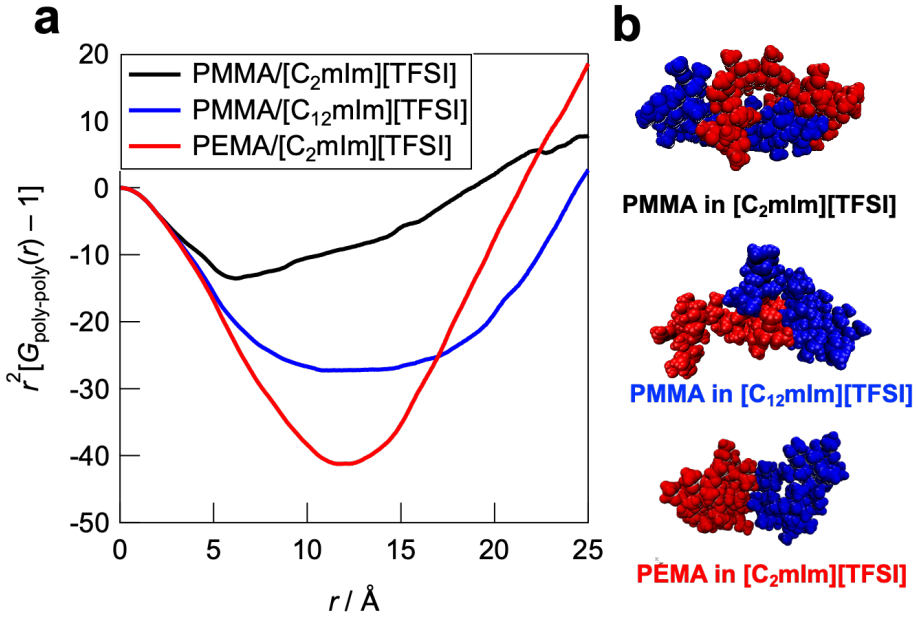

Figure 4-13. (a) Intermolecular contribution of the radial distribution function ($G_{poly\text{-}poly}(r)$) for the PMMA/[C2mIm][TFSI], PMMA/[C12mIm][TFSI], and PEMA/[C2mIm][TFSI] systems. (b) Representative snapshot of two adjacent polymers in ILs extracted from the MD simulation boxes.

4.8 Conclusions

In conclusion, UHMW gels, which were formed solely by physical entanglements of *in situ* polymerized UHMW polymers in ILs, were fabricated from various IL/monomer structures. In the rheological measurements, all UHMW gels exhibited a wide rubbery plateau without crossover of G' and G'' over wide frequency and temperature region, indicating that UHMW ion gels can maintain solid-like integrity over long timescales. Tensile tests suggested that stress-strain curves of UHMW ion gels were significantly dependent on the IL/polymer chemical structures. In particular, the PMMA/[C_2mIm][IM_{14}] UHMW ion gel showed the highest fracture stress despite relatively low T_g, implying that the nanoscale phase separation of long perfluoroalkyl chain might affect the tensile property of UHMW ion gels. Self-healing properties of UHMW ion gels evaluated by tensile tests revealed the trade-off relationship between the stiffness and the healing efficiency, whereas some UHMW gels deviated from the trade-off line. MD simulations for different polymer/IL structures revealed that the intramolecular polymer conformations as well as interpolymer interactions were dependent of the polymer/IL structures. In the combination of polymer/IL for the UHMW ion gel that shows high self-healing efficiency, the polymer chain can take an extended conformation in the IL, and that different polymer chains are likely to be present in close proximity to each other. In the field of polymer gel science, “the style of cross-linking”, “polymer network”, and “solvent” are known as the three major components of gels. So far, efforts have been made to realize effects of the style of cross-linking and polymer network towards unprecedented functions and excellent mechanical properties of gels. However, solvents engineering of gels has never been received any special attention. The ability to control the mechanical properties of gels by changing the solvent structure is a unique strategy that is not found in other gels such as hydrogels and organogels. Further, our insights into the effects of the chemical structure on the mechanical and self-healing properties of UHMW ion gels provide not only fundamental knowledges on polymer gel science but also a useful progress for the development of a new class of ion gels for wearable and flexible devices with desirable physicochemical properties.

Reference

[1] Noda, A.; Hayamizu, K.; Watanabe, M. *J. Phys. Chem. B* **2001**, *105*, 4603-4610.

[2] Jorgensen, W. L.; Maxwell, D. S.; Tirado-Rives, J. *J. Am. Chem. Soc.* **1996**, *118*, 11225-11236.

[3] Cornell, W. D.; Cieplak, P.; Bayly, C. I.; Gould, I. R.; Merz, K. M.; Ferguson, D. M.; Spellmeyer, D. C.; Fox, T.; Caldwell, J. W.; Kollman, P. A. *J. Am. Chem. Soc.* **1995**, *117*, 5179-5197.

[4] Canongia Lopes, J. N.; Pádua, A. A. H. *J. Phys. Chem. B* **2006**, *110*, 19586-19592.

[5] Low, K.; Wylie, L.; Scarborough, D. L. A.; Izgorodina, E. I. *Chem. Commun.* **2018**, *54*, 11226-11243.

[6] Harrisson, S.; Mackenzie, S. R.; Haddleton, D. M. *Chem. Commun.* **2002**, 2850-2851.

[7] Suzuki, Y.; Shinagawa, Y.; Kato, E.; Mishima, R.; Fukao, K.; Matsumoto, A. *Macromolecules* **2021**, *54*, 3293-3303.

[8] He, Y.; Boswell, P. G.; Bühlmann, P.; Lodge, T. P. *J. Phys. Chem. B* **2007**, *111*, 4645-4652.

[9] Noro, A.; Matsushita, Y.; Lodge, T. P. *Macromolecules* **2008**, *41*, 5839-5844.

[10] Ma, X.; Usui, R.; Kitazawa, Y.; Tamate, R.; Kokubo, H.; Watanabe, M. *Macromolecules* **2017**, *50*, 6788-6795.

[11] He, X.; Kong, M. Q.; Niu, Y. H.; Li, G. X. *Macromolecules* **2020**, *53*, 7865-7875.

[12] Liu, G.; Fang, D.; Dan, Y.; Luo, H.; Luo, C.; Niu, Y.; Li, G. *Phys. Chem. Chem. Phys.* **2022**, *24*, 16388-16396.

[13] Liu, Z.; Wang, W.; Stadler, F. J.; Yan, Z. C. *Polymers (Basel)* **2019**, *11*.

[14] Diodati, L. E.; Wong, A. J.; Lott, M. E.; Carter, A. G.; Sumerlin, B. S. *ACS Appl. Polym. Mater.* **2023**, *5*, 9714-9720.

[15] Airey, G. D.; Mohammed, M. H. *Rheologica Acta* **2008**, *47*, 751-763.

[16] Ishii, S.; Kokubo, H.; Hashimoto, K.; Imaizumi, S.; Watanabe, M. *Macromolecules* **2017**, *50*, 2906-2915.

[17] Lo Celso, F.; Appetecchi, G. B.; Simonetti, E.; Zhao, M.; Castner, E. W.; Keiderling, U.; Gontrani, L.; Triolo, A.; Russina, O. *Front. Chem.* **2019**, *7*.

[18] Fujii, K.; Kanzaki, R.; Takamuku, T.; Kameda, Y.; Kohara, S.; Kanakubo, M.; Shibayama, M.; Ishiguro, S.-i.; Umebayashi, Y. *J. Chem. Phys.* **2011**, *135*.

[19] Sun, T. L.; Kurokawa, T.; Kuroda, S.; Ihsan, A. B.; Akasaki, T.; Sato, K.; Haque, M. A.; Nakajima, T.; Gong, J. P. *Nat. Mater.* **2013**, *12*, 932-937.

[20] Wang, Z.; Gangarapu, S.; Escorihuela, J.; Fei, G.; Zuilhof, H.; Xia, H. *J. Mater. Chem. A* **2019**, *7*, 15933-15943.

Summary

I developed a quite new class of functional soft material composed of ionic liquids (ILs) and ultra-high molecular weight (UHMW) polymers and investigated its physicochemical and mechanical properties. It was found that radical polymerization of vinyl monomers in ILs specifically produces high molecular weight polymers, resulting in gelation without the addition of cross-linking agents that were commonly required chemicals. The effect of molecular weight on the physical properties of the resulting ion gels, i.e., UHMW ion gels, was clarified by rheological and dynamic light scattering measurements. The stress-strain behavior of the UHMW ion gels was evaluated by tensile tests. It was found that the ion gels exhibited superior mechanical properties compared to conventional chemically crosslinked gels. The potential influence of micro-solvation structure on self-healing properties was revealed at the molecular level by molecular dynamics (MD) simulation. Furthermore, the chemical structures of polymers and IL solvents were also found to govern the mechanical properties including self-healing properties of UHMW ion gels. The conclusions from the chapters are summarized in detail below.

Chapter 2

In situ radical polymerization of MMA in an IL, [C_2mIm][TFSI], resulted in a significant increase in molecular weight compared to that in toluene, a common organic solvent. Even at extremely low initiator concentrations, UHMW PMMA was formed while maintaining almost 100% conversion. A transparent freestanding gel was formed solely by physical entanglement of UHMW PMMA chains. The effect of the viscosity of the polymerization solvent on the high molecular weight was investigated by comparing the different IL as polymerization solvent with a viscosity-tuned conventional molecular liquid (toluene) system. The viscosity of the polymerization solvent had little effect on the increase in molecular weight, suggesting a decrease in the activation energy due to the interaction between the IL ions and the propagation radicals. In addition, the molecular weight of PMMA obtained by polymerization in IL was larger than that obtained by bulk polymerization, supporting the acceleration of polymerization by ILs. Rheological measurements revealed that the terminal relaxation behavior at high temperatures and low frequencies is suppressed with increasing molecular weight, resulting in excellent shape stability. Dynamic light scattering measurements also confirmed the disappearance of the flow-diffusion mode of the polymer with increasing molecular weight, suggesting the formation of a robust three-dimensional network with entangled cross-linking points.

Chapter 3

The mechanical properties of ion gels consisting of the entanglement of ultra-high molecular weight PMMA in ionic liquids were investigated by tensile tests, and the results showed that UHMW ion gels

exhibit excellent mechanical properties, such as [1] excellent stretchability, [2] recyclability by hot-pressing, [3] rapid self-healing ability at room temperature, which are not observed in conventional chemically cross-linked ion gels. The self-healing properties of the ion gels are attributed to the diffusion of polymer chains across the cut interface and the reformation of physical entanglement. This is in contrast to self-healing materials based on reversible bonds such as hydrogen bonding, host-guest interactions, and dynamic covalent bonds, which have been extensively studied in recent years. It is also suggested that the nonequilibrium state of the cut interface plays an important role in the self-healing process. With the appropriate combination of polymer and solvent structures, UHMW gels exhibit rapid self-healing behavior at room temperature. MD simulation results suggest that the self-healing properties of ion gels depend on slight differences in chemical structure and may be influenced by the micro-solvation of the polymer in IL.

Chapter 4

UHMW gels were fabricated from various IL/monomer structures. In the rheological measurements, all UHMW gels exhibited a wide rubbery plateau without crossover of G' and G'' over wide frequency and temperature region, indicating that UHMW ion gels can maintain solid-like integrity over long timescales. Tensile tests suggested that stress-strain curves of UHMW gels were significantly dependent on the IL/polymer chemical structures. In particular, the PMMA/[C_2mIm][IM_{14}] UHMW ion gel showed the highest fracture stress despite relatively low T_g, implying that the nanoscale phase separation of long perfluoroalkyl chain might affect the tensile property of UHMW ion gels. Self-healing properties of UHMW ion gels evaluated by tensile tests revealed the trade-off relationship between the stiffness and the healing efficiency, whereas some UHMW ion gels deviated from the trade-off line. MD simulations for different polymer/IL structures revealed that the intramolecular polymer conformations as well as interpolymer interactions were dependent of the polymer/IL structures. In the combination of polymer/IL for the UHMW ion gel that shows high self-healing efficiency, the polymer chain can take an extended conformation in the IL, and that different polymer chains are likely to be present in close proximity to each other. In the field of polymer gel science, “the style of cross-linking”, “polymer network”, and “solvent” are known as the three major components of gels. So far, efforts have been made to realize effects of the style of cross-linking and polymer network towards unprecedented functions and excellent mechanical properties of gels. However, solvents engineering of gels has never received any special attention. The ability to control the mechanical properties of gels by changing the solvent structure is a unique strategy that is not found in other gels such as hydrogels and organogels. Further, our insights into the effects of the chemical structure on the mechanical and self-healing properties of UHMW ion gels provide a useful basis for the development of a new class of ion gels for wearable and flexible devices with desirable physicochemical properties.

Thus, a new robust ion gel composed of physical entanglement of UHMW polymers has been successfully developed. It was found that these gels exhibit unique mechanical properties not found in conventional chemically crosslinked gels. The universal concept of stretchable and self-healing polymer gels based on the physical entanglement of UHMW polymers is expected to be extended to a variety of polymer systems. Due to the simplicity of the current UHMW ion gel concept, synergistic effects on mechanical properties are also expected by combining the UHMW ion gel strategy with other toughening strategies such as block copolymer self-assembly, nanocomposites, and supramolecular interactions. Furthermore, I found that the mechanical properties of UHMW ion gels can be precisely controlled by the chemical structure of the solvent as well as the polymer. The control of the mechanical properties of ion gels by the solvent, ILs, may enable further functionalization of polymeric materials with ILs.

Finally, I conclude that this study provides a new strategy for a soft material design, UHMW ion-gel, which can contribute to society through the field of soft electronics.

List of publications

Original papers comprising this thesis

1. Kamiyama, Y.; Tamate, R.; Hiroi, T.; Samitsu, S.; Fujii, K.; Ueki, T.
   Highly stretchable and self-healable polymer gels from physical entanglements of ultrahigh-molecular weight polymers.
   Sci. Adv. **2022**, *8*, eadd0226.
2. Kamiyama, Y.; Tamate, R.; Fujii, K.; Ueki, T.
   Controlling mechanical properties of ultrahigh molecular weight ion gels by chemical structure of ionic liquids and monomers.
   Soft Matter **2022**, *18*, 8582-8590.

Other papers

1. Yoshitake, M.; Kamiyama, Y.; Nishi, K.; Yoshimoto, N.; Morita, M.; Sakai, T.; Fujii, K.
   Defect-free network formation and swelling behavior in ionic liquid-based electrolytes of tetra-arm polymers synthesized using a Michael addition reaction.
   Phys. Chem. Chem. Phys. **2017**, *19*, 29984-29990.
2. Kamiyama, Y.; Shibata, M.; Kanzaki, R.; Fujii, K.
   Lithium-ion coordination-induced conformational change of PEG chains in ionic-liquid-based electrolytes.
   Phys. Chem. Chem. Phys. **2020**, *22*, 5561-5567.
3. Tamate, R.; Peng, Y.; Kamiyama, Y.; Nishikawa, K.
   Extremely Tough, Stretchable Gel Electrolytes with Strong Interpolymer Hydrogen Bonding Prepared Using Concentrated Electrolytes to Stabilize Lithium-Metal Anodes.
   Adv. Mater. **2023**, *35*, e22116

Books

1. 玉手亮多、上山祐史、上木岳士
   第 12 章 ゲル, 4「イオン液体を用いた自己修復性ソフトマテリアル」 大内幸雄監修(シーエムシー出版)
   2022, pp. 237-244

Patents

1. 上山祐史、玉手亮多、上木岳士
   「イオンゲルの製造方法、イオンゲル、固体電解質、及び、アクチュエータ」
   特開 2022147877 号
2. 上山祐史、玉手亮多、上木岳士
   「コーティング用組成物、膜、及び、積層体」
   特開 2022147878 号

Acknowledgement

This doctoral dissertation is based on research conducted from 2020 to 2024 in the research group of Associate Professor Ueki Takeshi, Department of Soft Matter, Graduate School of Life Sciences, Hokkaido University.

First of all, I would like to thank my academic supervisor, **Visiting Associate Professor Takeshi Ueki**. This dissertation is supported by his kind instruction in all aspects of my research content. He spent a lot of time with me from the drafting stage of this research, discussion of experimental results, and writing up the paper. When I started my research in this group, Although I was still inexperienced in materials science, I was able to learn a lot thanks to his kind guidance. He also provided me with a lot of advice and help when I ran into serious obstacles, and I was able to carry out this research until the end. As an educator and researcher, I would like to express my sincere gratitude for the wonderful research environment provided to me, and in gratitude for your kindness, I will continue my efforts to make a breakthrough as a full-fledged researcher as soon as possible.

I am also deeply grateful to **Dr. Ryota Tamate** of NIMS for his especially kind support of my research on viscoelasticity and mechanical properties of gels. He frequently took time to discuss experimental results from the early stages of the research, and taught me the fundamentals of the mechanical properties of polymeric soft materials.

I would also like to express my sincere gratitude to **Professor Kenta Fujii** of Yamaguchi University, who provided much support in the physical chemistry perspective of polymer-ionic liquid mixtures. He was also my advisor during my master's program, and it was his knowledge of physical chemistry and solution chemistry that enabled me to deepen this research. The molecular interpretation of this paper could not have been realized without discussions with him.

For the dynamic light scattering measurement, **Dr. Takashi Hiroi** of NIMS provided me with an excellent measurement environment. The measurement system he constructed was a very precious experience for me during the experiment, and I was able to spend meaningful time in my research activities. I would like to thank him for his guidance in experimental methods, data analysis, and interpretation.

I would like to thank **Dr. Sadaki Samitsu** of NIMS for his great help in compiling the original paper.I also appreciate his guidance on the value of this paper as materials science and its interpretation and significance from the viewpoint of polymer physics.

I would also like to thank to **Dr. Jun Nakanishi Group Leader** of NIMS, for his support in all research activities. He provided me not only an excellent research environment, but also had many opportunities of discussions with me in the execution of my research, which helped me to deepen this paper from an analytical chemistry point of view.

I am also grateful to **Yuna Osaka**, **Aya Saruwatari**, **Mai Kamiyama**, and **Tsubasa Naka**, who are members of the Ueki research group. At the beginning of my research, I was the first student in the group to silently continue experiments, but I was able to enjoy my research life with many new research members. I am also grateful to the members of Nakanishi's research group. In particular, **Dr. Shota Yamamoto** and **Dr. Kenta Homma** not only supported my daily research activities but also gave me meaningful suggestions in discussions about my daily research. I would also like to thank to the research technical staff of the Ueki group for their various supports in experiments. **Akiko Murai**, a secretary in the Nakanishi group, assisted us with procedures necessary to carry out our research. I would like to thank them as well.

I would also like to express my deepest gratitude to the Japan Society for the Promotion of Science (JSPS) and NIMS for their financial support.

Finally, I would like to thank my family, brother, and wife for their mental and financial support. My parents consulted with me when I entered the doctoral program and pushed me to pursue a career in academia. Also, my wife Mai Kamiyama and I promised to share a future together while I was in the doctoral program, and she has always supported me in my daily life.

I would like to express my sincere gratitude to all the people who have supported and helped me.

March, 2024

Yuji Kamiyama